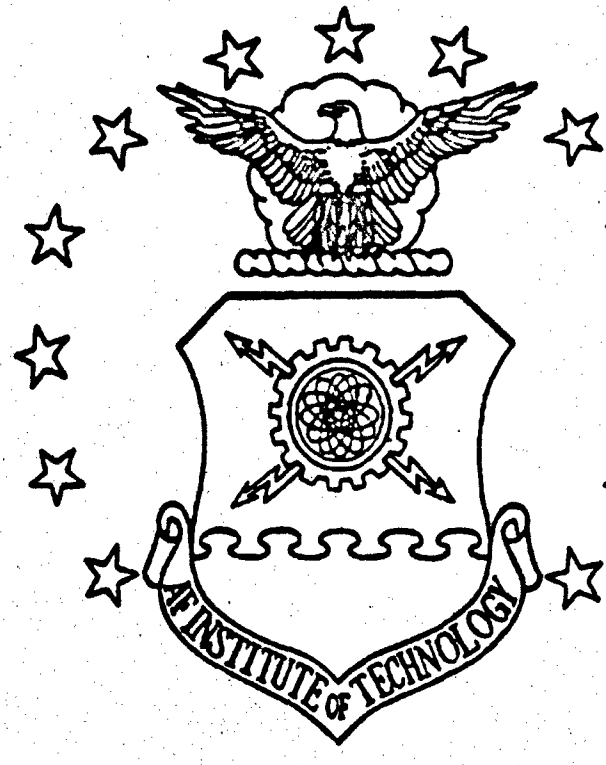

FATIGUE BEHAVIOR OF A CROSS-PLY CERAMIC MATRIX COMPOSITE SUBJECTED TO TENSION-TENSION CYCLING WITH HOLD TIME

THESIS

Scott A. Grant
Captain, USAF
AFIT/GAE/ENY/94D-16

DEPARTMENT OF THE AIR FORCE
AIR UNIVERSITY
AIR FORCE INSTITUTE OF TECHNOLOGY

Wright-Patterson Air Force Base, Ohio

AFIT/GAE/ENY/94D-16

FATIGUE BEHAVIOR OF A CROSS-PLY CERAMIC MATRIX COMPOSITE SUBJECTED TO TENSION-TENSION CYCLING WITH HOLD TIME

THESIS

Scott A. Grant
Captain, USAF
AFIT/GAE/ENY/94D-16

DISCLAIMER NOTICE

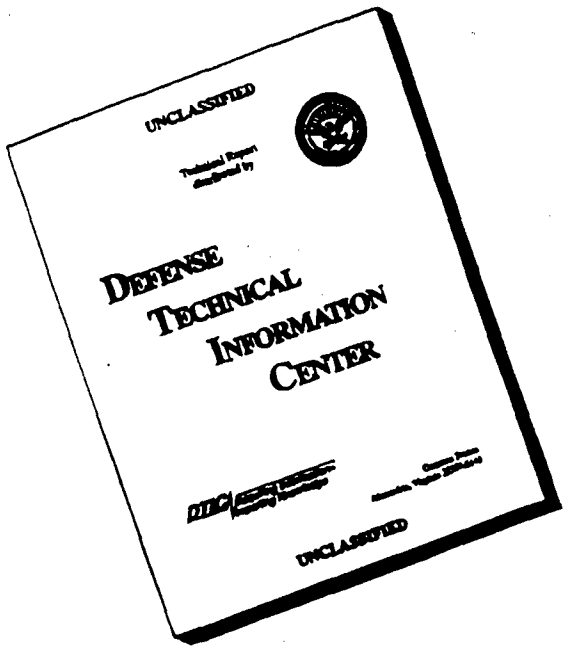

THIS DOCUMENT IS BEST QUALITY AVAILABLE. THE COPY FURNISHED TO DTIC CONTAINED A SIGNIFICANT NUMBER OF PAGES WHICH DO NOT REPRODUCE LEGIBLY.

AFIT/GAE/ENY/94D-16

FATIGUE BEHAVIOR OF A CROSS-PLY CERAMIC MATRIX COMPOSITE SUBJECTED TO TENSION-TENSION CYCLING WITH HOLD TIME

THESIS

Presented to the Faculty of the Graduate School of

Engineering of the Air Force Institute of Technology

Air University

in Partial Fulfillment of the

Requirements for the degree of

Master of Science in Aeronautical Engineering

Scott A. Grant

Captain, USAF

December 1994

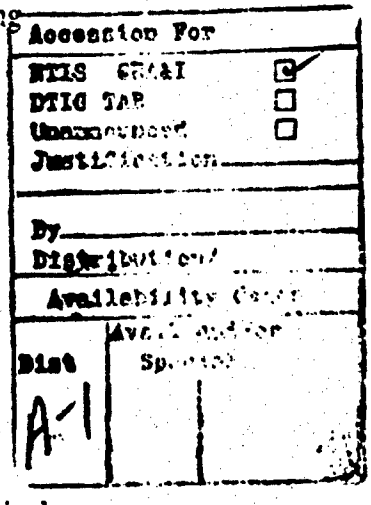

Approved for public release; distribution unlimited

Preface

In this study, the fatigue behavior of the SiC-MAS5 cross-ply composite was investigated at elevated temperatures with loading wave-forms combining the characteristics of high cycle fatigue and stress rupture. Published test data, two stress levels, and two temperatures were used to characterize this behavior. A series of tests were conducted to assess the fatigue life as a function of wave-form characteristic, temperature, and stress level. In addition, the mechanisms that control the fatigue life under these different conditions were investigated.

The people I would like to thank for their inputs and support are Dr. Shankar Mall for frequent visits to the laboratory to lend support and motivation, Dr. Larry Zawada for giving me advice on what works and what doesn't in post-mortem analysis, Dr. Anthony Palazotto and Capt. David Robertson for their comments on the draft, Mr. Mark Derriso for fielding a prodigious number of questions from graduate students trying to work the equipment for the first time. Also, I would like to thank Capt. Craig Steiner for the many late night phone calls from the lab on the status of my longer tests ("Hey, your test stopped....) and for the heads-up on tickets to concerts I would have otherwise never seen.

Finally, I would like to thank Mr. Ted Fecke of WL/POTC and Dr. Walter Jones of AFOSR/NA. Their sponsorship made this study possible.

Table of Contents

List of Figures

List of Tables

Abstract

A study was carried out to investigate the behavior of the SiC-MAS5, cross ply, $[0/90]_{8s}$ ceramic matrix composite when subjected to fatigue with loading wave-forms that combine the characteristics of stress rupture and high cycle fatigue. All tests were conducted under load control using four loading wave-forms, two elevated temperatures, and two stress levels.

All loading wave-forms were triangular with the combined loading and unloading rates of one hertz. Four hold times were applied at maximum load: 0, 1, 10, and 100 seconds. In order that the results from this study be compared to the previous study, 566 and 1093°C were chosen as the test temperatures.

Published elevated temperature tensile test data from the previous studies were used to select the two stress levels. The first, 103 MPa, was selected to represent a stress level slightly beyond the linear region of the monotonic stress-strain curve. The second, 138 MPa, was chosen as the representative of stress in the region of non-linearity of the monotonic stress-strain curve. These stress levels were chosen in order to introduce different levels of initial damage during the first fatigue cycle. All tests were done at the stress ratio, R ($\sigma_{min}/\sigma_{max}$) of 0.1.

The test results were compiled in the form of S-N (stress versus cycles to failure), S-T (stress versus exposure time which was computed as the cycle duration multiplied by the number of cycles at failure), S-S*T (stress versus stress-time parameter which was computed as the area under the cyclic loading curve multiplied by the number of cycles at failure), modulus degradation, variation of

strain, and characteristics of the stress-strain relationships during cycling. From the behavior demonstrated by these curves, relationships between the different effects of the loading wave-form on the fatigue behavior of the tested ceramic matrix composite were developed. In addition, a post-mortem SEM analysis of the fractured surfaces of all specimens were conducted to assess the fatigue damage mechanisms.

It was found that the S-N data followed the trend that as the hold time, temperature, or stress increased with all other factors constant, the number of cycles to failure decreased. In addition, a normalization was applied to reflect the amount of time the material was exposed to the elevated temperature environment under stress, and the application of this normalization technique revealed that the life expectancy of the material depended on a synergistic combination of oxidation due to temperature and cyclic fatigue--both contributed to varying degrees depending on the temperature and stress.

FATIGUE BEHAVIOR OF A CROSS PLY CERAMIC MATRIX COMPOSITE SUBJECTED TO TENSION-TENSION CYCLING WITH HOLD TIME

I. Introduction

A. Background

Ceramic matrix composites (CMCs) have applications in high temperature structures where metallic materials are undesirable due to creep or oxidation. Because of these limitations, the use of CMCs is on the rise in applications such as protective coverings/coatings (e.g. the protective tiles on the space shuttle) and extreme temperature structures (e.g. turbomachinery hot section components).

Monolithic ceramic materials all share one common disadvantage--the inability to tolerate flaws due to manufacturing or service hazards. Under high performance conditions, these flaws can cause stress concentrations that develop into cracks which propagate through the structure eventually causing catastrophic failure. The development of CMCs has helped to reduce the danger of failure due to flaws and increased the tolerance of ceramic structures to flaw related damage.

CMC materials tend to be more resistant to failure than monolithic ceramics due to the addition of ceramic fibers. These fibers arrest the propagation of cracks through the matrix for two reasons. First, the fibers apply a force opposite to the direction of crack opening. This tends to relieve the stress at the

crack tip stopping the propagation through the matrix. Second, the fiber provides a physical barrier that arrests the crack propagation until the stress at the crack tip becomes great enough to change the direction of propagation through the matrix. Unlike other composite materials such as fiber reinforced polymeric composites (PMCs), CMCs do not derive the majority of their strength from the fibers. In PMCs, the fibers have a modulus of elasticity that exceeds that of the matrix by a factor of ten [1]. In CMCs, the modulus of the fibers and matrix are of the same order. The addition of fibers give CMCs the toughness that monolithic ceramics lack.

The critical nature of the application of these advanced materials makes complete characterization a must. The designers must have information pertaining to not only the strength of the material, but also its fatigue and toughness characteristics. Since CMCs have applications typically in the aerospace industry, these characteristics are especially important due to the severe operating environments encountered and lower safety factors imposed by weight considerations. Typically, the tests performed are monotonic loading, cyclic fatigue, and stress rupture at a variety of temperatures and/or atmospheric conditions. With few exceptions, these tests are conducted independently. But these do not accurately represent the loading conditions encountered by an aircraft component. For example, a wing spar will encounter stress-rupture type loading throughout the flight due to the weight of the airframe it is supporting. It will encounter cyclic fatigue loading due to the mechanical vibrations from the engines

and aerodynamic forces. The temperature will change dramatically with changes in altitude and flight mach number. But the airframe as a whole will not suffer any of these stresses independently--there will always be some combination of these stresses acting on it at any time. Thus, an important addition to the typical types of material tests is one where the different types of loading are combined.

It is possible that the cumulative damage caused to a component under a period of service is some combination of mechanisms caused by the environment (temperature), cyclic fatigue, and stress rupture. In the case of a linear combination, it can be expressed as the following:

$$D_T = D_e + D_f + D_r , \qquad (1)$$

where D_T is the total damage, D_e is the damage caused by the environment, D_f is the damage due to cyclic fatigue, and D_r is the damage due to stress rupture. The long term goal of this study is to establish such relationships. However, as a first step in this direction, the study with the following objective was conducted.

B. Problem Statement/Scope

This objective was to investigate the relationship between the effects of temperature and combined stress-rupture/high cycle fatigue loading on the fatigue life of the silicon fiber (Nicalon) reinforced magnesium alumino-silicate (MAS5) CMC.

C. Approach

To achieve the stated objective, a test program was designed. This involved fatigue tests with a triangular wave-form with and without hold time at maximum load and elevated temperatures. All tests were conducted under load control on an MTS servohydraulic test machine under load control mode. Two elevated temperatures, two stress levels, and four loading wave-forms were used giving a total of sixteen tests. The two stress levels were chosen based on the published monotonic tensile and fatigue loading data from the previous studies and these were 103 and 138 MPa. The 103 MPa stress level is about 20 MPa above the fatigue limit at 566°C [2], and the 138 MPa stress level is about 66% of the tensile strength of the material [3]. Together, these stress levels represent the region just beyond linearity, and the region well into the non-linear range, respectively on the monotonic stress strain relationship. Hence, they introduced different levels of initial damage. The elevated temperatures of 566 and 1093 Celsius were chosen to correspond with previous studies [2,3] of this material in order to allow for comparisons and to some extent provide the verification. The loading rate for all wave-forms was 1 Hz with hold times of 0, 1, 10, and 100 seconds. The hold always occurred at maximum load level, and this allowed for varying proportions of stress rupture versus cyclic fatigue components in the loading. Figure 1 contains an illustration of the loading wave-forms used during the study.

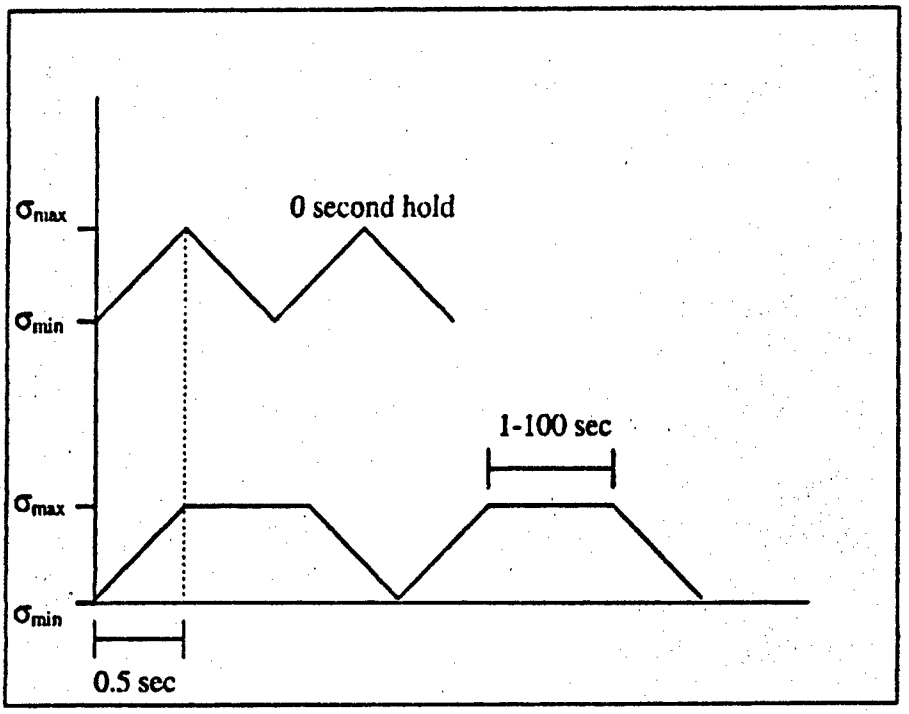

Figure 1. Loading Wave-forms.

During each test, various data were acquired periodically and these were load versus displacement (later converted to stress versus strain via the BASIC program listed in the Appendix), secant modulus, hysteretic loop energy, and maximum/minimum strain. The frequency of data acquisition was at first based on fatigue life estimates and later based on the fatigue life trends. The result was, ideally, 20-50 data sets per specimen test. Data were graphically presented based on the normalized life and/or the number of cycles, where appropriate.

Different fatigue life diagrams, i.e. the number of cycles to failure at a particular stress (S-N curve), the time exposure to the high temperature environment under a stress (S-T curve), and a parameter showing the combined

effect of stress and time under a stress (S-S*T curve, where S*T was the area under the cycling loading curve multiplied by the number of cycles at failure), were made to study the fatigue behavior of the material.

The degradation of the material due to fatigue were investigated from the plots of normalized modulus degradation, loop hysteretic energy, stress-strain, and maximum/minimum strain versus the number of cycles or normalized life. Trends from these plots were compared to the results of the S-N, S-T, and S-S*T curves and the results of these macroscopic comparisons were used to form a hypothesis on the controlling phenomena on the microscopic level.

Finally, a post-mortem microscopic analysis was conducted with the SEM and optical microscope on each failed specimen to identify the controlling damage mechanism and how it varies for different test conditions. These observations, along with the aforementioned data curves, formed a complete picture of the fatigue behavior of the composite and the varied mechanisms that contribute to the demise of the material under the condition of combined cycling and stress rupture loading.

II. Background

A. Experimental Background

The Nicalon-MAS5 ceramic matrix composite is representative of an emerging class of high temperature materials used in aggressive environments. The high temperature performance of this material has been improved with the addition of potassium borosilicate glass (BSG) as a second phase glass modifier. The boron in the BSG dopant diffuses into the MAS5 matrix and the SiC fibers during the manufacturing process and prevents oxygen embrittlement of the fiber/matrix interface--a condition that plagues conventional CMCs. The process of embrittlement begins with microcracks that form in the matrix upon initial loading. These cracks allow oxygen to infiltrate the material, oxidizing the fibers and the carbon interface between the matrix and the fibers causing the strength of the interfacial bond to increase. This is undesirable from the standpoint that a weak interfacial bond that allows some frictional sliding is a necessary feature of a "tough" CMC. The bond strength of the interface can (and will at elevated temperatures in oxidizing environments) increase to a point where matrix cracks simply propagate through the fibers. In short, the material begins to more like a monolithic ceramic [4].

The vast majority of testing of this and other like materials has been limited to monotonic tensile, high cycle fatigue, and stress rupture. Testing under the condition of combined loading has not been accomplished. But these tests are

important for two reasons. First, it is a more realistic representation of the type of loading the material will expect in service. Second, combined loading tends to be a more demanding condition to place on the material and in a sense, represents a worst-case scenario--desirable from the standpoint of conservative design practice.

Larsen [3] looked at the behavior of cross ply Nicalon-MAS5 at various levels of BSG doping at both 566 and 1093 °C under conditions of both stepped and constant stress rupture loading. At the lower temperature, it was found that the 5% BSG doped material achieved 200 hour run-out at 138 MPa where it was subsequently loaded to failure, which occurred at approximately 165 MPa. The stepped stress rupture tests resulted in approximately the same failure stress. For comparison, monotonic tensile failure occurred at approximately 262 MPa. At the higher temperature, 200 hour run-out was achieved with the 5% BSG material at a stress of 117 MPa where, upon rapid upload to failure, the test was terminated at a stress of 165 MPa. Monotonic tensile failure occurred at 234 MPa. These results represented a minor increase in durability over the un-doped materials at 566°C and a significant increase at the higher temperature where the effects of the oxygen environment are more pronounced. The fracture surfaces demonstrated brittle behavior at the edges with increased fiber pullout in other areas.

Wothem [2] examined the thermomechanical fatigue (TMF) properties of several ceramic matrix composites, including cross-ply Nicalon-MAS5. It was found that the fatigue life of the material decreased significantly when the TMF

was out of phase as compared to the in phase behavior. In addition, the uni-directional Nicalon-MAS5 specimens tested exhibited twice the fatigue life at a given loading condition implying the failure of the material was dominated by the fibers. Post-mortem analysis of the fracture surfaces showed brittle behavior at the edges with fiber pullout increasing toward the center. The area of brittle fracture increased with the out of phase TMF showing an increased effect of the environment or oxygen embrittlement. This brittle behavior at high temperatures was also experienced with the Nicalon-CAS material tested by Allen [5].

Headinger [6,7] tested an enhanced SiC-SiC material at 1100°C using three different wave-forms: triangular with a frequency of 0.5 hertz, trapezoidal with a loading frequency of 0.5 hertz with hold times of two and four seconds. It was discovered that the fatigue life of the material was inversely related to the hold time of the wave-form. Also, the time at maximum stress was applied as a normalization to the data. This tended to collapse the data to one curve indicating that the fatigue life is a strong function of the time at maximum stress.

The Nicalon-MAS5 [2,3,10], Nicalon-CAS [5,8] and SiC-SiC [6,7] systems are all high temperature CMCs that have a history of stress rupture and cyclic fatigue tests at elevated temperature. The Nicalon-CAS system has similar physical properties from the standpoint of matrix porosity and modulus. Although the SiC-SiC system has similar mechanical properties, the matrix porosity is much higher. The fact that the trend of similar and dissimilar CMCs tends to be the

same when comparing stress rupture and cyclic fatigue life implies that a common mechanism exists.

The aforementioned testing indicates the following trends: first, the fatigue life of ceramic matrix composites decreases with increasing stress and temperature. Second, the introduction of stress rupture components into the wave-form decreases the number of cycles to failure while the *time* under stress remains fairly constant to the point of failure. Third, the predominant failure mechanism is brittle behavior and subsequent micro-cracking caused by oxygen embrittlement.

B. Models and Predictions

Researchers have proposed two models for the prediction of modulus degradation due to cyclic fatigue [8]. One model was based on the experimental determination of matrix crack density compared to the modulus degradation. A linear function was developed that predicted the change in material modulus as a function of matrix crack density. Also proposed was a logarithmic correlation given by:

$$E/E_0 = A + B \text{ Log}(t \text{ or } N), \qquad (2)$$

where A is a constant and B is the slope of the line defined by plotting the normalized Young's modulus versus the log of the number of cycles. The model

accurately predicted the extent of modulus degradation with the limitation that it not be applied to cases where there is significant damage on the first loading cycle. Both models were based on experimental observations from Nicalon-CAS specimens.

Because the failure mechanisms in both Nicalon-MAS5 and Nicalon-CAS are similar, this model may be accurate for both materials. In addition, the parameter of time in the equation implies that the model may be used for the combined loading case since the failure of SiC-SiC was found to be a function of time at maximum stress.

III. Experimental Procedure

The set-up consisted of a servo-hydraulic test machine with water-cooled grips; a controller; heat lamps (each consisting of a water/air-cooled aluminum housing with four single filament quartz bulbs--each rated at 1 KW); thermocouple driven temperature controllers (each controlling one pair of bulbs); connections to centralized cooling water, compressed air and hydraulics; a PC running MATE, written by George Hartman of the University of Dayton Research Institute, controlling the data acquisition. This equipment applied the triangular wave-forms (with and without hold times) at elevated temperatures up to 1100°C and was used throughout the study.

A. Test Station

An MTS model 244.12 was used for all the material tests controlled by a model 458.20 controller. The configuration was somewhat unique and warrants mention. First, since the tests were conducted at elevated temperatures, the machine is oriented horizontally to relieve the heat load on the grips. Second, the cooled heat lamps were held in position by a jig fabricated in the AFIT machine shop. The Sylvania quartz heat lamps were rated for 1000 Watts. For even heating, a set of lamps were used--one on each side of the specimen with two active bulbs. Figure 2 illustrates the test station layout.

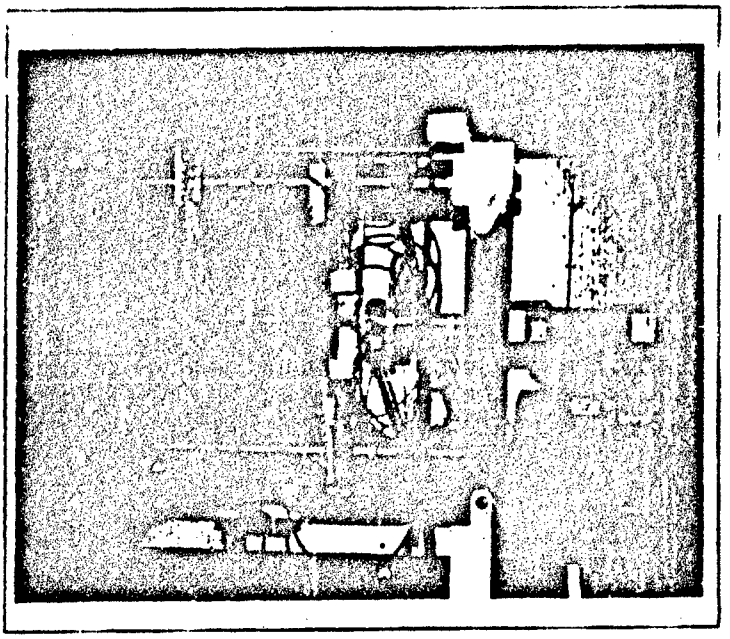

Figure 2. Test Station.

The tests were controlled by MTS proprietary software designed for the servohydraulic tester using a personal computer (PC), a 486 DX2. Approximately 1000 data points were acquired per data acquisition cycle. Strain data were acquired through the use of a MTS model 632.53E14 extensometer. The standard quartz extensometer rods were replaced with longer units to provide protection from the elevated temperatures of the test volume. The extensometer was calibrated at a gauge length of 1.27 cm.

B. Test Station Alignment

The alignment was performed to ensure that each test specimen would be subjected to an axial load without any bending or torsional components. The test

station was aligned using a square cross-section aluminum calibration specimen instrumented with eight strain gauges-two per side. These were configured such that all bending modes could be detected. After verifying the condition of the un-installed calibration specimen by noting that all the strains were negligible (that is, not bent or damaged), it was installed in the tester and aligned. The grips were then adjusted until all the strains in the calibration specimen were within 100 microstrains. At this point, the test station was assumed to be aligned.

C. Material Description

SiC-MAS5 is in an emerging class of glass ceramic materials with weak fiber/matrix bond. This type of bond is desirable from the standpoint that the weekly bonded fibers will tend to bridge matrix microcracks arresting their progression. The fibers are manufactured by Nippon Carbon Company under the brand name Nicalon. The fibers are made of amorphous silicon carbide and are approximately 15 μm in diameter. The matrix is made of 5% BSG doped magnesium alumino-silicate (hence the name SiC-MAS5). The addition of this dopant improves the durability of the composite material in oxidizing environments at elevated temperatures. Table 1 contains the material properties of the SiC-MAS5 composite.

Table 1: Properties of SiC-MAS5.

Room Temperature Properties of SiC-MAS5	
E_f	200 GPa
V_f	0.39
ν_f	0.25
α_f	$4x10^{-6}$
E_m	138 GPa
ν_m	0.25
α_m	$2.4x10^{-6}$
Porosity	~1%

Note: E=modulus of elasticity, V=volume fraction, ν=Poisson's ratio, α=coefficient of thermal expansion, subscripts f and m are fiber and matrix, respectivcly

D. Specimen Preparation

The SiC-MAS5 material from Corning was received as a 15X15X0.3 cm (approximate) plate that was sectioned as shown in Figure 3 into thirty 15X0.5X0.3 cm (approximate) specimens before polishing. The specimens were machined by using the Buehler Isomet® radial low speed saw using a diamond blade and Isocut® cutting oil. A guide was fabricated at the AFIT machine shop to ensure that the plate was held squarely in place during the cutting operation. The cutting operation for each specimen began with the machining of three 0.3 cm deep pilot cuts 0.2 inches from the edge of the plate. This technique was used in order to ensure the thin cutting blade did not deviate from parallel to the edge. This eliminated the need for excessive polishing and further ensured the consistency of the specimens. The saw is shown in Figure 4. The final dimensions of the specimens are listed in Table 2.

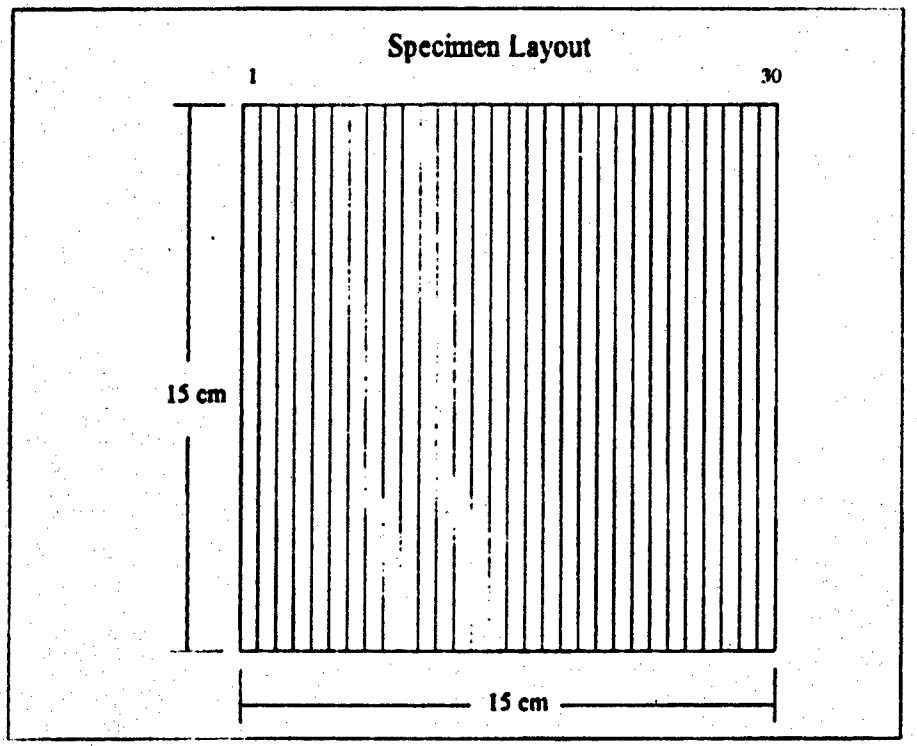

Figure 3. Specimen Layout on Master Plate

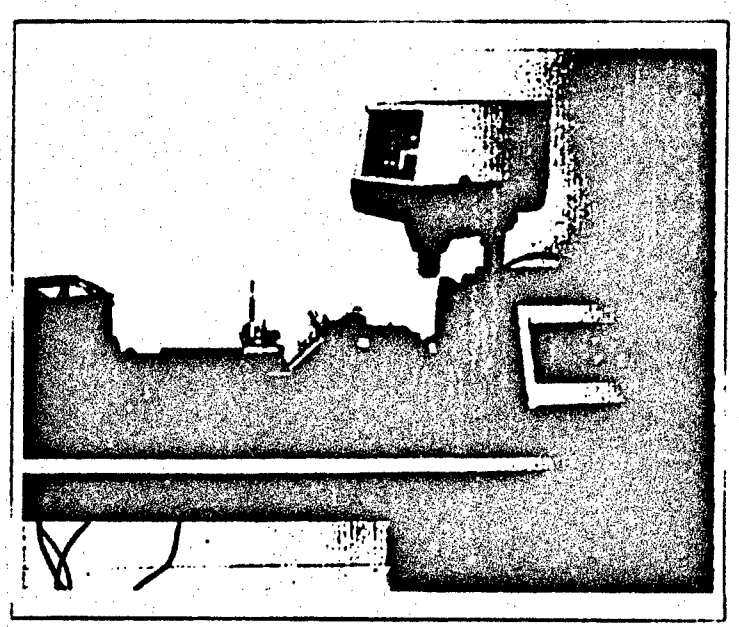

Figure 4. Low Speed Saw (middle).

Table 2: Specimen Dimensions.

Specimen Number	Length (cm)	Width (cm)	Thickness (cm)	Cross-sectional Area (cm^2)
24	15	0.447	0.320	0.1430
7	15	0.463	0.320	0.1482
23	15	0.409	0.320	0.1309
30	15	0.479	0.320	0.1533
25	15	0.466	0.320	0.1491
27	15	0.461	0.320	0.1475
26	15	0.461	0.320	0.1475
2	15	0.431	0.320	0.1379
13	15	0.408	0.320	0.1306
17	15	0.462	0.320	0.1478
19	15	0.445	0.320	0.1424
21	15	0.462	0.320	0.1478
15	15	0.465	0.320	0.1488
16	15	0.461	0.320	0.1475
20	15	0.451	0.320	0.1443
28	15	0.449	0.320	0.1437

Specimen preparation started with the removal of the initial blemishes along the machined edge caused by the cutting process, followed by a finish polishing with successively finer grinding compounds until a finish suitable for replicating was obtained. A Texmet® pad with Metadi® 45 micron diamond suspension fluid combined with fluid extender was used for the initial removal of edge roughness. This initial smoothing continued until microscopic inspection revealed a consistent surface. The process continued with Metadi® 9, 3, and finally 1 micron fluid combined with fluid extender on an Texmet® polishing cloth. Successively finer grades of fluid were applied when microscopic inspection revealed a consistent surface. The last step in the preparation of each specimen

was the installation of ductile aluminum tabs using heat resistant epoxy at the tensile tester grip locations. This prevented damage to the brittle material due to the gripping operation. The polisher is shown in Figure 5.

E. Experimental Procedure

Each test followed a standardized procedure that involved the installation of the specimen in the tester, installation of the thermocouples, zeroing of the extensometer, ramping to temperature, measurement of the initial modulus, and initiation of the test regimen.

Specimen installation consisted of three steps: alignment, gripping, and stress zeroing. Alignment consisted of ensuring that the entire aluminum pad was within the jaws of the grip and using a fabricated gauge to manually locate each end of the specimen at equal positions laterally within the grip. At this point, the left (fixed) grip was closed. Because of the brittle nature of SiC-MAS5, the grip pressure was kept at about 3.5 MPa. This pressure was arrived at through some trial and error and represented the pressure that would slightly deform the ductile aluminum pads and no more. The data confirmed that this pressure was sufficient to prevent the specimen from slipping during the sometimes lengthy tests that followed. In addition, all the specimens failed far from the aluminum tabs indicating that the grip pressure caused no significant pre-test damage. Next, the high pressure hydraulic system was brought to operating temperature by applying the triangle wave output of a function generator to the displacement controller for

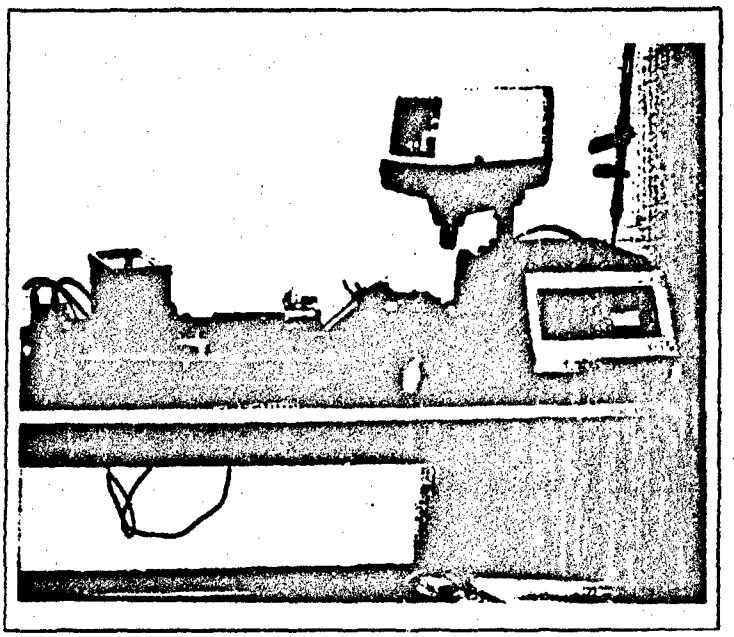

Figure 5. Specimen Polisher (right).

a period of five minutes. After the warm-up was complete, control was transferred to the load controller and the right (actuated) grip closed. The load was then manually zeroed. The specimen was now ready for the installation of the thermocouples.

The type K (chromel-Alumel) thermocouples were installed in the middle on both sides of the specimen held in place with silica adhesive applied to the thermocouple weld region. The installation was such that each thermocouple controlled two quartz bulbs in a heat lamp on the opposite side of the specimen. In addition, the bulbs were mounted in a staggered configuration in order that the specimen be heated evenly across the width of the heat lamps (approximately

7.6 cm). The curing of the silica adhesive occurred at 150° C for a period of two hours.

The extensometer was then zeroed manually at a gauge length of 1.27 cm on the edge of the specimen at room temperature with the thermocouple approximately in the center of the quarts rods. The pressure on the extensometer rods was the minimum required to hold them in place on the specimen. The specimen was then brought to the test temperature.

The process of ramping up to the test temperature was accomplished in the same manner for both the 566 and 1093° C. First, the thermocouples were checked by verifying that both indicated room temperature (about 27 °C) and were within about one or two degrees of each other. Then the specimen was heated at a constant rate of approximately three degrees per second. After the test temperature was reached, it was allowed to stabilize for about five minutes before the load was applied. A certain amount of thermal strain was introduced at each test temperature--0.00070 at 566°C and 0.00140 at 1093°C. These values were verified before the start of each test to confirm that the extensometer rods had not slipped. Figure 6 shows a specimen installed in the servohydraulic tester.

The initial cycle of all tests was applied manually through the use of the BETASTAT program, written by Brian Sanders, an AFIT PhD student. In a fashion similar to the MATE program, BETASTAT collected stress versus strain data. The use of this program was not redundant. Because of the initial workload on the computer during the start of the test, the first data acquisition cycle was not

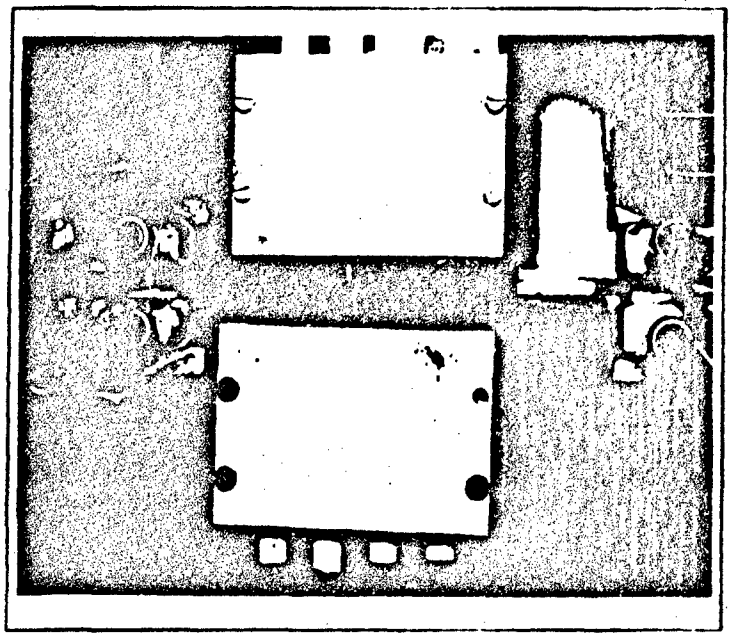

Figure 6. Specimen Installation.

accomplished until the third loading cycle at best. This was not acceptable as the analysis required the initial (undamaged) modulus of the specimen. Since a large amount of damage occurs during the first loading cycle, the use of BETASTAT was essential. First, the load was calculated based on the stress level desired for the particular test and the specimen cross section (unique after polishing). Then the heated specimen was brought to the maximum load manually by the operator via the controller. The rate of load application for varied slightly from test to test but was approximately 0.05 Hz.

To initiate the remainder of the test, necessary data (specimen dimensions, requested data acquisition cycle, maximum stress, hold time, etc.) was entered into the MATE program in an interactive fashion. Subsequent cycles were initiated by

the PC via the controller. Displacement limits were entered into the controller so that at the time of specimen failure, the hydraulic systems in the servohydraulic tester would shut down preventing other than cyclic damage to the specimen caused by excessive grip displacement.

IV. Results and Discussion

This study was carried out to identify the relationship between an elevated temperature environment, stress rupture loading, cyclic fatigue, and how each contributes to the failure of the ceramic matrix composite, SiC-MAS5. This was accomplished through the use of S-N (stress versus cycles to failure), S-T (stress versus exposure duration), S-S*T (stress versus total area under the cycling curve to the point of failure), modulus degradation, stress-strain loop hysteretic energy, stress-strain, and minimum/maximum strain curves.

The data used to construct the modulus degradation and stress-strain loop hysteretic energy curves were smoothed as much as possible based on the envelope of the raw data in order to reflect the pertinent trends. Also, any extensometer slippage will be reflected in the raw strain data from the extensometer and, if necessary, applied to the reduced data to reflect the true trends. These envelope plots are included in Appendix B for the reader to refer. The data from the 1093°C/138 MPa/100 second hold test is absent from all but the fatigue life plots. This is due to the test completing before a single cycle could be completed, i.e. the specimen failed during the first cycle. In addition, some of the other high temperature tests terminated in rapid fashion, resulting in only one or two cycles of data acquisition. Finally, a post-mortem Scanning Electron Microscope (SEM) analysis of the fractured surface and an optical microscopic survey of the polished edge were conducted. The results of this examination were

compared to the mechanical behavior. This required a total of sixteen load controlled tests shared between two elevated temperatures. Table 3 summarizes the test matrix and the number of cycles at failure for each specimen.

First, fatigue tests without any hold time were conducted at both temperatures. Then the remaining fourteen tests were conducted--seven at each temperature. The rate of load application varied with the maximum stress achieved which was 207 MPa/s for the 103 MPa tests and 276 MPa/s for the 138 MPa tests. The initial modulus at 566 and 1093°C was obtained by Steiner [9] and was found to be 117 and 97 GPa, respectively. This compares well with the monotonic tensile data presented by Larsen [3]. Based on the initial modulus at 566°C, the initial strain rates were approximately 0.00088/s and 0.00110/s to a maximum stress of 103 and 138 MPa, respectively. At 1093°C, the initial strain rates were approximately 0.0010/s and 0.00130/s to a maximum stress of 103 and 138 MPa, respectively. Loading and unloading were accomplished at a one hertz rate. The R value (ratio of maximum stress to minimum stress or $\sigma_{max}/\sigma_{min}$) was 0.1 for all tests.

A. Fatigue Life Diagrams

The fatigue data for tests at both elevated temperatures was compiled in several ways. First, S-N curves were created to get an initial comparison of the trends formed by the variation of stress and wave-form. Table 4 contains a summary of the results.

Table 3: Summary of Test Results: Cycles at Failure.

Specimen Number	Test Temperature (°C)	Hold Time (s)	Maximum Stress (MPa)	Cycles to Failure	Fracture Location (from center, mm)
24	566	0	103	425,299	10
7	566	1	103	101,834	5
23	566	10	103	91,739	6
30	566	100	103	5,135	6
25	566	0	138	1,156	0
27	566	1	138	1,195	4
26	566	10	138	265	6
2	566	100	138	14	25
13	1093	0	103	20,237	30
17	1093	1	103	6,017	30
19	1093	10	103	216	32
21	1093	100	103	10	28
15	1093	0	138	32	21
16	1093	1	138	18	20
20	1093	10	138	11	20
29	1093	100	138	***	21

*** Less than one cycle

At 566°C, the data followed the trend that the number of cycles completed at failure varied inversely with hold time. The maximum number of cycles completed at this temperature was 425,299 and occurred at a stress and hold time of 103 MPa and 0 seconds, respectively. The minimum of 14 cycles occurred at a stress and hold time of 138 MPa and 100 seconds, respectively.

At 1093 °C, the trend was the same. The maximum number of cycles was 20,237 and occurred at a stress and hold time of 103 MPa and 0 seconds, respectively. The minimum was less than one cycle, lasting approximately 60 seconds into the 100 second hold segment of the first cycle (for the purposes of

Table 4: Summary of Test Results: Exposure Duration.

Stress (MPa)	Temperature (°C)	Hold Time (s)	Cycles at Failure	Exposure Time (s)	Figure Number Showing Fractured Surface
138	566	0	1156	1156	52,70
138	566	100	14	1414	53,71
138	566	1	1195	2390	54
138	566	10	265	2915	55,80
103	566	1	101834	203700	56
103	566	0	425299	425299	57,68
103	566	100	5135	518635	58,69
103	566	10	91739	1009129	59,79
138	1093	0	32	32	60,74
138	1093	1	18	36	61
138	1093	100	1	101**	62,75
138	1093	10	11	121	63,78
103	1093	100	10	1010	64,73
103	1093	10	216	2376	65,76,77
103	1093	1	6017	12030	66
103	1093	0	20237	20237	67,72

** Less than one cycle

the fatigue life diagrams, this will be considered one cycle). This occurred at a stress level of 138 MPa and a hold time of 100 seconds. When comparing the S-N results between the two temperatures, the number of cycles to failure decreases with increased temperature, holding all other variables constant. Figures 7 and 8 illustrate these trends.

Figure 9 illustrates the effect of hold time at both temperatures. It shows that the effect of hold time is to decrease the number of cycles by the same *factor regardless of the stress or temperature*. This implies a strong dependence on the temperature of the oxidizing environment and will be explored further.

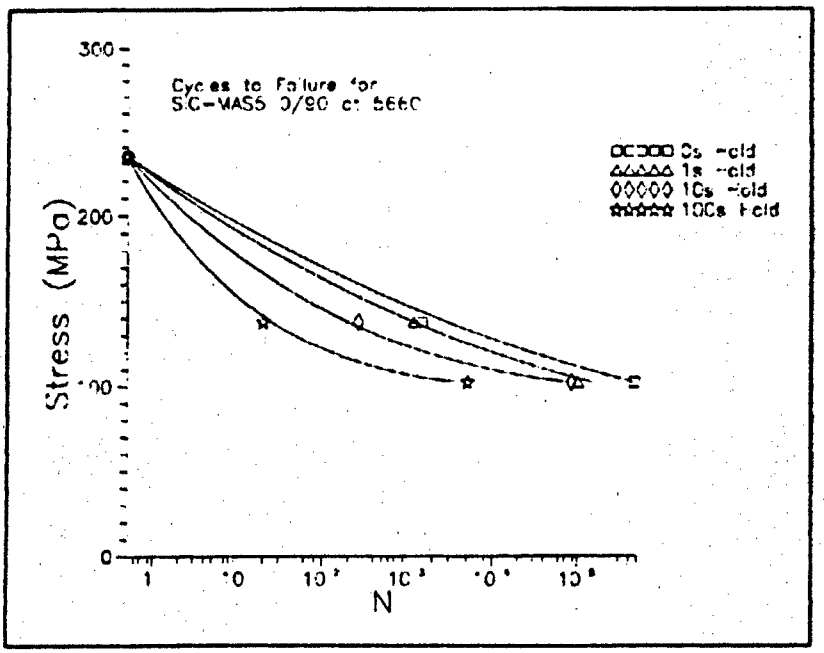

Figure 7. Cycles to Failure at 566°C.

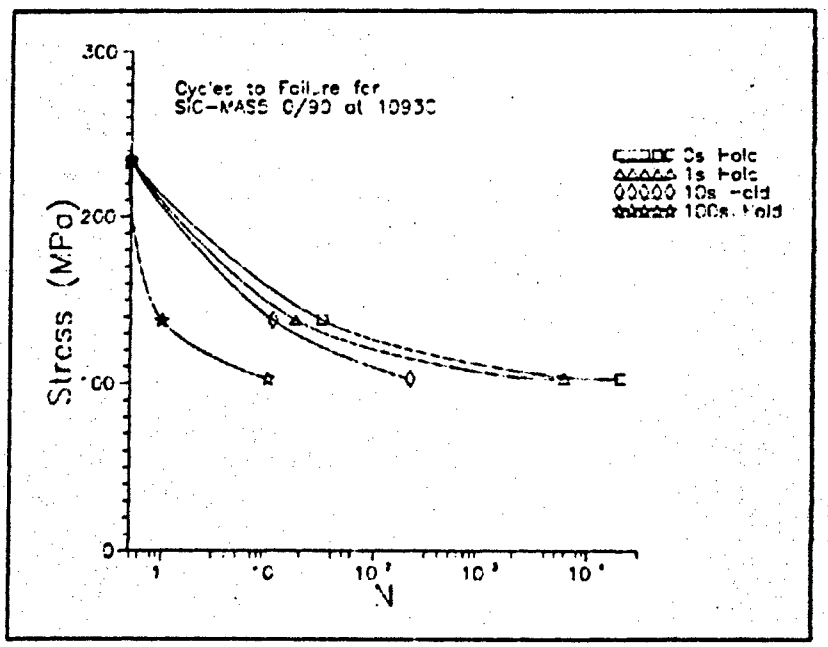

Figure 8. Cycles to Failure at 1093°C.

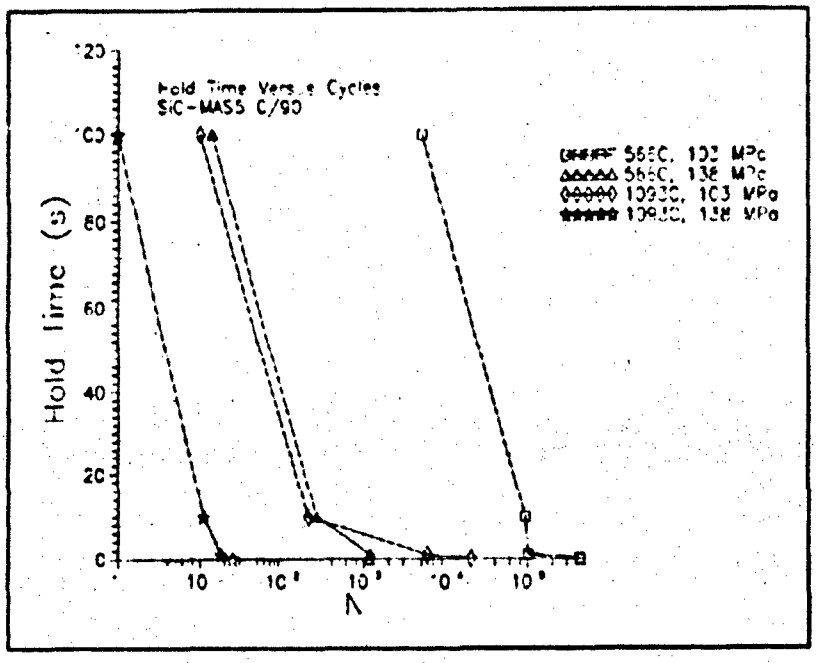

Figure 9. Effect of Hold Time On Life.

Expanding on the results of Figure 9, plots of the specimen stress versus the exposure duration to the high temperature environment were created from the S-N data. In addition to the data from the present study, the stress-rupture data presented by Larsen [3] at 1093°C was also plotted. The exposure duration to the environment was defined as the number of cycles to failure multiplied by the duration per cycle. It was assumed that the exposure began at the start of load application (beyond the minimum specified by the value of R) and ended when the stress returned to the minimum value. For example, if the cycle hold time was one second with a one hertz ramp rate, the total exposure would be two seconds. Figures 10 and 11 illustrate the result of this normalization technique.

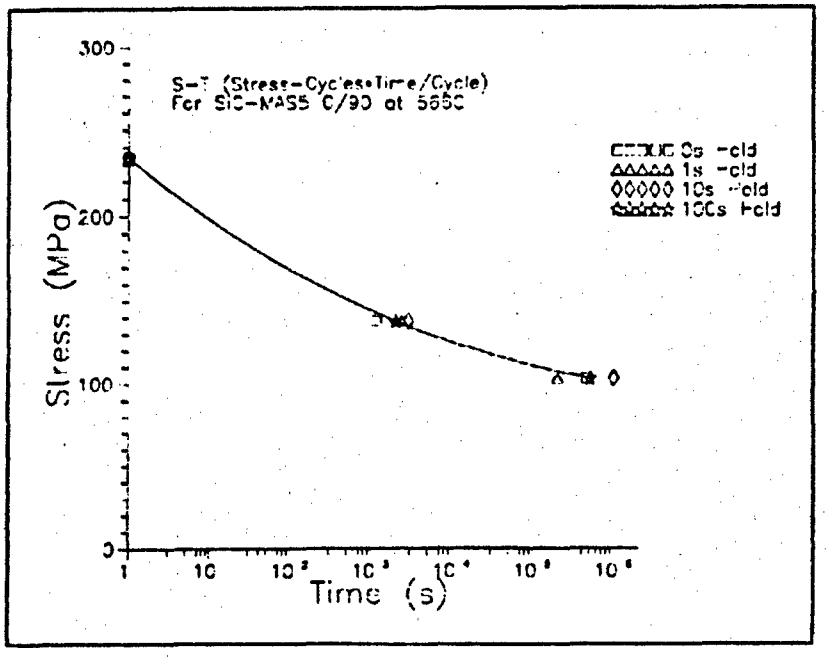

Figure 10. S-T Curves for 566°C.

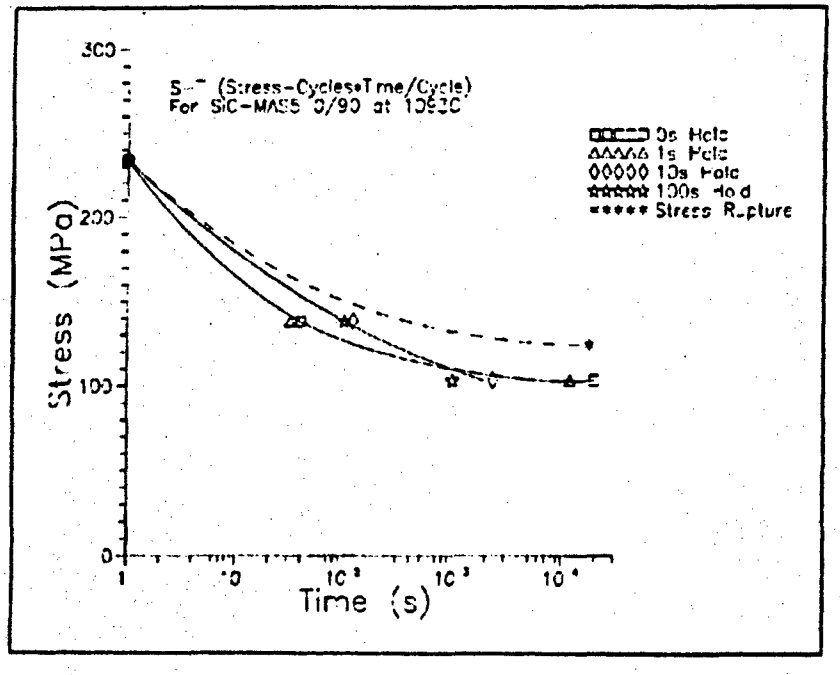

Figure 11. S-T Curves for 1093°C.

At 566°C, the S-T data collapses to within a factor of two--a normal scatter in fatigue experiments. In contrast, the spread in the S-N data is approximately the same at both stresses--two orders of magnitude. This reduction of data spread is caused by the normalization technique, that is, the introduction of the exposure time parameter normalizes the data to account for the effect of the environment. The fatigue life of the material at this temperature is almost totally dependent on the exposure time under stress with a negligible effect from the cyclic fatigue.

At 1093°C, the reduction in spread from the S-N data to the S-T data is not as extensive. In addition, the reduction varies with the stress level with the higher stress experiencing a greater reduction than the lower. This is due to the larger contribution of the cyclic fatigue mechanism at this temperature. At 1093°C, the rate of oxidation is far greater than at 566°C. This coupled with the mechanical interactions at the micro-level will tend to expose new material to the effect of the environment on successive cycles, causing the material to rapidly accumulate damage from the environment. This phenomena is demonstrated by the large data spread at low stress (where the number of cycles is relatively great) and the relative collapse at the higher stress (where the number of cycles is much less).

Another normalization technique applied to the S-N data was the introduction of a parameter defined as the area under the loading wave-form (in units of stress*time) multiplied by the number of cycles to failure. This parameter is a combination of stress level and exposure duration. The data normalized to this parameter is presented in Figures 12 and 13. At both temperatures, the data

from different test conditions did not tend to merge to a single curve, implying that this parameter was not a meaningful normalization method.

The fact that the fatigue life decreases with increasing stress is an expected result of all S-N curves as Figures 7 and 8 show. However, the decrease of cyclic fatigue life with hold time implies the effect of a damage mechanism that is predominantly time dependent. This hypothesis is supported by the collapse of the 566°C data illustrated in Figures 10. But the 1093°C data does not follow this simple relationship. It appears that the fatigue life in the higher temperature case is a function of both the exposure time and cycling. In addition, the stress rupture result [3] appears to be significantly different than that of any of the hold times.

In fact, close examination of Figure 11 will reveal differing regions of contribution from cyclic fatigue and the environment. For example, as the stress increases, the curves tend to collapse as in Figure 10. But as the stress decreases, the effect of the cycling increases, causing the data to spread. In addition, the data in Figure 11 have split into three separate curves--one representing the shortest hold times (0 and 1 second), one representing the longest hold times (10 and 100 seconds), and one representing the pure stress-rupture result. The effect of the cycling is largest at the lowest hold times (as evidenced by a lowering of the curve), while the curve representing the longer hold times is closer to the pure stress-rupture result. This follows logically since the longer hold times contain larger stress-rupture components.

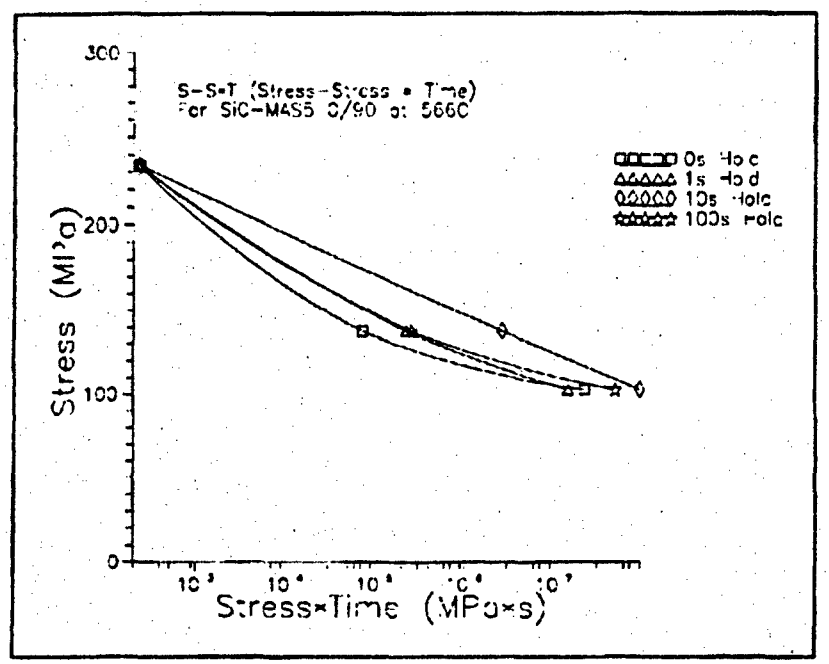

Figure 12. S-S*T Curves for 566°C.

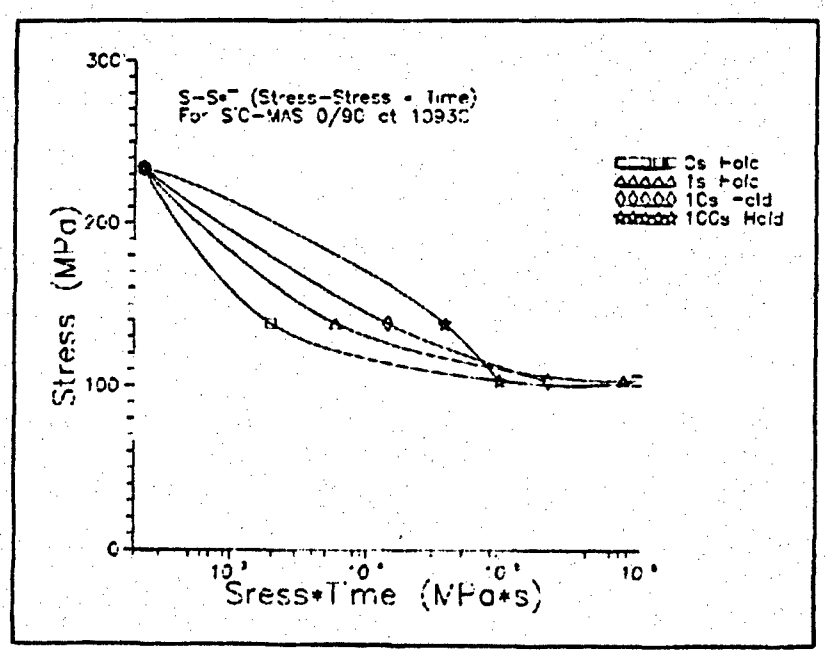

Figure 13. S-S*T Curves for 1093°C.

The data from the pure stress rupture test [3] does not fall on the S-T curve for two reasons. First, the failure of the material must be a function of both the cycling *and* environmental temperature. One mechanism will dominate over the other as the temperature and loading wave-form vary. Second, the rate of oxidation in most materials is not constant. In the absence of flaking, the oxide provides a protective layer that inhibits further oxidation.

It is possible that, in the case of SiC-MAS5, the rate of oxidation follows a logarithmic decay as it progresses in a steady state problem. This would explain why a pure stress rupture specimen will have a longer life than one in which the identical stress level is applied but cycled. The rate of oxidation (or damage) in the stress rupture specimen will slow to nearly zero with time because there will be no additional un-oxidized surface exposed as the test progresses.

In contrast, the specimen experiencing cyclic fatigue will encounter the synergistic effect of oxidation occurring at the fibers and continuing to a much larger extent due to the mechanical action of crack opening and closing resulting in the exposure of un-oxidized surfaces to the environment at the interface. In addition, cycling will cause the crack density to increase over time exceeding that of the stress rupture specimen, and, presumably, provide additional paths for oxidation to occur.

In summary, an increase in the hold time at a constant stress and temperature causes a decrease in the cycles at failure. The damage after initial loading is due to the synergistic effect of the elevated temperature environment

combined with the micro-mechanical interactions caused by the cycling. The extent to which this damage progresses is heavily dependent on the temperature of the environment. At 566°C, the rate of oxidation is low enough so that the synergistic effect of the cycling and oxidation does not occur to a significant extent. At 1093°C, the rate of oxidation is much larger, and the effect of the environment coupled with the cycling has a significant effect on the fatigue life. This effect is proportional to the number of cycles and *decreases* with increasing stress. Finally, the S-S*T normalization illustrated in Figures 12 and 13 resulted in some collapse of the data, but to an insignificant extent. This implied that the normalization technique was not useful and, therefore, was not explored further.

B. Modulus Degradation

The degradation of the modulus during cycling was also plotted to analyze the fatigue behavior. The data was compiled in two ways. First, the normalized modulus was plotted as a function of the number of cycles completed on the log scale. The normalized modulus was defined as the modulus of the material at a particular cycle as shown in Appendix B divided by the initial modulus computed from BETASTAT. Then, an additional normalization was applied to the life of the specimen because of the wide variation in the number of cycles to failure depending on the combination of wave-form and stress applied. The data in this case is plotted as a function of normalized life. The normalized life was defined as the cycle of interest divided by the cycles at failure. The normalized modulus-

normalized life plots were created in order to compare the trends of the moduli from a group of specimens with a wide variation in the number of cycles at failure at statistically meaningful points. But because the largest amount of damage occurs during the first few cycles, the normalized modulus-log cycles plots were created to recover the resolution lost at the beginning of the longer tests by the former method. The technique used to compute the modulus was the secant method and is illustrated in Figure 14.

At 566°C/103 MPa, the rate of modulus degradation (change in normalized modulus/cycle) is dependent on the hold time, i.e. the larger the hold time, the larger the degradation. At 566°C/138 MPa, the modulus is fully degraded by the fourth cycle with less dependence on hold time. In addition, the moduli at the lower stress level tend to degrade over the course of the test, while

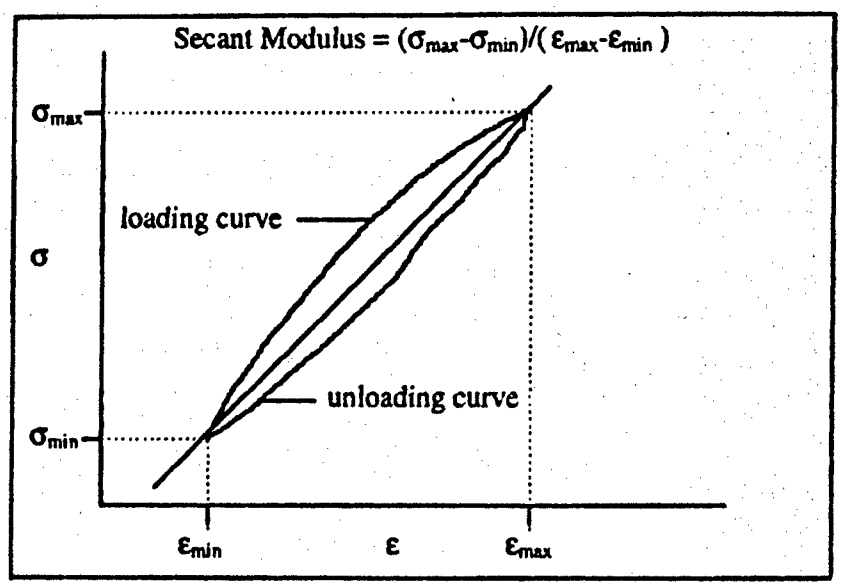

Figure 14. Calculation of Secant Modulus.

the moduli of the 138 MPa tests tend to degrade immediately then stabilize. In all cases, the modulus eventually degrades with hold time, i.e. the longer the hold time, the greater the degradation. These trends are illustrated in Figures 15 and 16.

At 1093°C, the behavior is different in that the lower stress shows a random ordering of rates of modulus degradation. Also, all normalized moduli are within the range of 0.86 to 0.94 after the first few cycles. The higher stress at 1093°C shows the same tendency as the 566°C tests at high stress in that the modulus fully degrades within the first few cycles then stabilizes. In this case, the stabilized value is 0.45 to 0.5. In addition, the low stress tests show an interesting tendency for a modulus recovery as the test progresses. This phenomena was also observed by Harris [4] and is due to the accumulation of debris in the cracks or possibly to changes in the bond strength at the fiber matrix interface. The high temperature modulus degradations are shown in Figures 17 and 18.

Figures 19 and 20 group the aforementioned tests with respect to temperature. Plotted in this way, it can be seen that the data separates into two groupings--those at 103 MPa and those at 138 MPa.

The normalized life plots are shown in Figures 21-26. They clearly show the overall trend of the modulus for a variety of hold times and cycles at failure.

At 566°C, the 103 MPa tests show a definite dependence on hold time as shown in Figure 21. In general, as the hold time increases, the extent of modulus

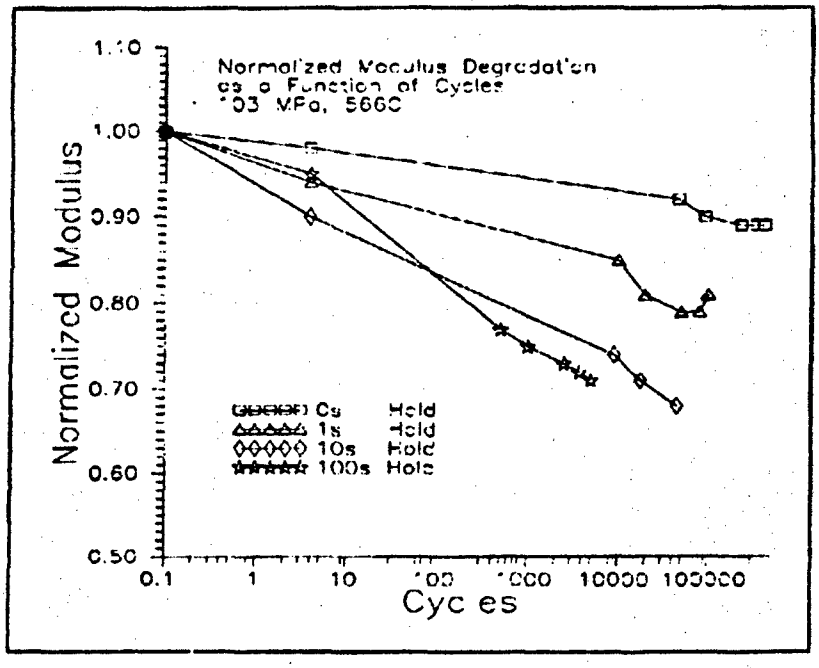

Figure 15. Normalized Modulus Degradation at 566°C, 103 MPa.

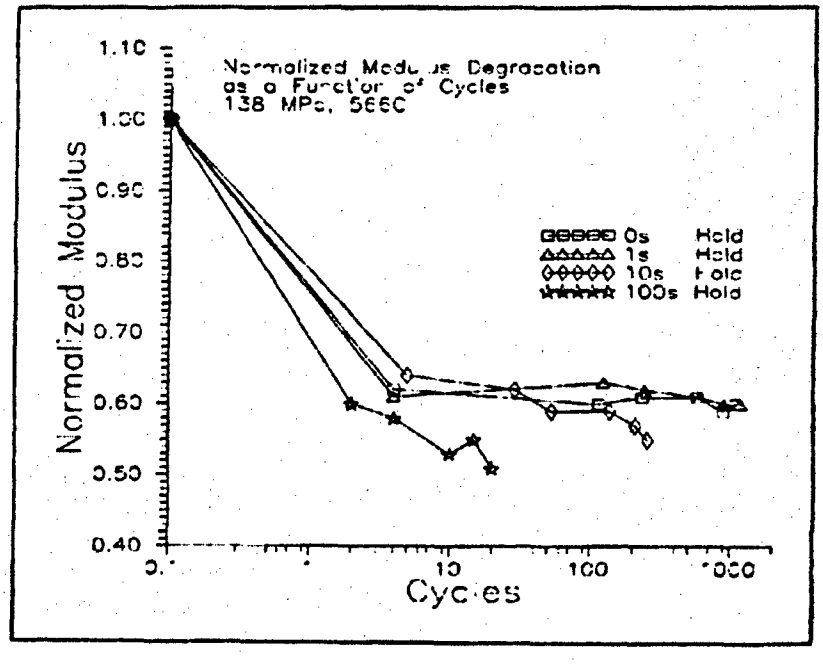

Figure 16. Normalized Modulus Degradation at 566°C, 138 MPa.

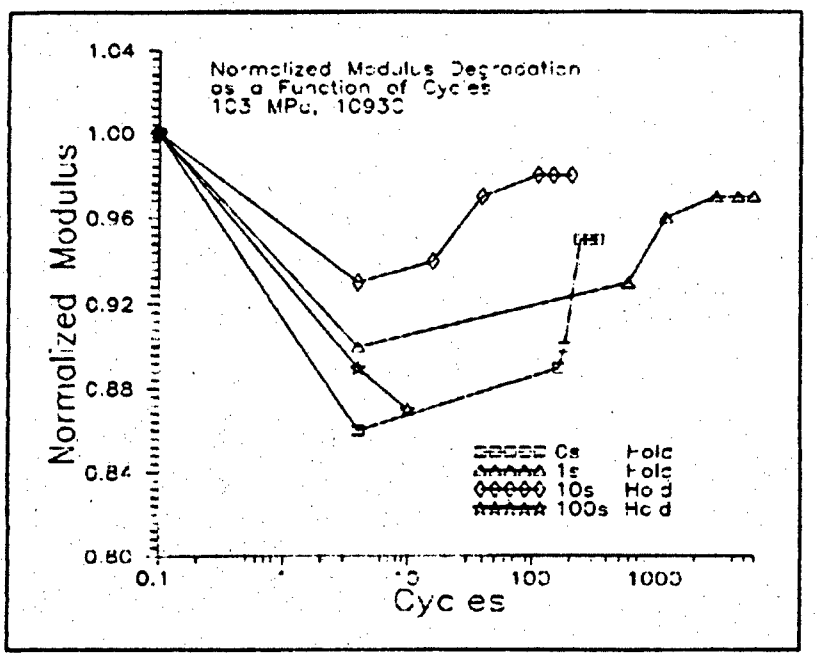

Figure 17. Normalized Modulus Degradation at 1093°C, 103 MPa.

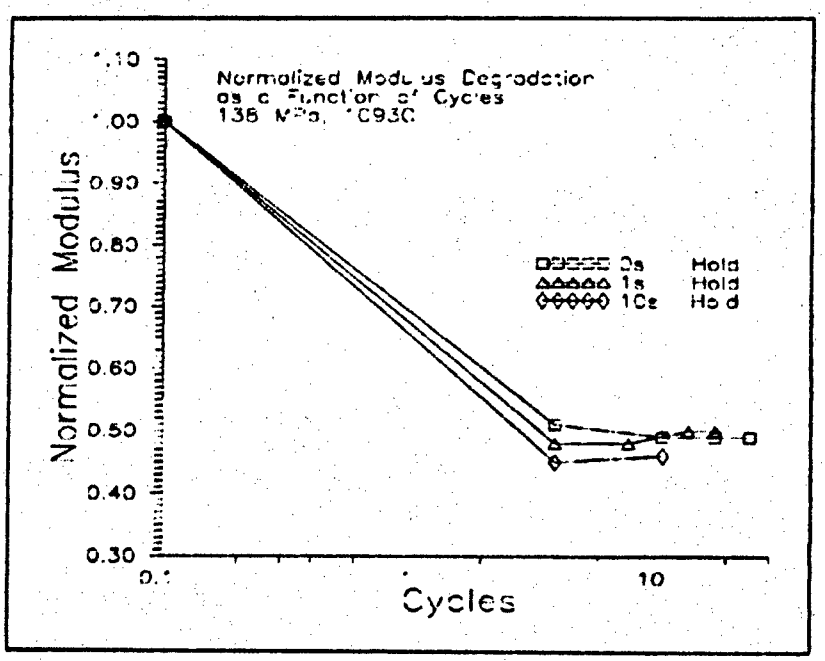

Figure 18. Normalized Modulus Degradation at 1093°C, 138 MPa.

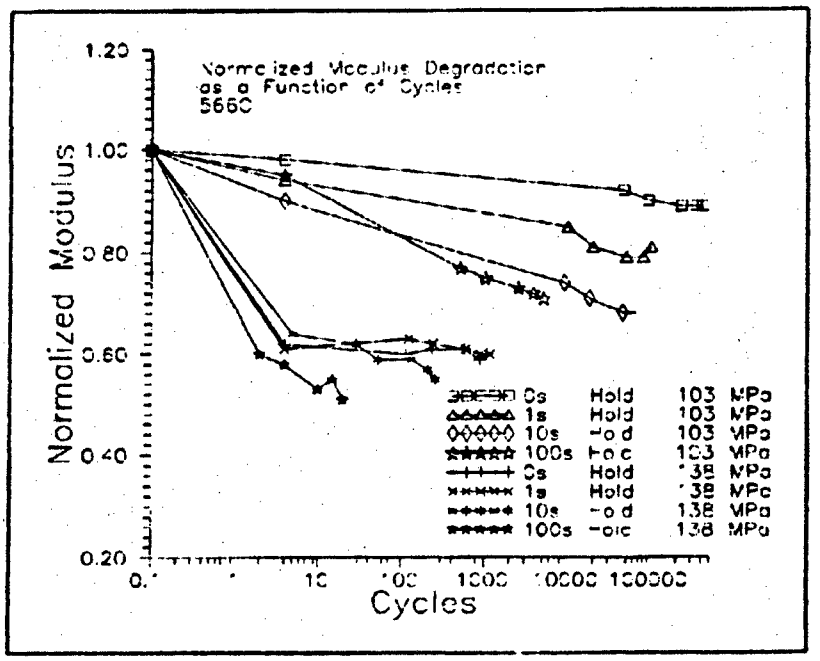

Figure 19. Normalized Modulus Degradation at 566°C.

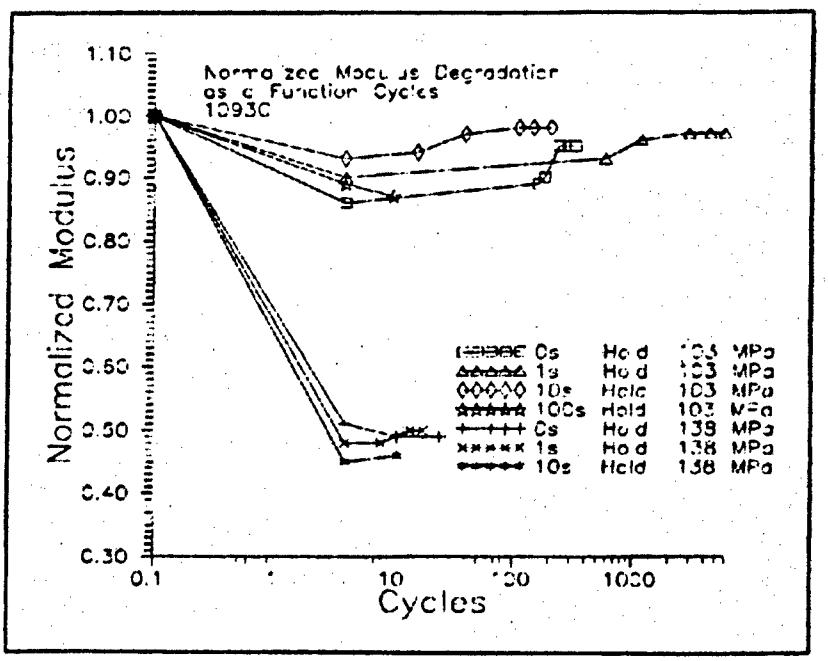

Figure 20. Normalized Modulus Degradation at 1093°C.

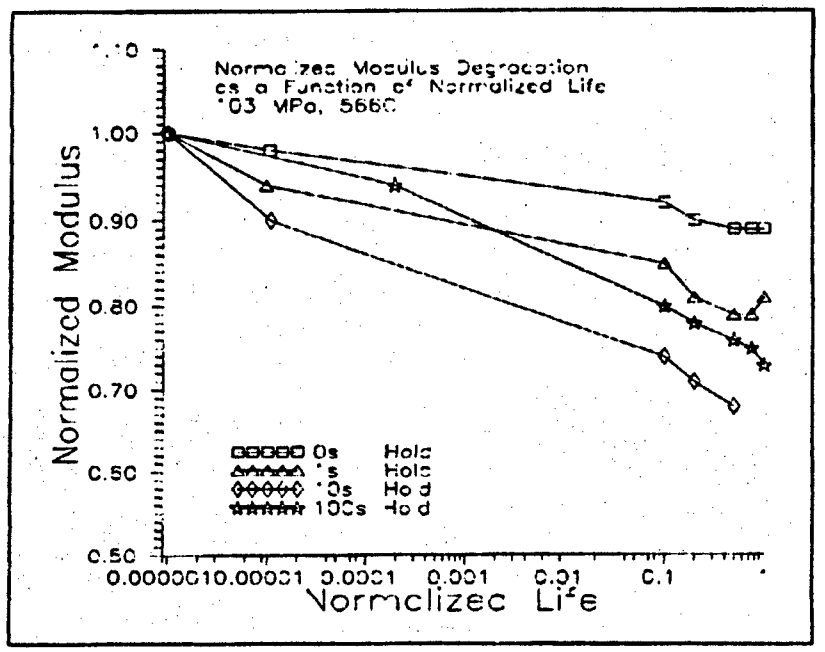

Figure 21. Normalized Modulus Degradation/Life for 566°C, 103 MPa.

degradation also increases. At failure, the normalized moduli for this combination of stress and temperature vary between 0.7 and 0.9. When the stress is increased to 138 MPa, the normalized modulus stabilizes to approximately 0.6 after the first few cycles as shown in Figure 22.

At 1093°C, the 103 MPa tests all show a tendency to recover some of the modulus lost after the first few loading cycles. The normalized moduli of all hold times start within a range of 0.86 to 0.94 and end within the range of 0.94 to 0.98.

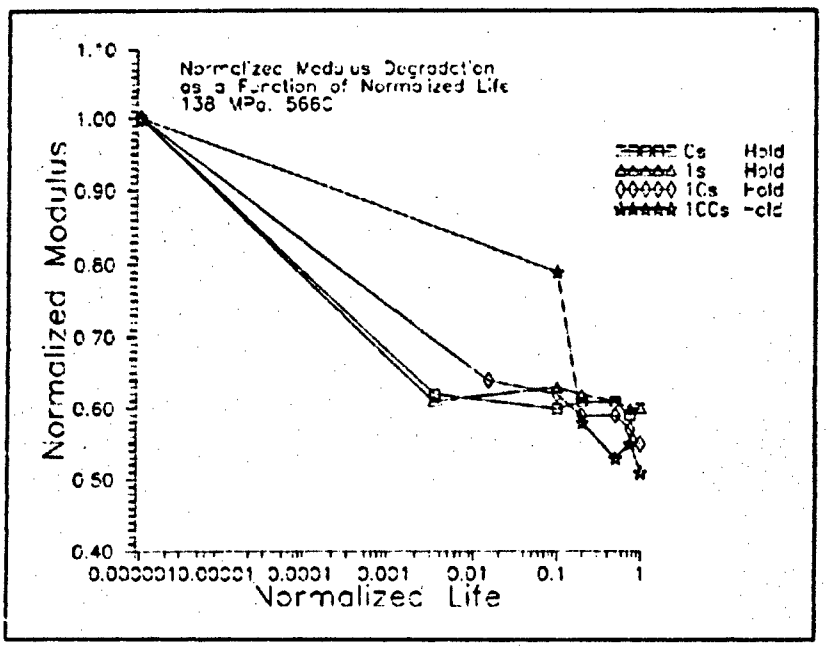

Figure 22. Normalized Modulus Degradation/Life at 566°C, 138 MPa.

Throughout the tests at this temperature and hold time, the moduli are within 6-8% of one another as shown in Figure 23. This small variation implies that the degradation of the modulus under the high temperature/low stress condition is not a function of hold time. However, the longest hold time of 100 seconds did correspond to the largest modulus decrease. At the higher stress, all normalized moduli fall within the first few cycles to 0.45 to 0.5. Again, as in the low temperature case, the stabilized value of normalized modulus is not dependent

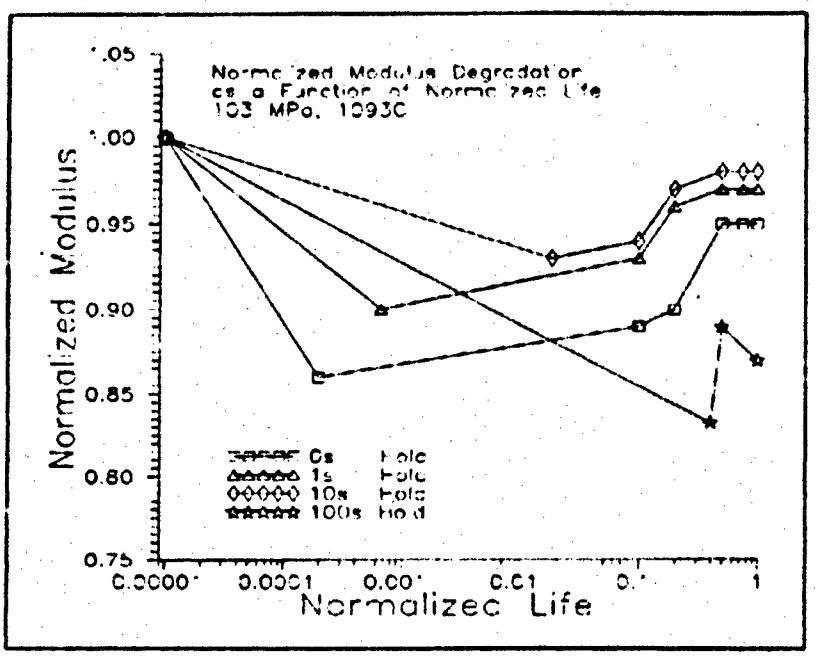

Figure 23. Normalized Modulus Degradation/Life at 1093°C, 103 MPa.

on the hold time. Figure 24 illustrates the trends at this combination of temperature and stress.

When grouped according to temperature, the data clearly shows that the effect of hold time is significant only at the low temperature, low stress condition. All other loading conditions show a minimal dependence on hold time. These trends are shown in Figures 25 and 26.

The differing extent to which the S-T data collapsed at 566°C as compared to 1093°C (as shown in Figures 10 and 11) combined with the dependence of modulus degradation on hold time at low stress implies a combined effect from the cycling and the environment. This differs from the 138 MPa behavior in

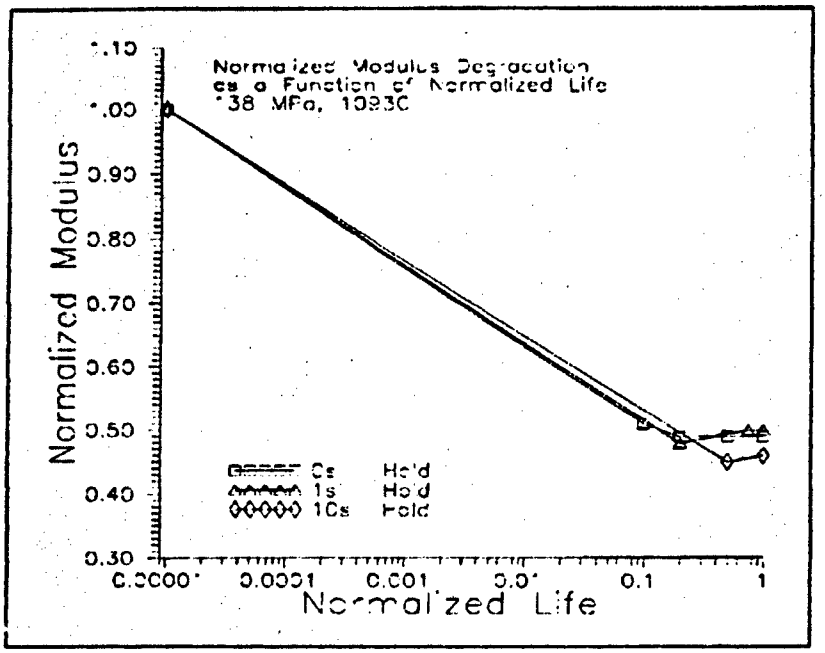

Figure 24. Normalized Modulus Degradation/Life at 1093°C, 138 MPa.

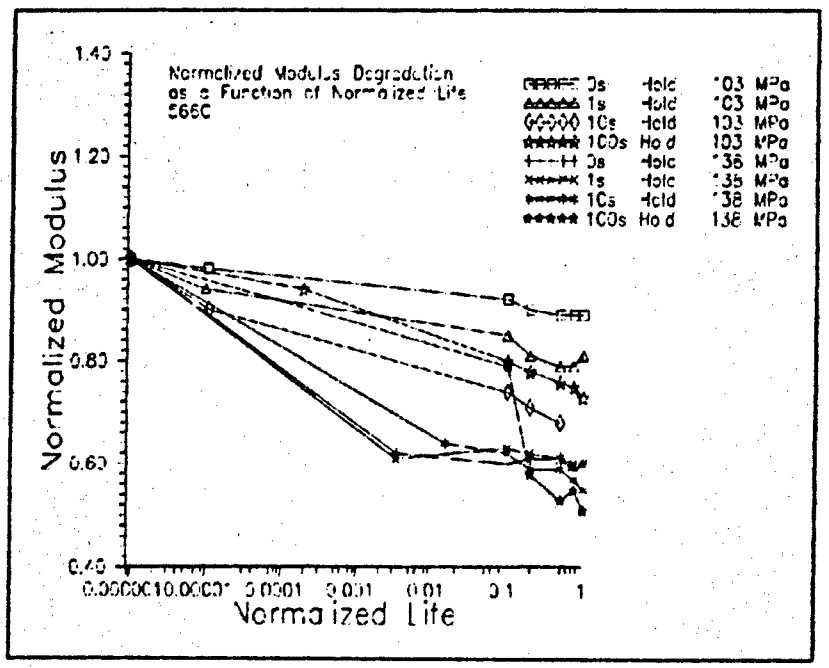

Figure 25. Normalized Modulus Degradation/Life at 566°C.

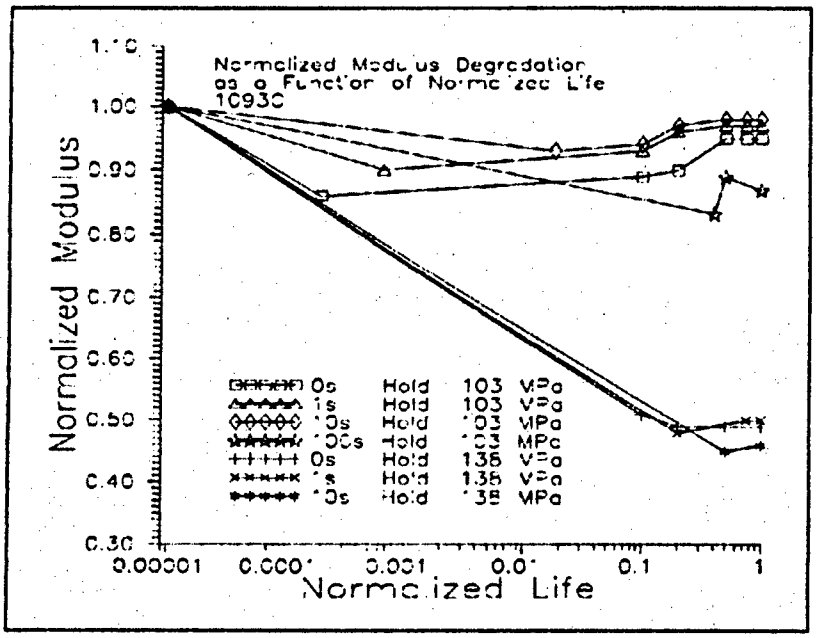

Figure 26. Normalized Modulus Degradation/Life at 1093°C.

that at this higher stress level, the initial damage occurs almost immediately (as evidenced by a large drop in normalized modulus within the first few cycles). The normalized modulus then stabilizes at this degraded value until the point of failure. The initial modulus degradation at the higher stress is consistent with the limiting value predicted by the total discount method assuming the 90° plies have failed. The modulus of the undamaged composite is given by

$$E=l/n*E_L+m/n*E_T. \qquad (3)$$

where E is the modulus of the composite; E_L and E_T are the longitudinal and transverse moduli of the laminae, respectively; n, m, and l are the total number of

plies, the number of plies with fibers running in a direction transverse to the load, and the number of plies with fibers running in a direction parallel to the load, respectively. When the 90° fibers have failed totally, the second term is equal to zero and,

$$E=l/n*E_L \qquad (4)$$

In addition, after the density of cracks has saturated, or reached a maximum, the majority of the load will be supported by the fibers and,

$$E=l/n*E_f \qquad (5)$$

Where E_f is the modulus of the fibers. In this case, the modulus for the $[0/90]_{2S}$ material will become approximately V_f*E_f, where V_f is the volume fraction of the fibers, or 80 GPa. This represents a normalized modulus of 0.4 at room temperature. Assuming the normalized value remains the same at elevated temperatures, this is in line with the experimental observations when one considers that the total discount method assumes all the transverse fibers have failed--definitely the case when the stress level is beyond the "knee" in the stress-strain curve. The "knee" is defined as the stress level on the monotonic tensile curve where the slope (modulus) instantaneously decreases due to the failure of the 90° plies. Also, the contribution from the matrix in the longitudinal plies will vary based on the crack density which is a function of the stress. The 0.4 value

represents a "worst case" that is approached by the stabilized modulus of the high temperature/high stress tests. Based on the monotonic tensile tests conducted by Larsen (4), the major 'knee" occurs at 110 MPa at 566°C and 83 MPa at 1093°C. This compares well with the experimental observations in that at 1093°C the difference in modulus degradation between the two stress levels is more pronounced than at 566°C.

In summary, the effect of hold time is to increase the rate and extent of modulus degradation at the low temperature/low stress condition. This implies an environmental effect that dominates over the effect of the cycling and is reinforced by the collapse of the S-T data in Figure 10. The rate is also dependent on the relationship between the location of the "knee" in the monotonic tensile curve and the maximum stress. Loading to a stress level beyond this point in the curve will result in the vast majority of the damage occurring in the first few cycles. After that, the fatigue life is dependent on the effect of the environment as illustrated by the collapse of the S-T data in Figures 10 and (at the high stress only) Figure 11. In addition, an increase in temperature generally caused an increase in the rate and extent of modulus degradation and was probably due to the lower "knee" stress. The long term, high temperature tests tended to experience an increase in modulus after the initial decrease. This was possibly due to an accumulation of debris in the matrix cracks [4] combined with the oxidation and subsequent stiffening of the carbon fiber/matrix interface [10]. The combination of a relatively large number of cycles combined with the high rate of

oxidation caused a synergistic effect to occur that tended to spread the high temperature/low stress data on the S-T curve as shown in Figure 11. The most severe test conditions resulted in a stabilized modulus value in line with the prediction based on the transverse fibers being totally discounted and the matrix saturated with cracks.

C. Loop Hysteretic Energy

The stress-strain loop hysteretic energy was also plotted as a function of the percentage of the test completed. This parameter is equal to the area traced by the loading and unloading curves (in units of stress) and is indicative of the extent of damage the material is sustaining on a per cycle basis.

First, the results were examined on the basis of temperature. At 566°C, 103 MPa, the data is rather random, but all are within 20% of an approximate mean of 1.35 KPa. At 138 MPa, the trend becomes less ambiguous with the longest and shortest hold times resulting in the greatest and least loop hysteretic energy, respectively. These trends are shown in Figure 27. This falls in line with the observations of the moduli reductions. The 103 MPa modulus reductions were small and within 10% of an approximate normalized modulus of 0.9 while the 138 MPa reductions were far greater at a normalized modulus of approximately 0.6. In fact, the 33% increase in stress from 103 MPa to 138 MPa resulted in an increase of approximately 500% in the value of loop hysteretic energy and a degradation increase of 50% at a given normalized life.

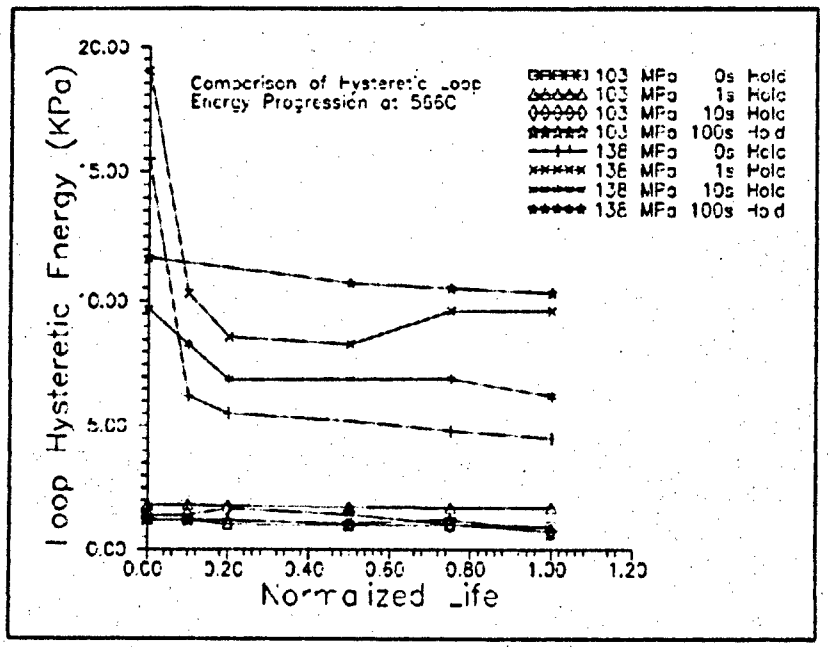

Figure 27. Loop Hysteretic Energy at 566°C.

At 1093°C, the trend continued as shown in Figure 28 with the difference in loop hysteretic energy between the two stress levels increasing to a factor of 10.

This disproportionate behavior between the increase in stress and the increase in loop hysteretic energy is due to the extent of cracking and damage in the matrix. At the lower stress level, transverse matrix cracks have just begun to form with the associated decrease in modulus, while at the higher stress, the damage to the 90° fibers has progressed to the point they can be reasonably discounted and provide no contribution to the strength of the material. This is to be expected since, at the higher temperature, 103 MPa falls right at the "knee" with 138 MPa well into the range where the transverse fibers have failed. At 566°C, 103 MPa falls below the point where extensive damage to the transverse

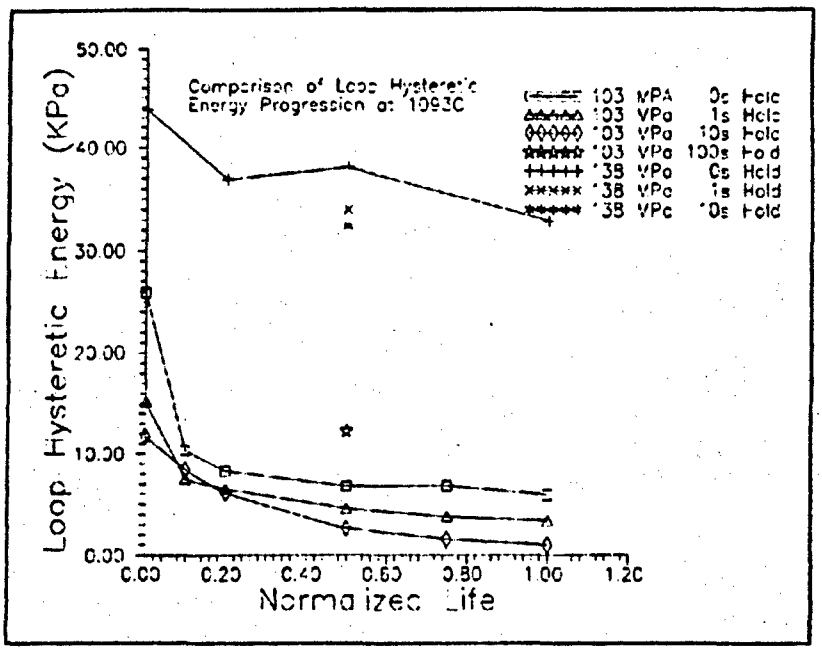

Figure 28. Loop Hysteretic Energy at 1093°C.

plies will occur (although some cracking will probably take place) while at the higher temperature, 103 MPa is right at this critical point. Figures 29 and 30 illustrate the 566°C, 103 MPa and 566°C, 138 MPa trends, respectively. Figures 31 and 32 extend this to 1093°C.

The loop hysteretic energy plots follow the trends of the modulus in that the vast majority of the damage, or the highest energy, occurs during the initial cycles of the test at the high temperature and stabilizes as the test progresses. Unlike some of the modulus plots, there is no tendency for increase toward the end of the test. This makes sense when one considers that the effect of oxidation may be to increase the modulus, and this increase will tend to diminish the area between the loading and unloading curves decreasing the hysteretic loop energy.

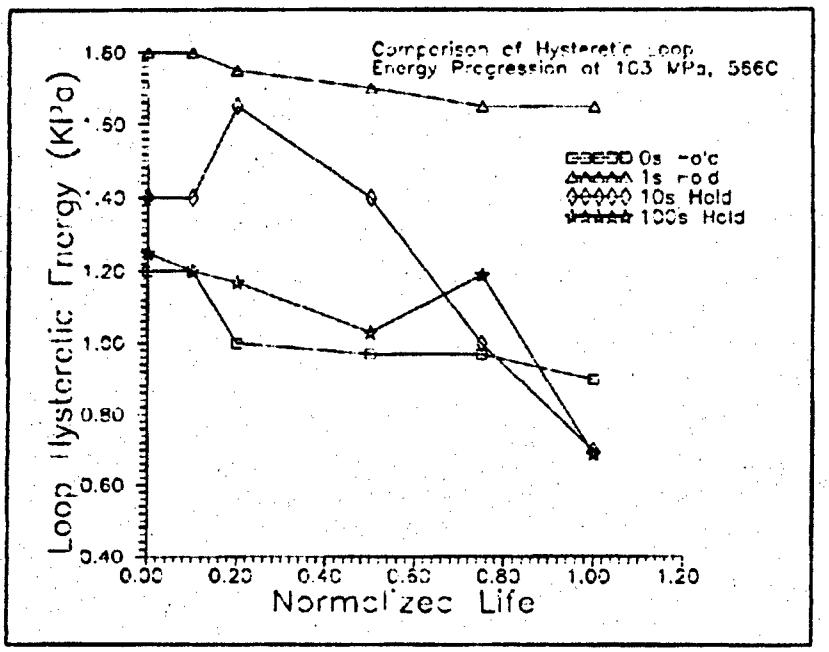

Figure 29. Loop Hysteretic Energy at 566°C,103 MPa.

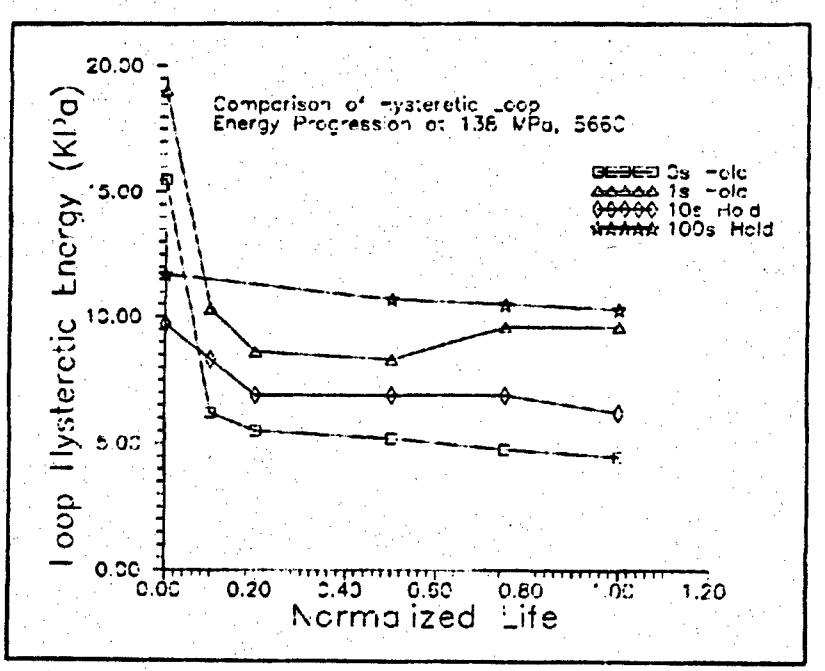

Figure 30. Loop Hysteretic Energy at 566°C, 138 MPa.

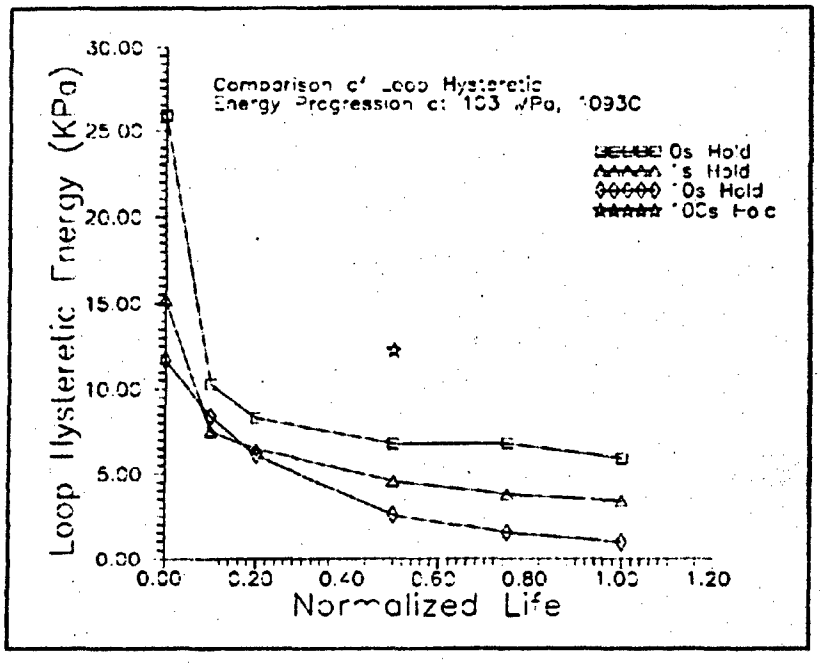

Figure 31. Loop Hysteretic Energy at 1093°C, 103 MPa.

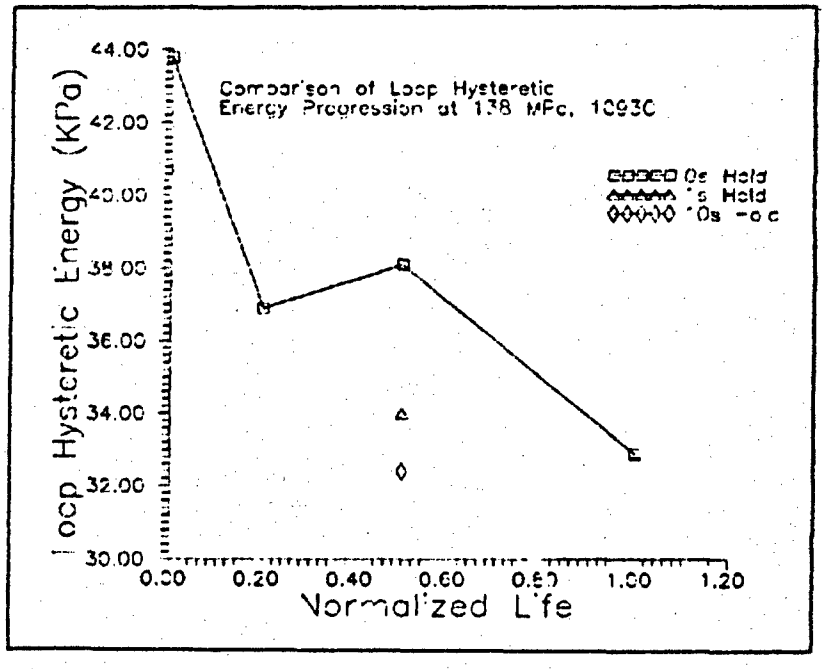

Figure 32. Loop Hysteretic Energy at 1093°C, 138 MPa.

This is illustrated by fact that while the modulus remains constant or increases slightly, the hysteretic loop energy continues to decrease throughout the test as shown in the aforementioned figures which illustrate the trend for 103 MPa/566°C, 138 MPa/566°C, 103 MPa/1093°C and 138 MPa/1093°C respectively. Finally, an increase in hold time usually caused an increase in the hysteretic loop energy at all points throughout the test. This trend was ambiguous at the low stress levels and much clearer as the stress increased to 138 MPa. It is possible that the lower stress levels display random behavior due to the similar contributions of the various mechanisms, while the higher stress allowed the effect of the environment and creep to become dominant. In addition, the effect of the environment is to increase the strength of the interfacial bond (causing the composite to become more brittle) [10].

In summary, the loop hysteretic energy follows the trend of the modulus degradation. An incremental increase in the stress level caused a disproportionate increase in the loop hysteretic energy. This was due to the larger value of stress being beyond the "knee" of the monotonic tensile curve that represents the point of irreversible damage to the 90° plies.

D. Stress-Strain Relationships

The load versus displacement data from the cycles of interest was converted to stress versus strain data and plotted for values of 0, 0.5, and 1.0 of normalized life (displaced for clarity where necessary). As expected, the majority

of the damage to the material was inflicted on the first few cycles based on the increased curve area. This compares favorably with the trends from the loop hysteretic energy data.

At 566°C/103 MPa, the curves show the tendency for an apparent decrease in slope with increasing hold time, however, the area traced by the loading and unloading curves does not change appreciably indicating a fairly constant rate of damage to the material. This is due to the level of stress in relation to the "knee" at 566°C. 103 MPa is well below this critical value at the lower temperature, and the damage on successive cycles is relatively small. These loading curves are shown in Figures 33 through 36.

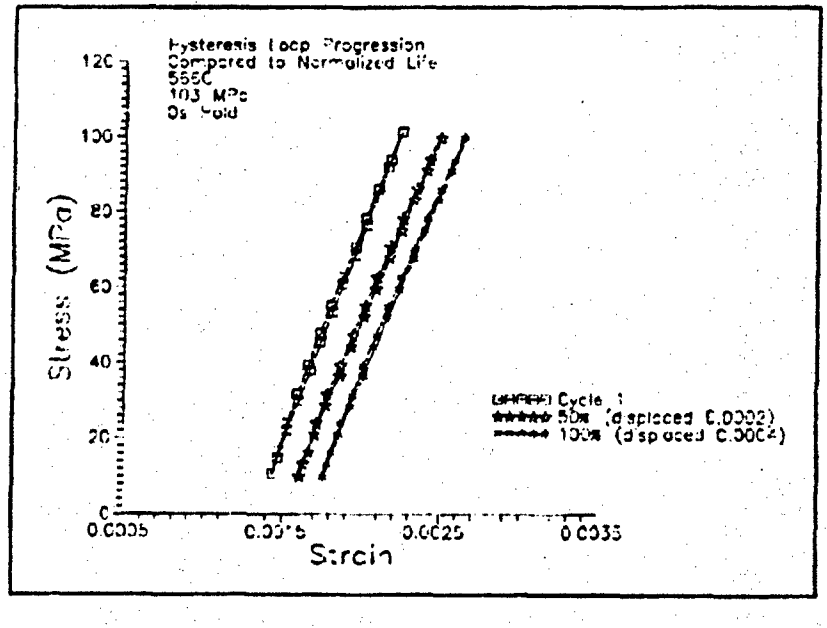

Figure 33. Loading Curves for 566°C, 103 MPa, 0 Second Hold.

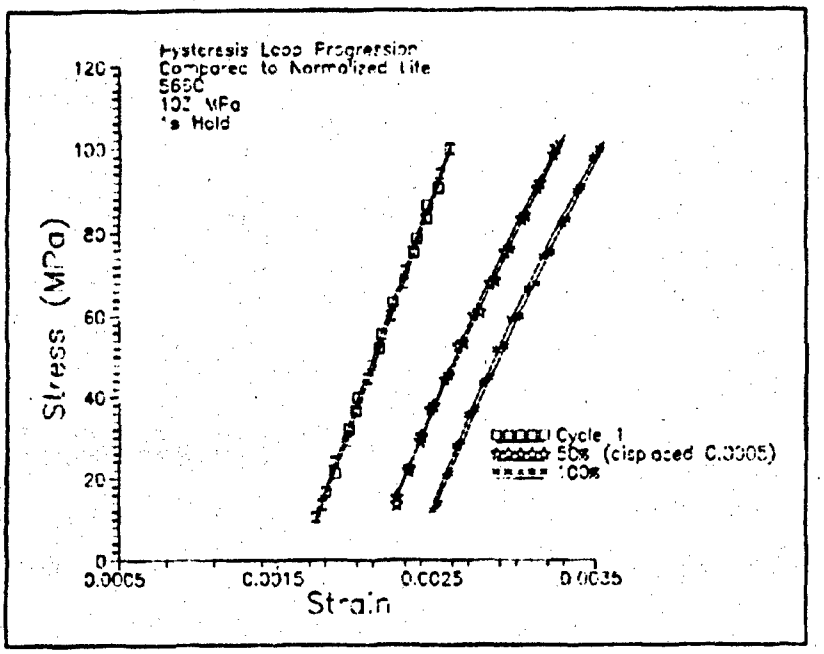

Figure 34. Loading Curves for 566°C, 103 MPa, 1 Second Hold.

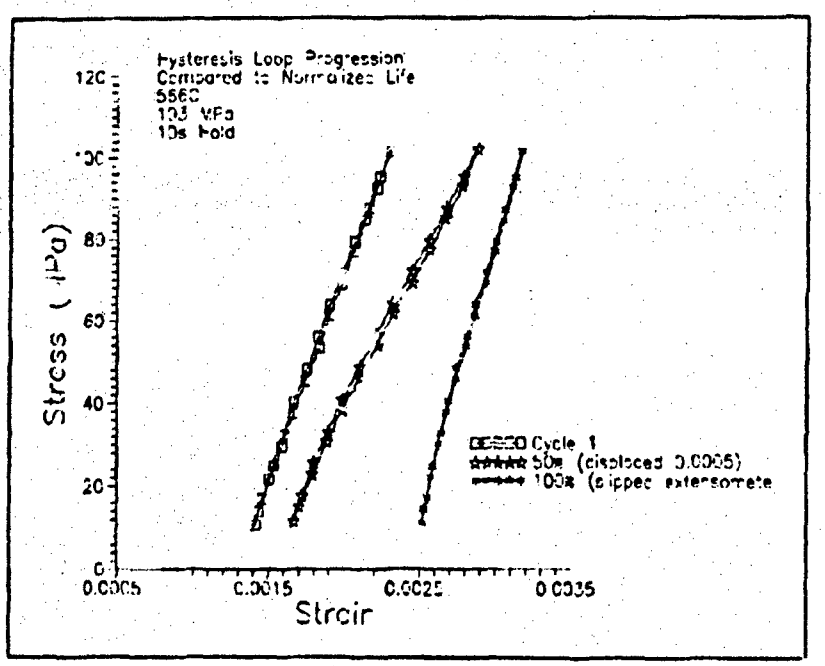

Figure 35. Loading Curves for 566°C, 103 MPa, 10 Second Hold.

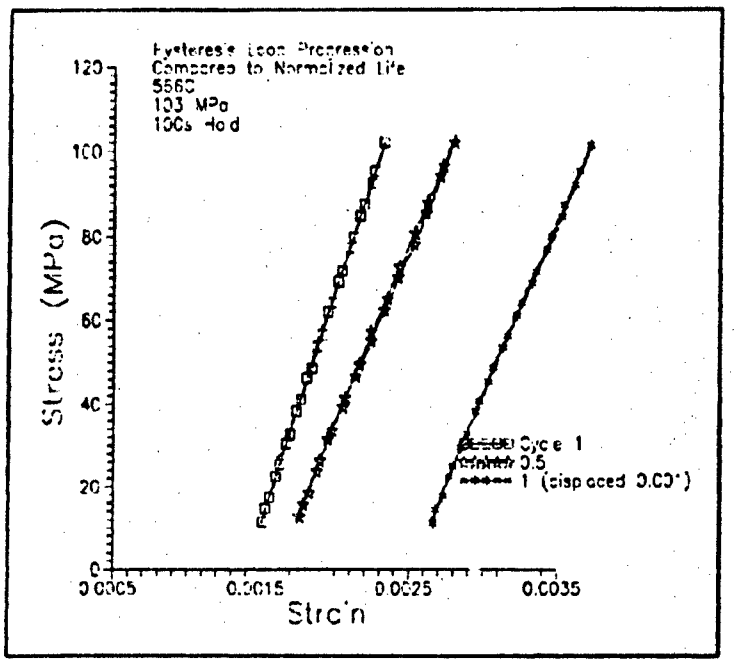

Figure 36. Loading Curves for 566°C, 103 MPa, 100 Second Hold.

This is in contrast to the 138 MPa data which shows a large traced area on the initial cycle, followed by a decreasing area with successive cycles. Like the 103 MPa data, this data shows a tendency for slope decrease as the hold time increases. This is due to the stress at the "knee" being exceeded. At this level, the 90° plies are destroyed on the first few loading cycles (as evidenced by the area traced by the loading curves), and, after that, the curve area remains relatively constant to the point of failure. These loading curves are shown in Figures 37 through 40.

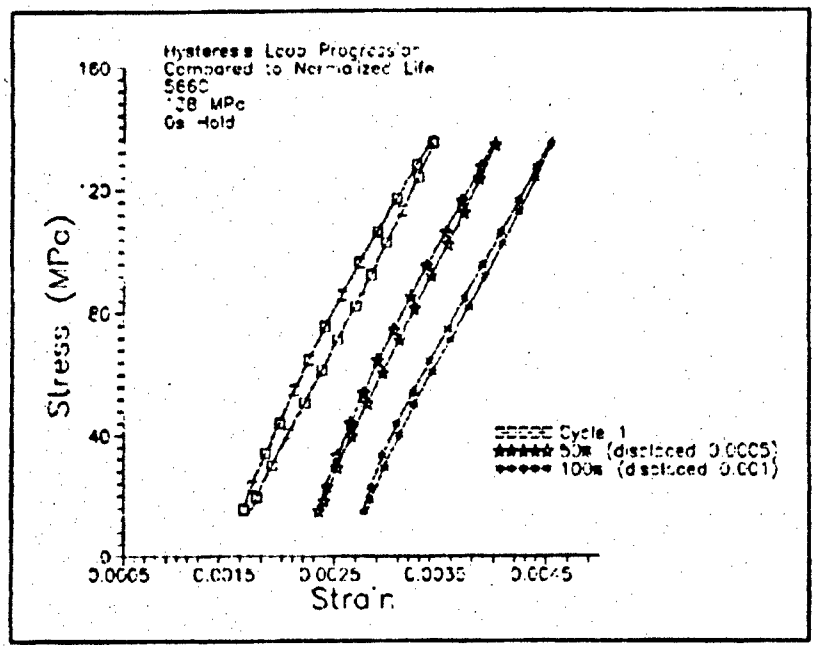

Figure 37. Loading Curves for 566°C, 138 MPa, 0 Second Hold.

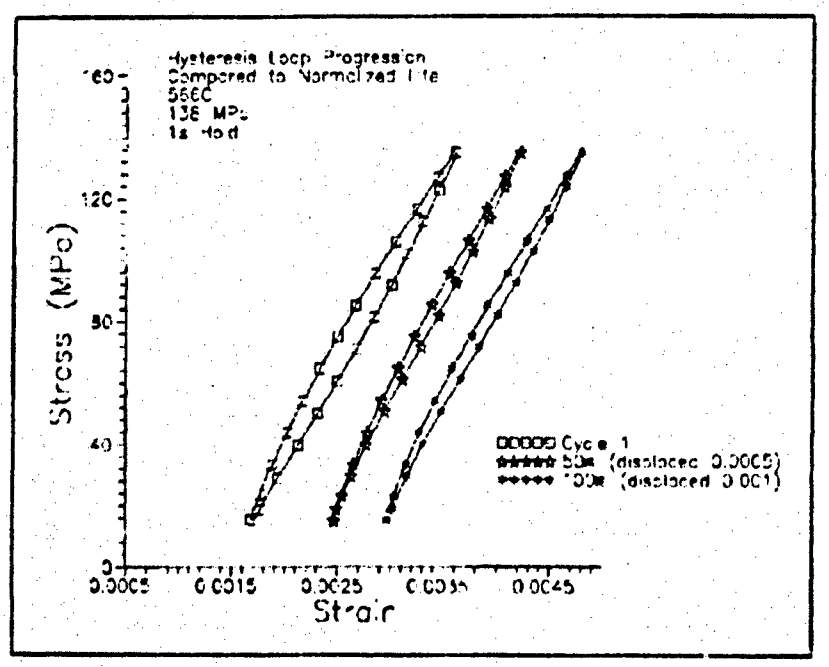

Figure 38. Loading Curves for 566°C, 138 MPa, 1 Second Hold.

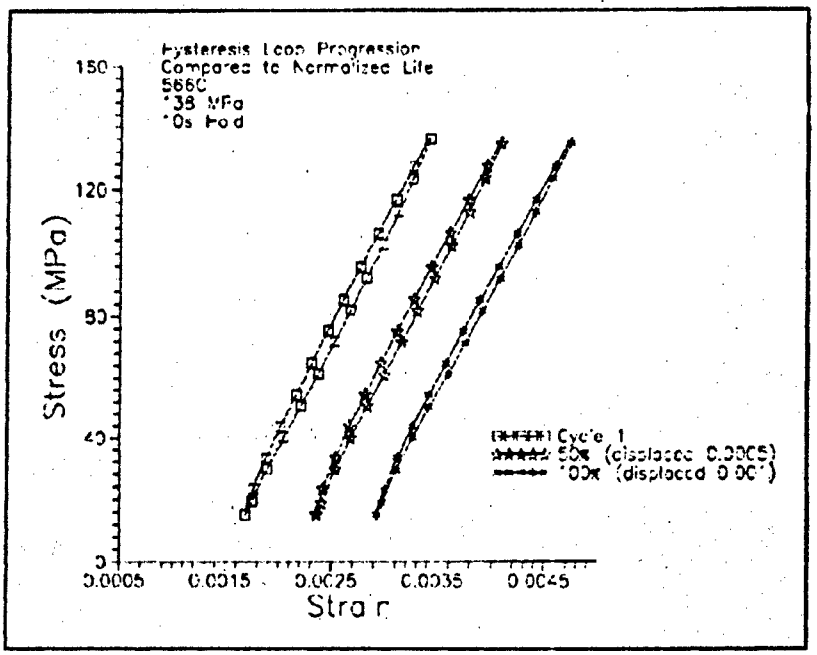

Figure 39. Loading Curves for 566°C, 138 MPa, 10 Second Hold.

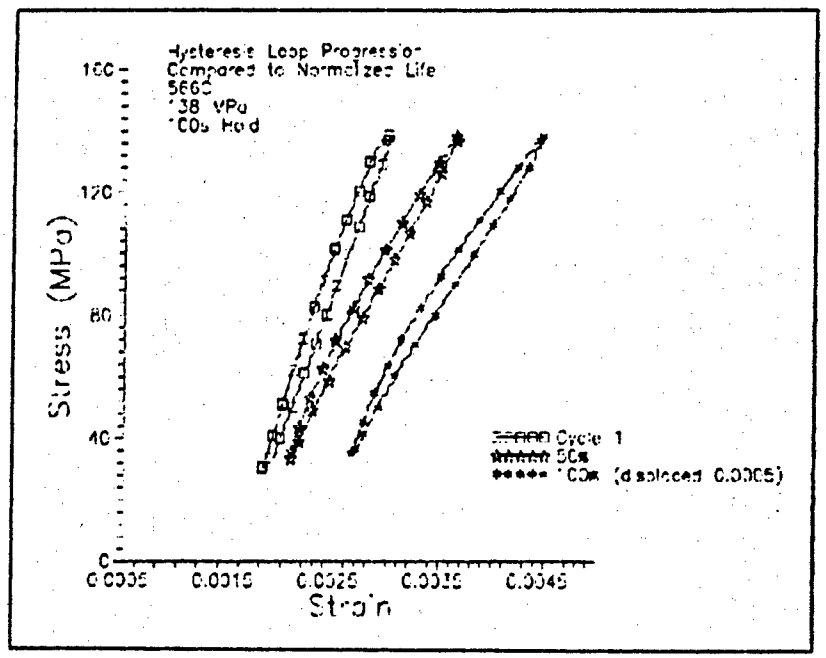

Figure 40. Loading Curves for 566°C, 138 MPa, 100 Second Hold.

At 1093°C, the loading curves show behavior that is quite different from the lower temperature. The lower stress level shows the majority of the damage being done on the initial cycles, while the latter cycles show a relatively constant traced area. This is due to the failure of the 90° plies occurring at a lower stress as the material is degraded at this higher temperature. At this temperature, 103 MPa falls right at the "knee", and the behavior is similar to the 566°C, 138 MPa curves as shown in Figures 41 through 44. At 138 MPa, the area traced out by the loading curves are consistently large from the start to the end of the test. Since the modulus is fully degraded within the first few cycles and the effect of the environment is to stiffen the fiber/matrix interface (inhibiting slip), the relatively large area of the loading curves must be due to creep.

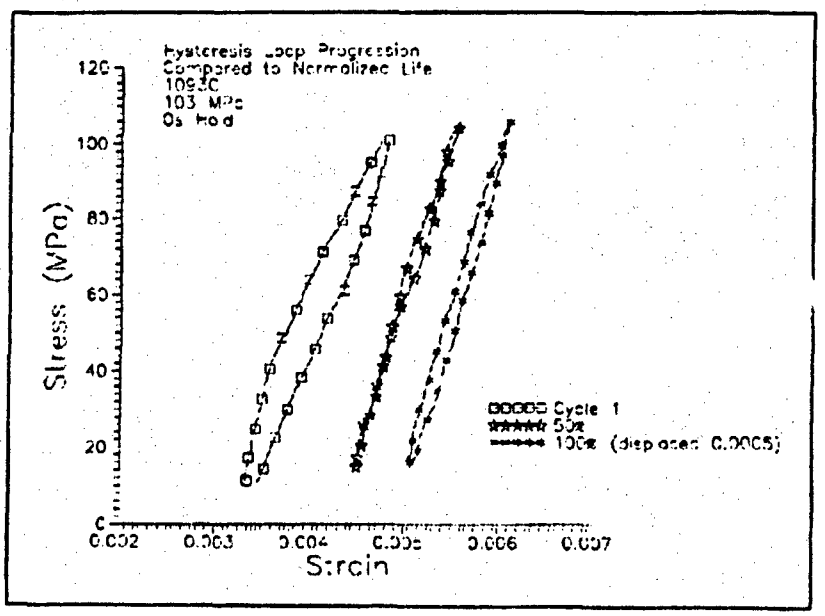

Figure 41. Loading Curves for 1093°C, 103 MPa, 0 Second Hold.

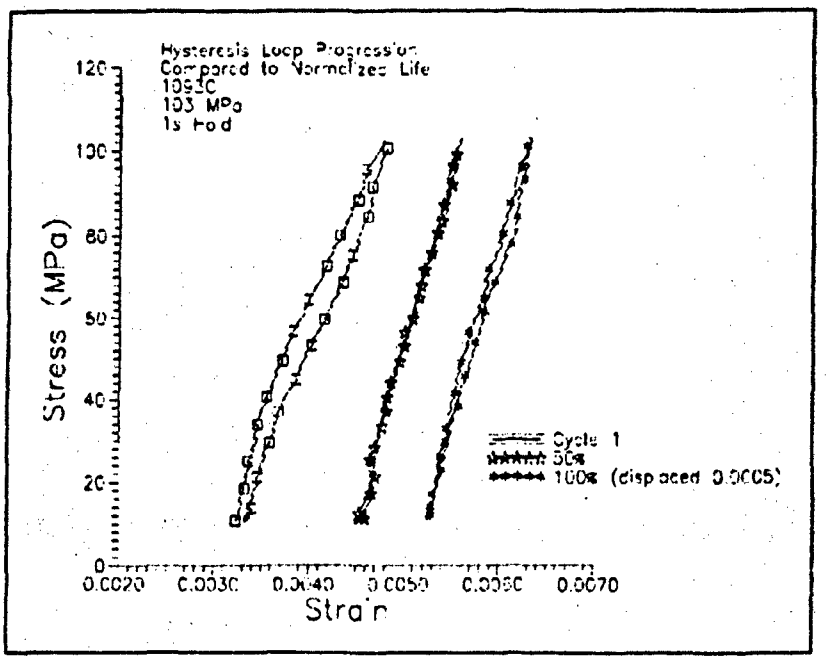

Figure 42. Loading Curves for 1093°C, 103 MPa, 1 Second Hold.

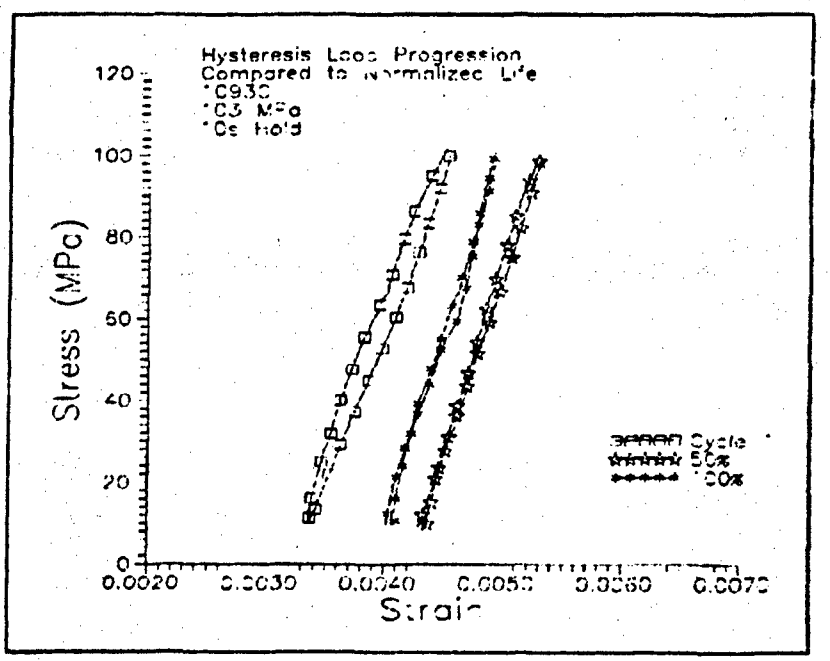

Figure 43. Loading Curves for 1093°C, 103 MPa, 10 Second Hold.

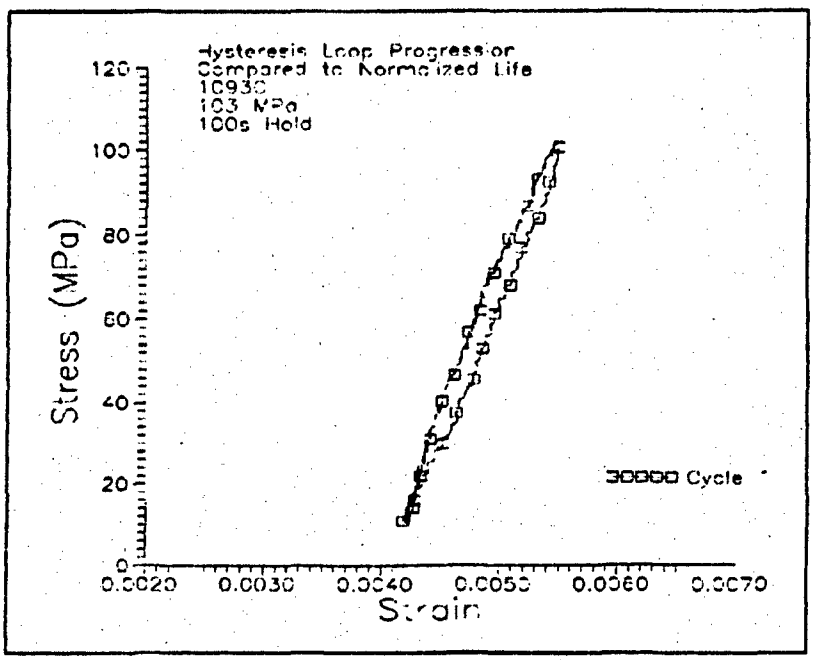

Figure 44. Loading Curves for 1093°C, 103 MPa, 100 Second Hold.

This follows logically when one considers that the effect of creep increases with increasing stress and temperature. These loading curves are shown in Figures 45 through 47.

To summarize, the change in slope and in size of the hysteresis loops agrees with the observations of modulus degradation and loop hysteretic energy, respectively. Once again, the stress level in relation to the stress at which the 90° plies fail is an important factor in the size of the traced area of the loading curves. The effect of hold time is to decrease the apparent slope of the loading curves at

the latter stages of the test. This is especially apparent at the low stress condition where the damage to the 90° plies has not fully progressed after the first few cycles.

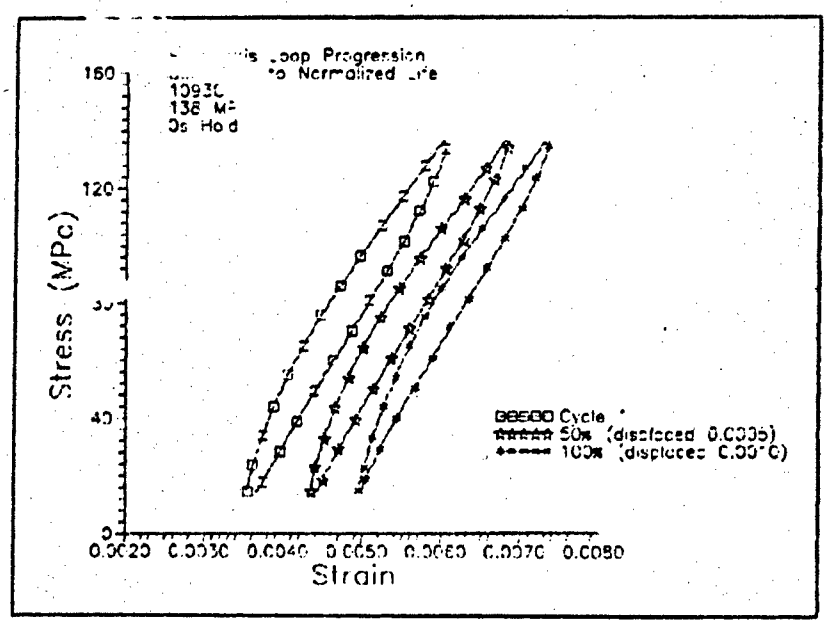

Figure 45. Loading Curves for 1093°C, 138 MPa, 0 Second Hold.

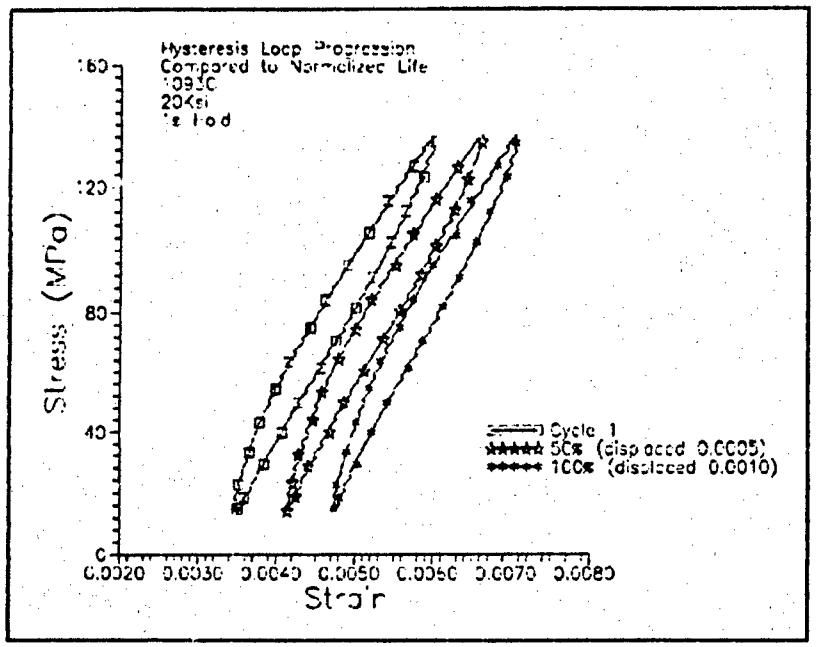

Figure 46. Loading Curves for 1093°C, 138 MPa, 1 Second Hold.

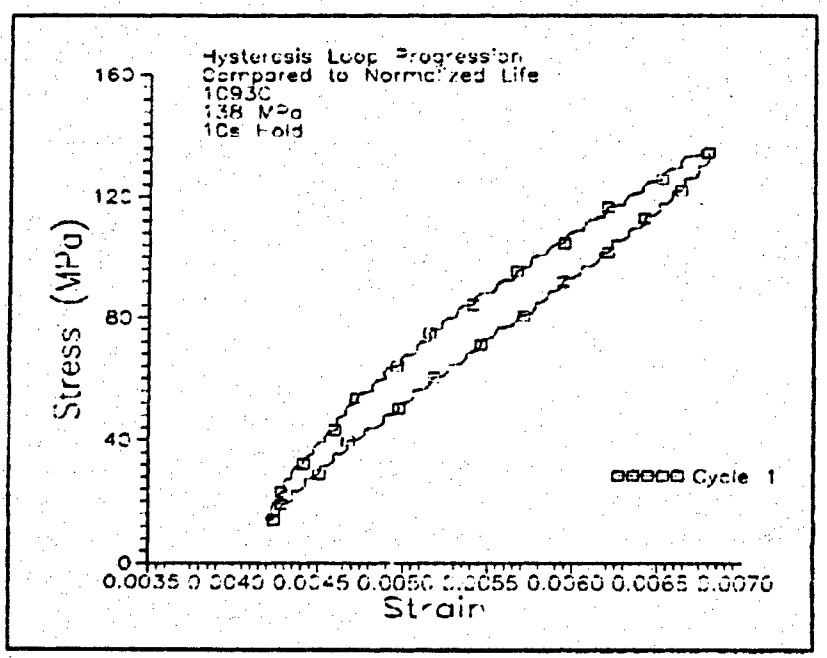

Figure 47. Loading Curves for 1093°C, 138 MPa, 10 Second Hold.

E. Strain Progression

From the stress-strain curves, the variation of maximum and minimum strain with test progression was plotted at points representing 0, 0.1, 0.2, 0.5, 0.75, and 1.0 (where possible) of the normalized fatigue life for each specimen. It was found that, in general, the envelope of the strains (ε_{max}-ε_{min}) was constant with the strains increasing initially followed by a stabilization to the point of failure. This trend was repeated at both temperatures.

At the 566°C, 103 MPa loading condition, the strains tend to gradually increase over the duration of the test as illustrated in Figure 48. This compares well with the tendency of the modulus to gradually decrease over the same period as shown previously in Figure 21. When the stress is increased to 138 MPa, the strains again follow the trend of the modulus. The modulus tends to degrade within the first few cycles, and correspondingly, the strains tend to increase within the first few cycles then stabilize as shown in Figure 49.

At 1093°C, the strains again follow the trend of the modulus in that ε_{max} and ε_{min} both increase within the first few cycles (corresponding to the modulus decrease) then stabilize as shown in Figures 50 and 51. The slight increase in modulus experienced after the initial damage at low stress is not clearly indicated by a corresponding decrease in the strain data. This is due to the competing effect of the microcracks (which tend to decrease the modulus and increase the strain), the progressive oxidation and stiffening of the fiber matrix interface (which may tend to increase the modulus and decrease the strain), and the accumulation of

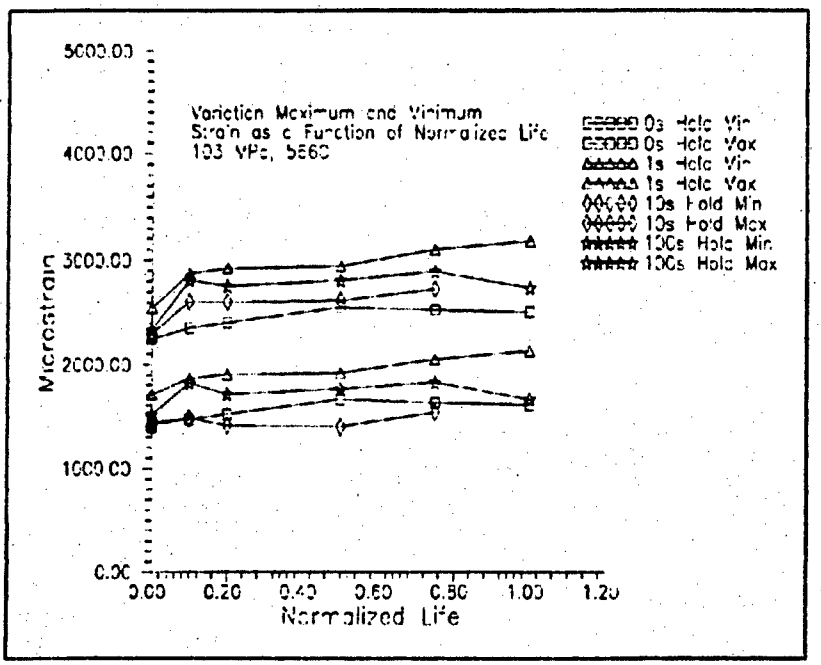

Figure 48. Variation of Min/Max Strain, 566°C, 103 MPa.

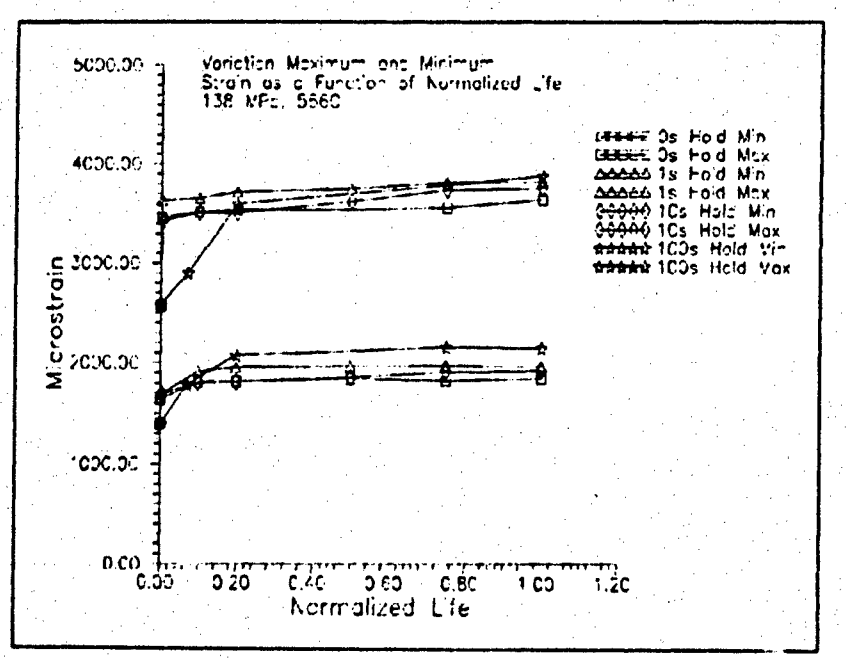

Figure 49. Variation of Min/Max Strain, 566°C, 138 MPa.

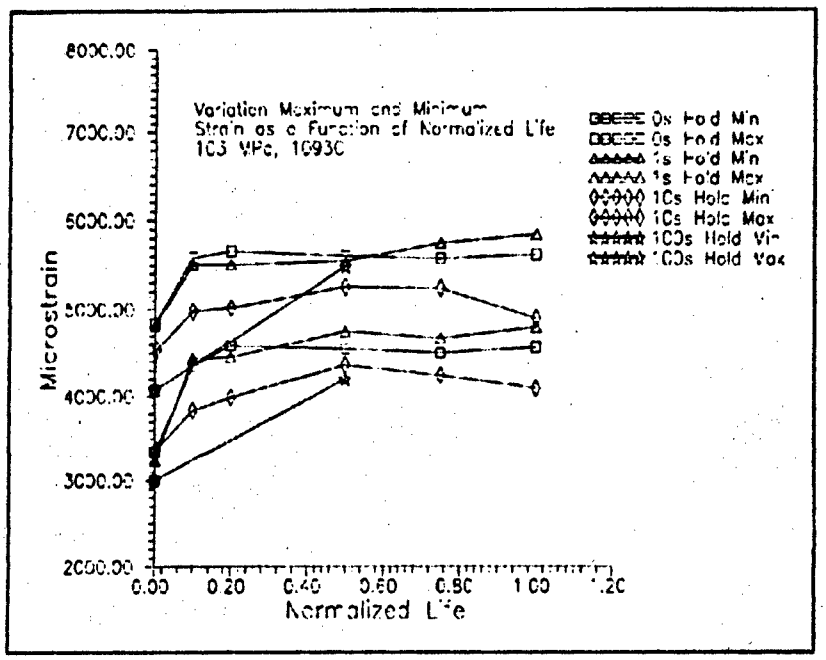

Figure 50. Variation of Min/Max Strain, 1093°C, 103 MPa.

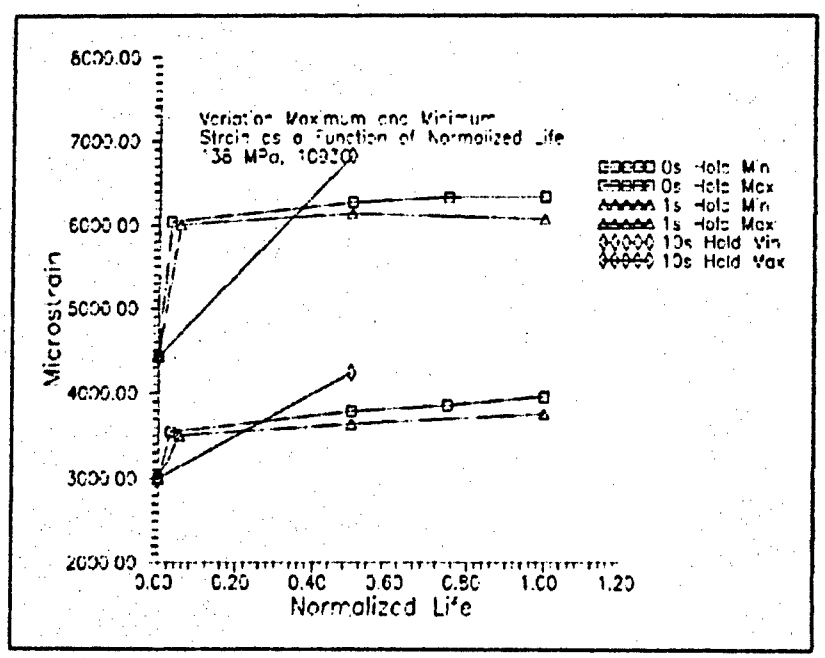

Figure 51. Variation of Min/Max Strain, 1093°C, 138 MPa.

debris in the matrix cracks (which will tend to increase the modulus and decrease the strain). The extent of matrix cracking (at a stress level below the "knee") is a function of the number of cycles as is the accumulation of debris in the matrix cracks. The extent of oxidation at the fiber/matrix interface is a function of both the cycling and the temperature of the environment as shown by the 1093°C S-T data in Figure 11. The 1093°C, 103 MPa tests were most conducive to a combination of the aforementioned mechanisms working in concert causing the relationship between modulus reduction and strain progression to become ambiguous.

Furthermore, all the strain data show a tendency for $\varepsilon_{max} - \varepsilon_{min}$ to remain constant after the initial damage has been done. Also, ε_{max} and ε_{min} tend to gradually increase. Since the modulus tends to remain constant after the initial damage occurs, the strain data indicate the presence of creep. In this case, "creep" is defined as a time dependent, permanent deformation of the material--not in the sense that a plastic deformation is occurring as in metallic materials, but instead in the form of accumulation of various forms of damage at the microlevel.

The strain data (ε_{max} and ε_{min}) will change with increasing cycles for a variety of reasons. First, elongation due to creep effects will be indicated by an increase in both ε_{max} and ε_{min} equally as previously stated. Cyclic damage from micro-cracks, on the other hand would be indicated when ε_{min} remains relatively constant while ε_{max} continues to increase over time (or cycles) in a load controlled test. This would indicate a progressive decrease in modulus, and, while this

occurred to a small extent at the low stress/low temperature combination of 103 MPa/566°C, all other stress/temperature combinations produced an initially large modulus decrease followed by a constant *or slightly increasing* value of normalized modulus.

In summary, the progression of the maximum and minimum strains follows a trend indicative of creep in that ε_{max} and ε_{min} are both slightly increasing with $\varepsilon_{max} - \varepsilon_{min}$ remaining relatively constant. In addition, the data from the plots of modulus degradation lend support to the creep hypothesis.

F. Damage Mechanisms

Finally, the fractured surface of the failed specimens was analyzed under the SEM under magnifications of ranging from 100 to 1800. An oblique view was used in all cases. The parameters of interest were the extent and trend of the fiber pullout, the condition of the fibers, and how both related to a given loading condition.

At 566°C, the length of fiber pullout tended to be constant over the entire fracture surface. The extent of pullout, however, varied directly with the exposure time (T=cycles*time/cycle) to which a specimen was exposed to the environment. The longer the exposure time, the less extensive (shorter) the fiber pullout tended to be. Figures 52 through 59 show the fracture surfaces in logical order of increasing exposure time at 138 and 103 MPa as listed in Table 4.

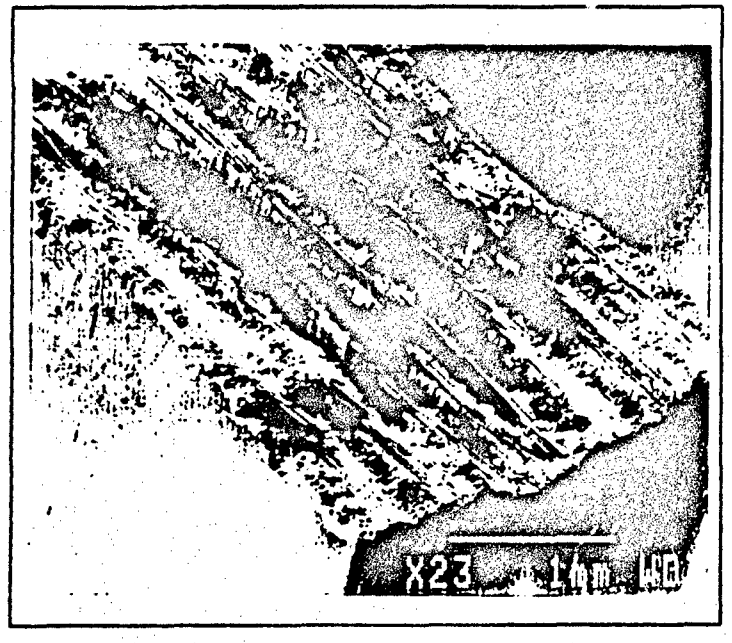

Figure 52. Fractured Surface at T=1156 seconds.

Figure 53. Fractured Surface at T=1414 seconds.

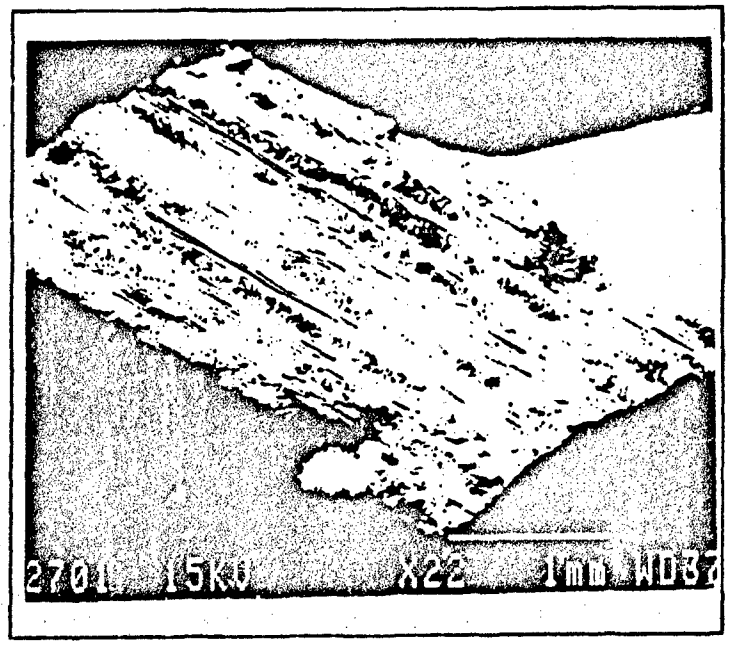

Figure 54. Fractured Surface at T=2390 seconds.

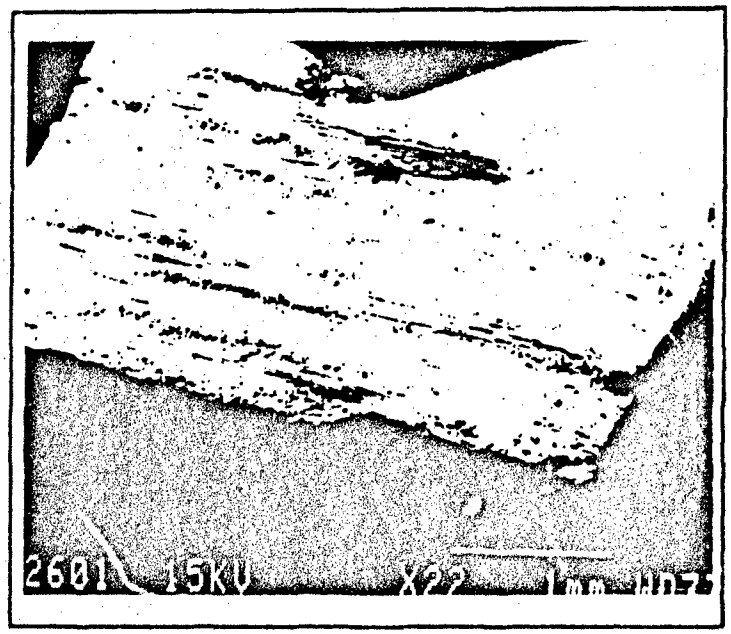

Figure 55. Fractured Surface at T=2915 Seconds.

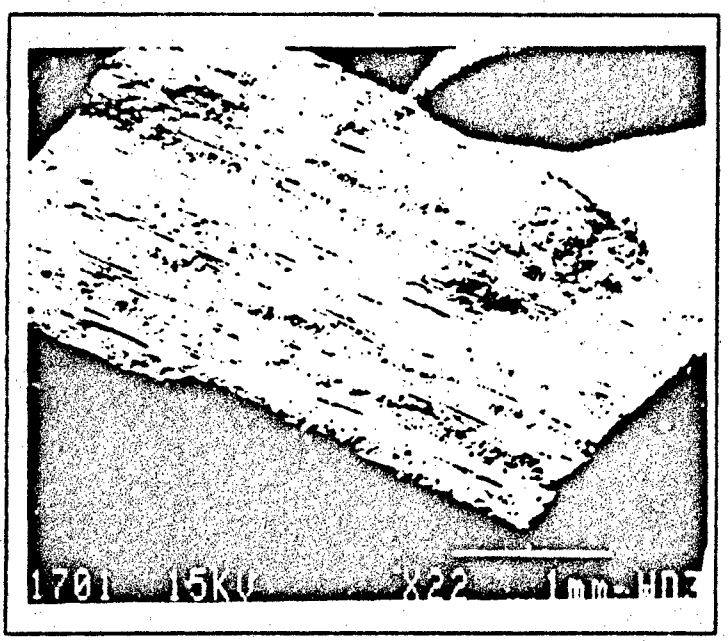

Figure 56. Fractured Surface at T=203700 seconds.

Figure 57. Fractured Surface at T=425299 seconds.

Figure 58. Fractured Surface at T=518635 seconds.

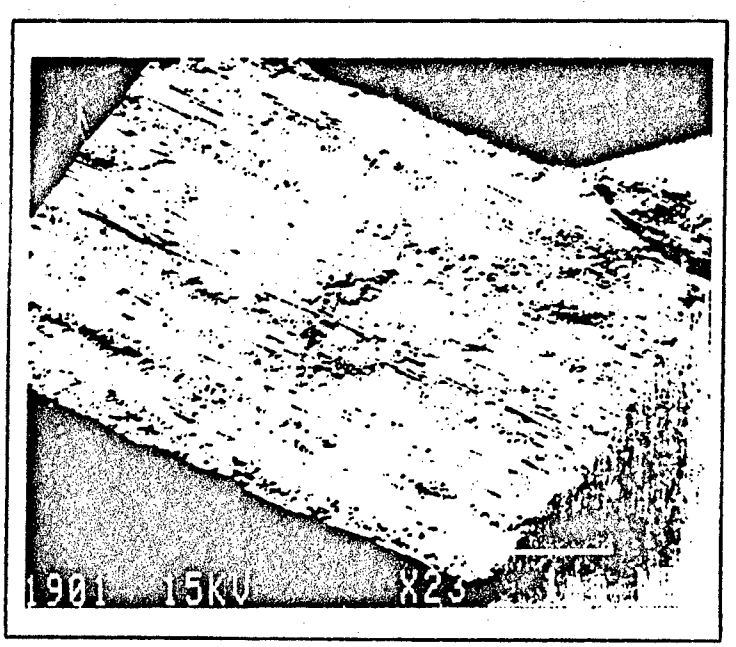

Figure 59. Fractured Surface at T=1009129 seconds.

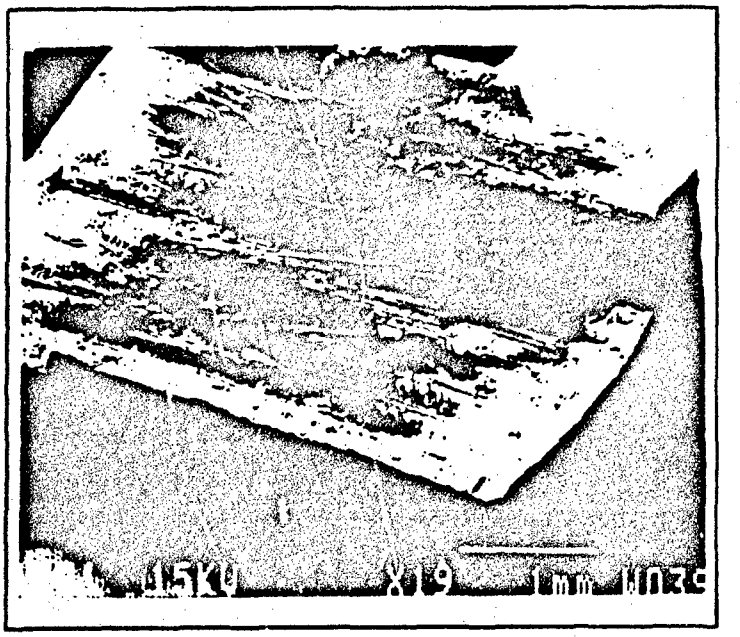

Figure 60. Fractured Surface at T=32 seconds.

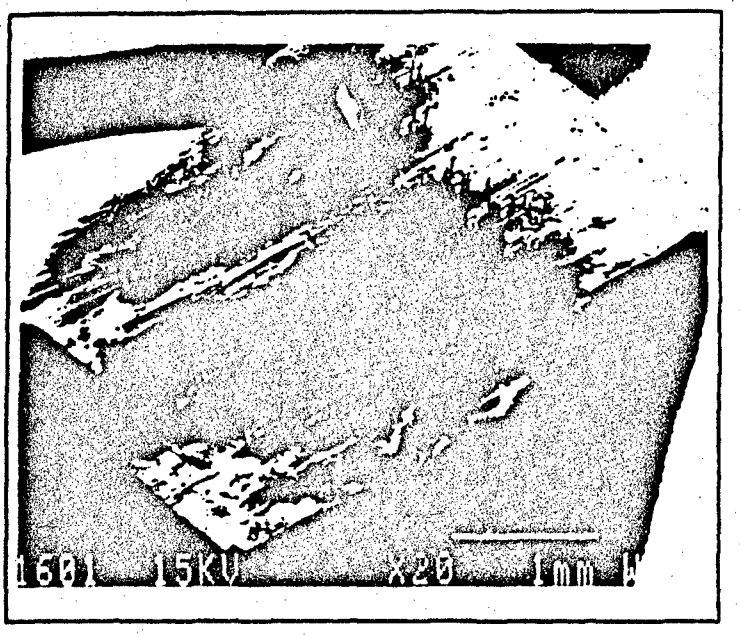

Figure 61. Fractured Surface at T=36 seconds.

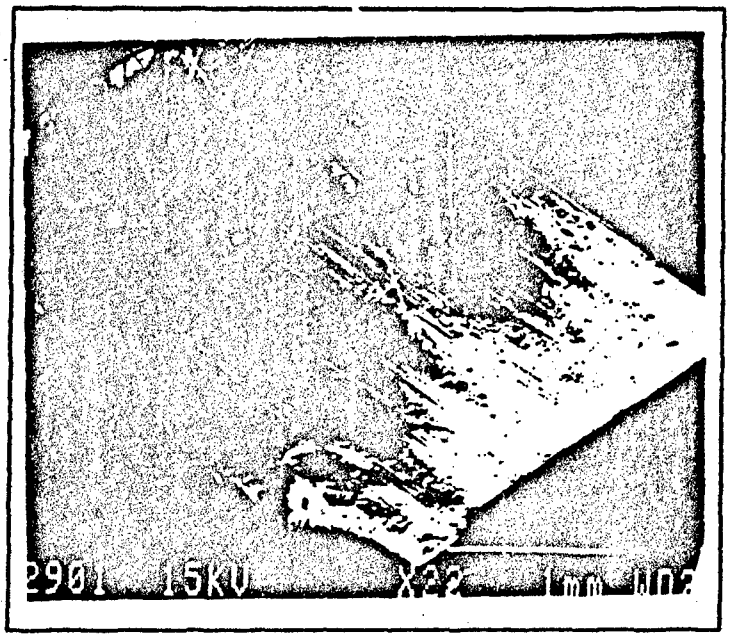

Figure 62. Fractured Surface at T=101 seconds.

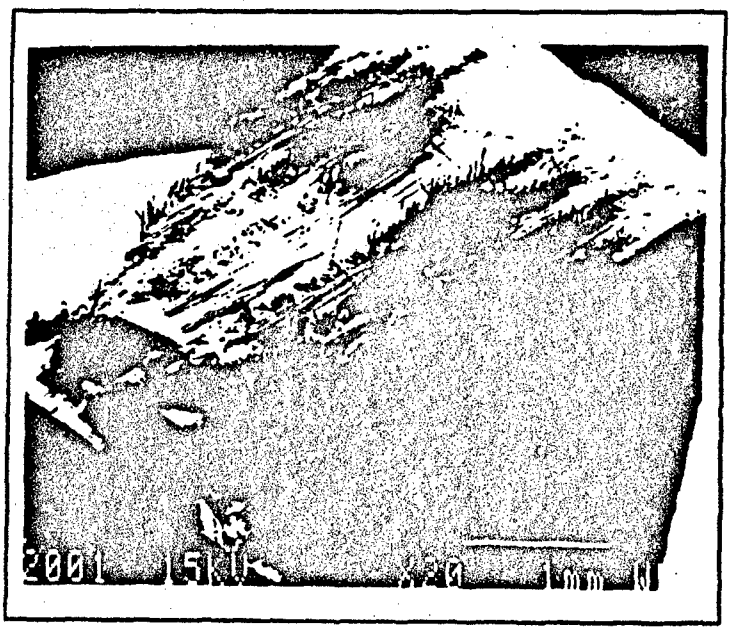

Figure 63. Fractured Surface at T=121 seconds.

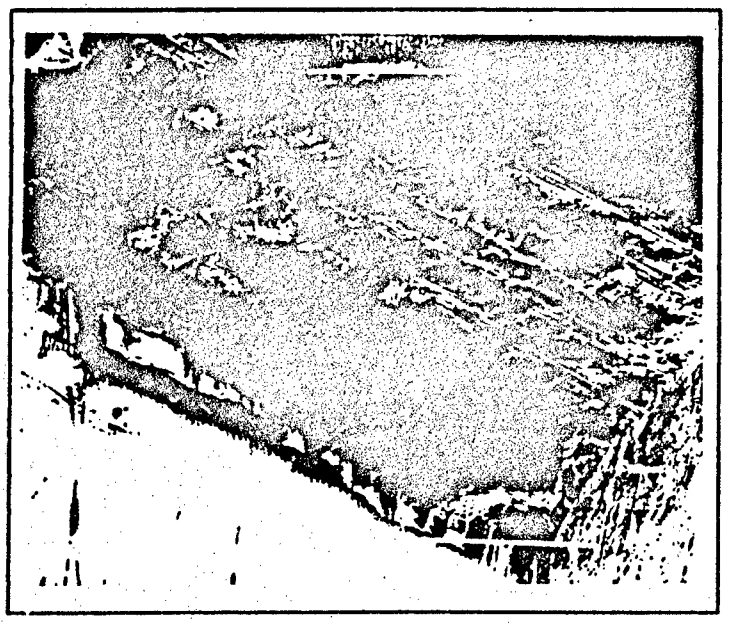

Figure 64. Fractured Surface at T=1010 seconds.

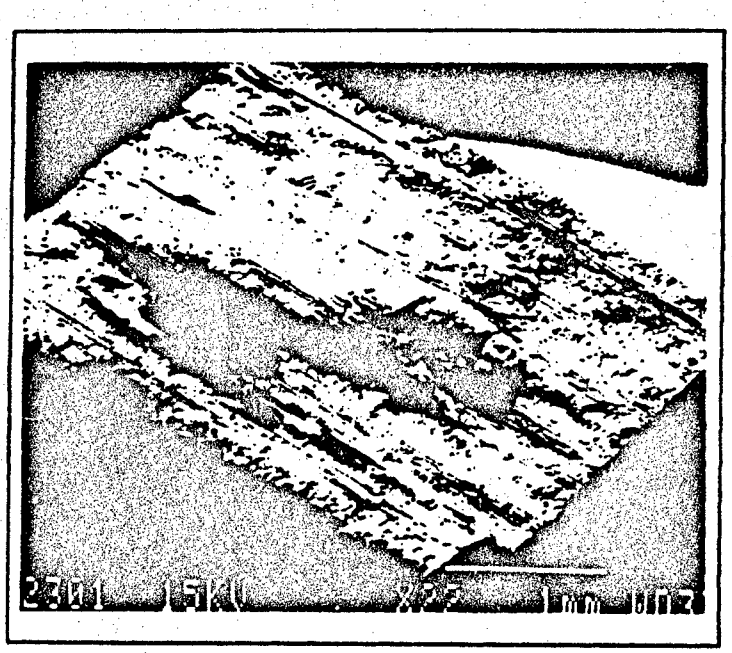

Figure 65. Fractured Surface at T=2376 seconds.

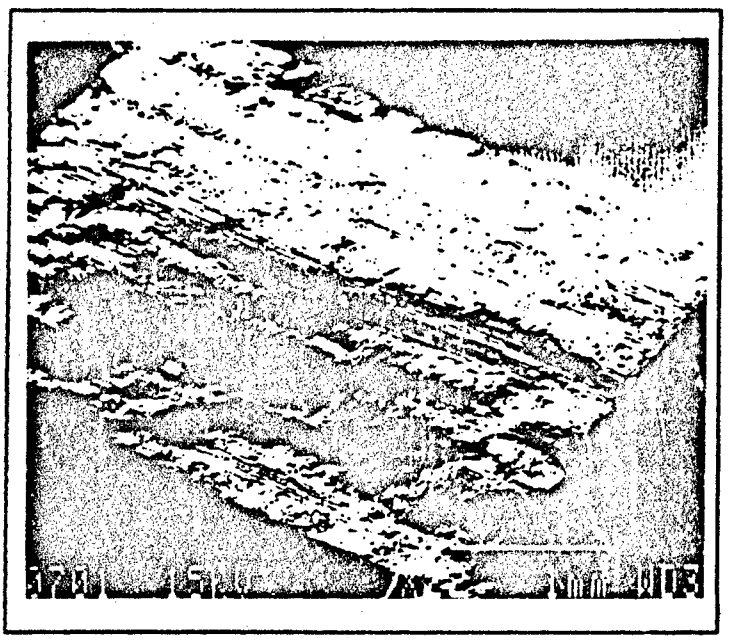

Figure 66. Fractured Surface at T=12030 seconds.

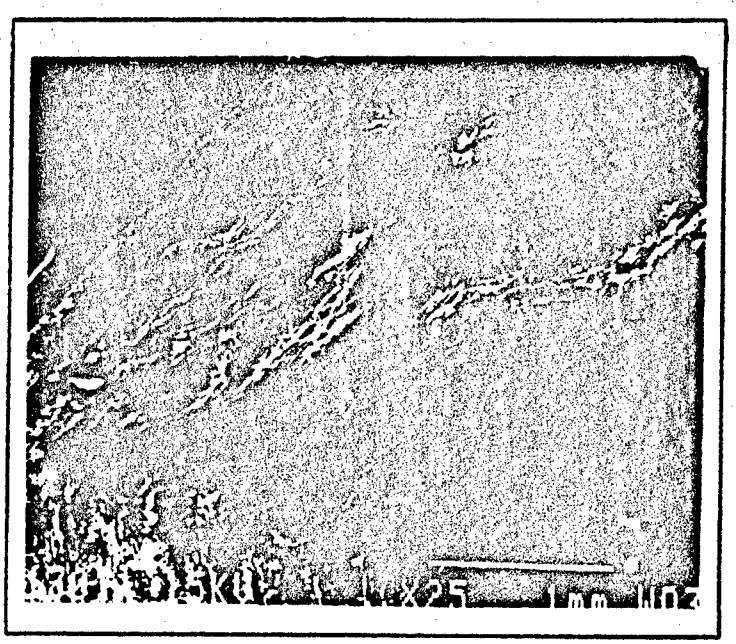

Figure 67. Fractured Surface at T=20237 seconds.

extreme values of hold time (0 and 100 seconds) corresponding to each combination of stress and temperature were analyzed for a total of eight cases. In addition, fibers at both the edge and the center of each case were analyzed. Unlike the previously discussed fracture surfaces, the SEM analysis of the fibers was not conducted with respect to exposure time (although the exposure times are listed for reference).

It was found that all fibers examined from the 566°C tests contained little or no evidence of oxidation. Only the 138 MPa tests showed any evidence of damage from the environment. Figures 68 to 71 illustrate the condition of the fibers at the surface in order of increasing hold time for the edge and center of each case.

Figure 68. Fiber Condition for 566°C, 103 MPa, 0 Second Hold (T=425299s).

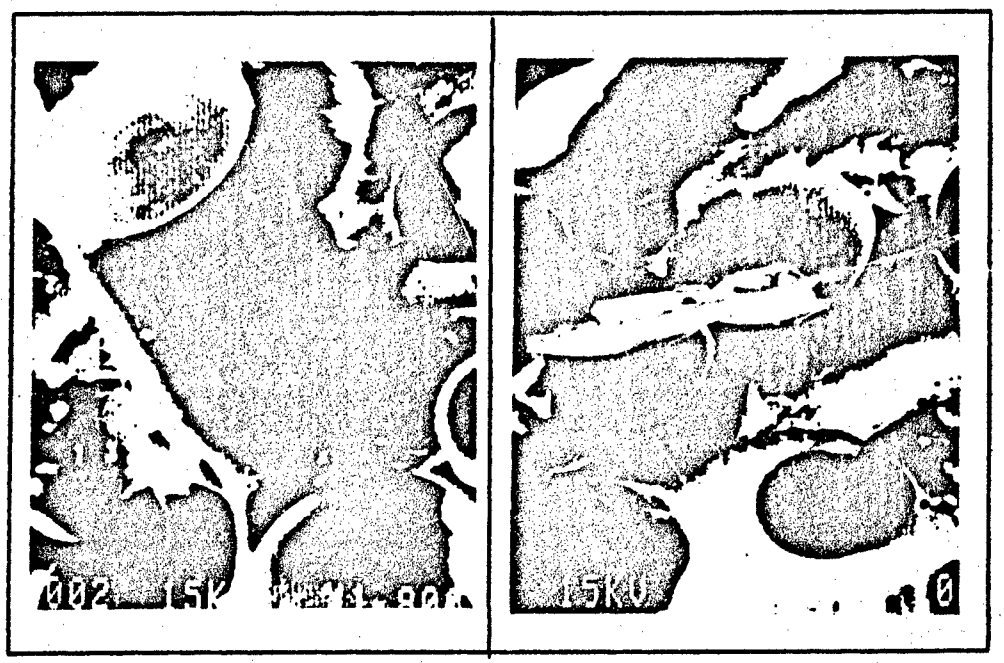

Figure 69. Fiber Condition for 566°C, 103 MPa, 100 Second Hold (T=518635s).

Figure 70. Fiber Condition for 566°C, 138 MPa, 0 Second Hold (T=1156s).

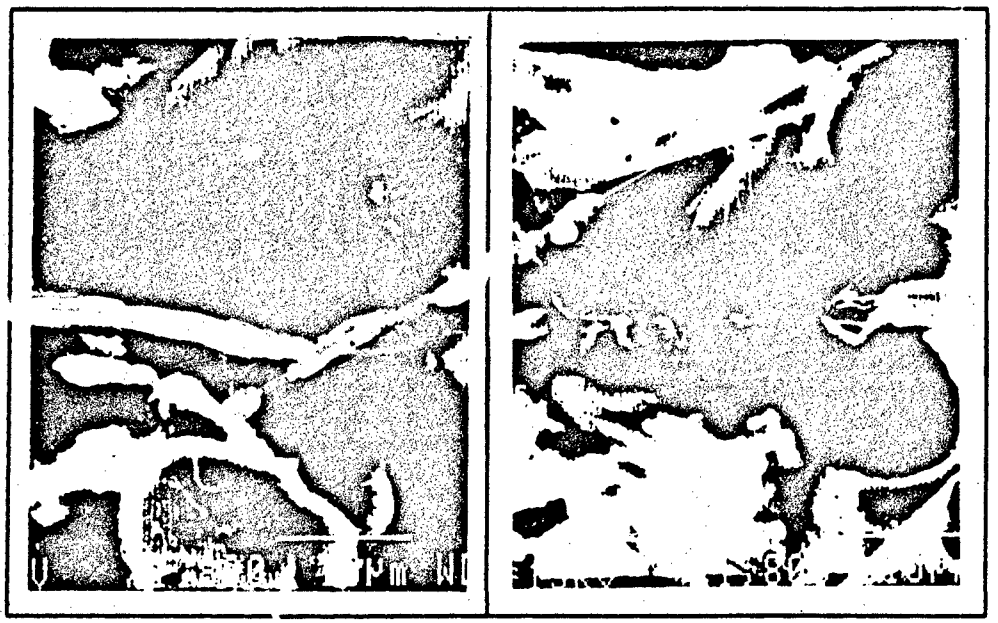

Figure 71. Fiber Condition for 566°C, 138 MPa, 100 Second Hold (T=1414s).

The 1093°C tests, on the other hand, showed extensive damage to the fibers. In addition, the damage done to the fibers near the edge of the fractured surface was much greater than those near the center. This is consistent with the macroscopic analysis of the fractured surfaces. The illustrations of the fibers at 1093°C are arranged in logical order of increasing hold time for the edge and center of each fractured surface case as shown in Figures 72 through 75.

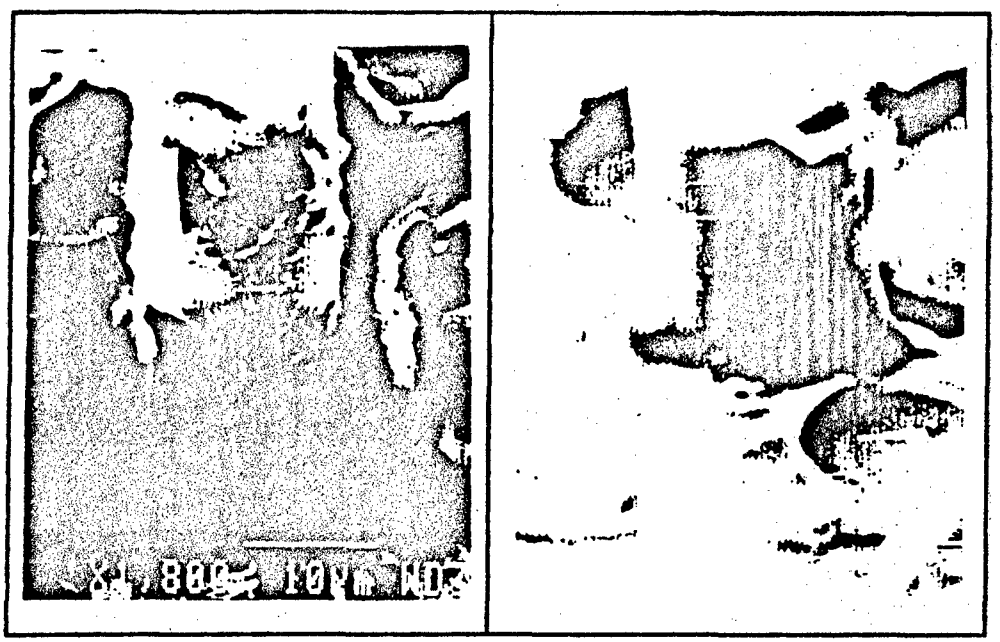

Figure 72. Fiber Condition for 1093°C, 103 MPa, 0 Second Hold (T=20237s).

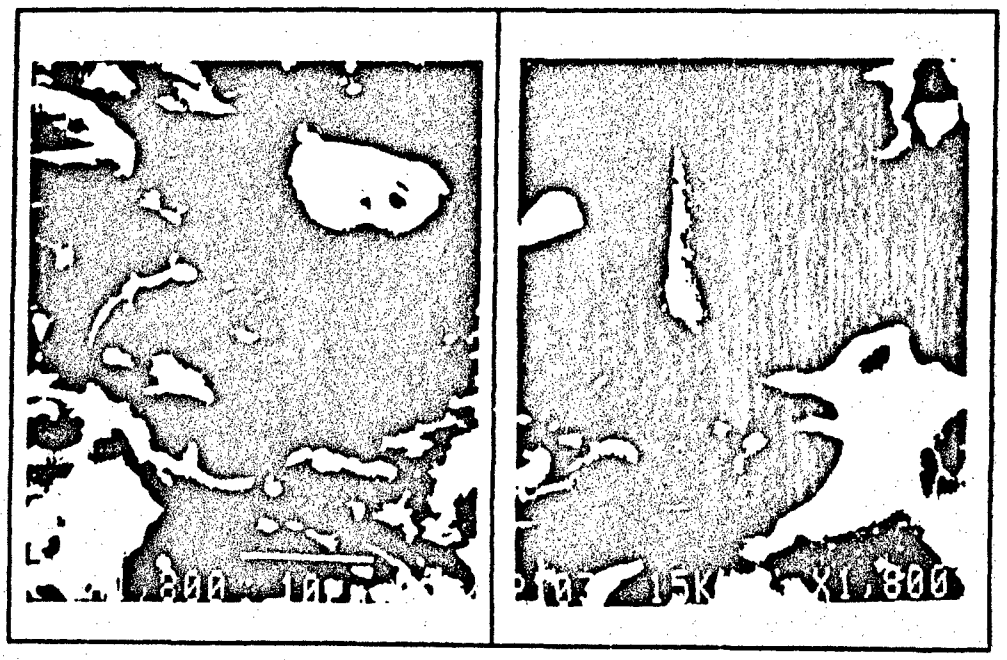

Figure 73. Fiber Condition for 1093°C, 103 MPa, 100 Second Hold (T=1010s).

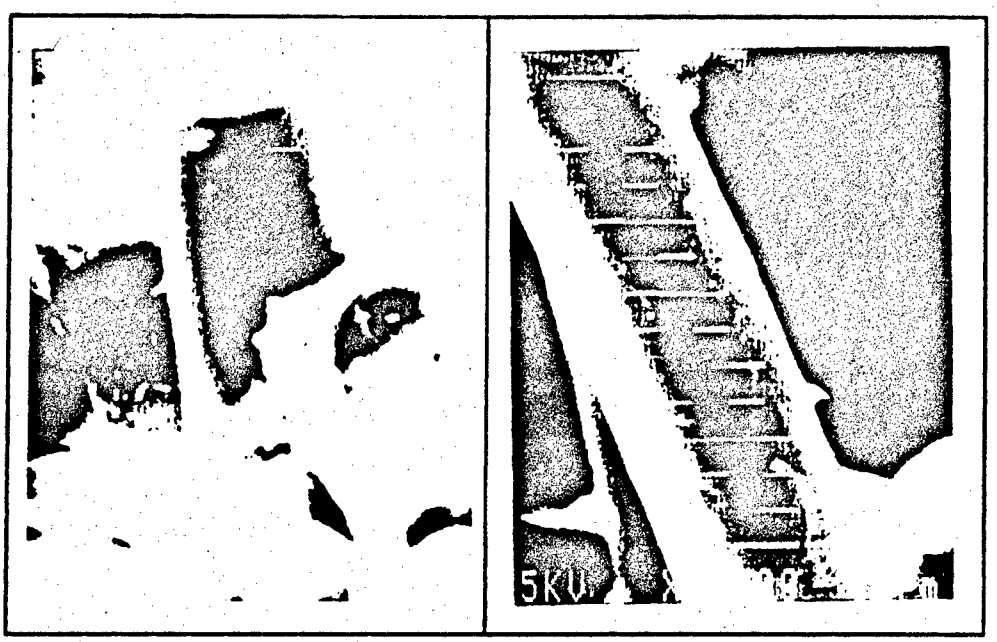

Figure 74. Fiber Condition for 1093°C, 138 MPa, 0 Second Hold (T=32s).

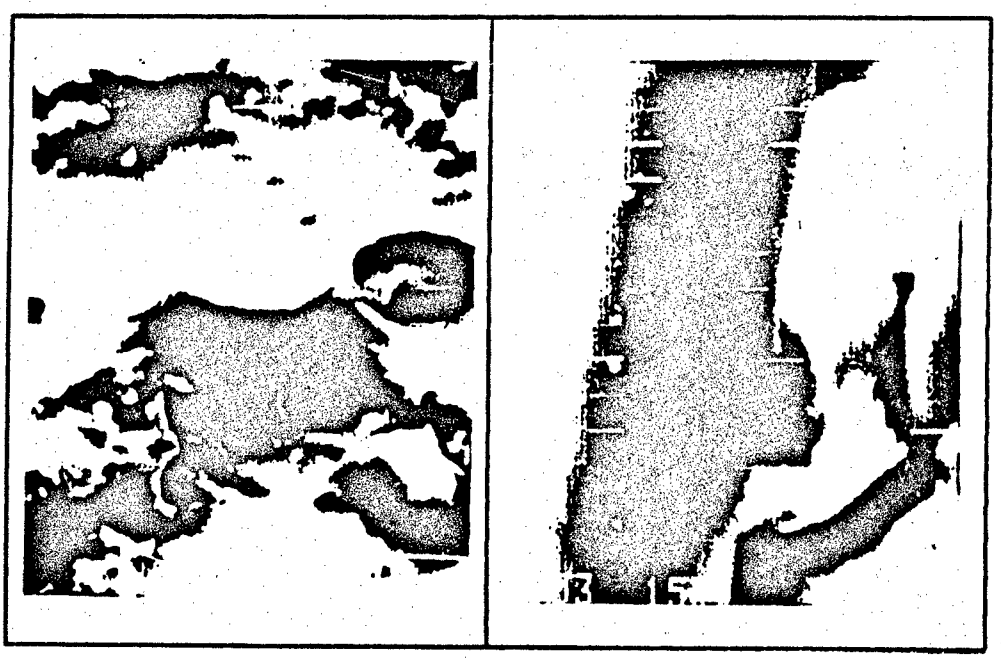

Figure 75. Fiber Condition for 1093°C, 138 MPa, 100 Second Hold (T=101s).

Additionally, an optical microscopic analysis was performed on four of the specimens--each representing the ten second hold specimen of one temperature/stress regime contained in Table 4. It was found that brittle behavior was prevalent in the high temperature/low stress regime. This is illustrated by the crack in Figures 76 and 77. The crack appears to have a preferential direction that, when magnified further in Figure 77, reveals cracking through the fibers. This is indicative of a fully embrittled fiber-matrix interface. The high temperature, high stress specimen shown in Figure 78 illustrates a combined

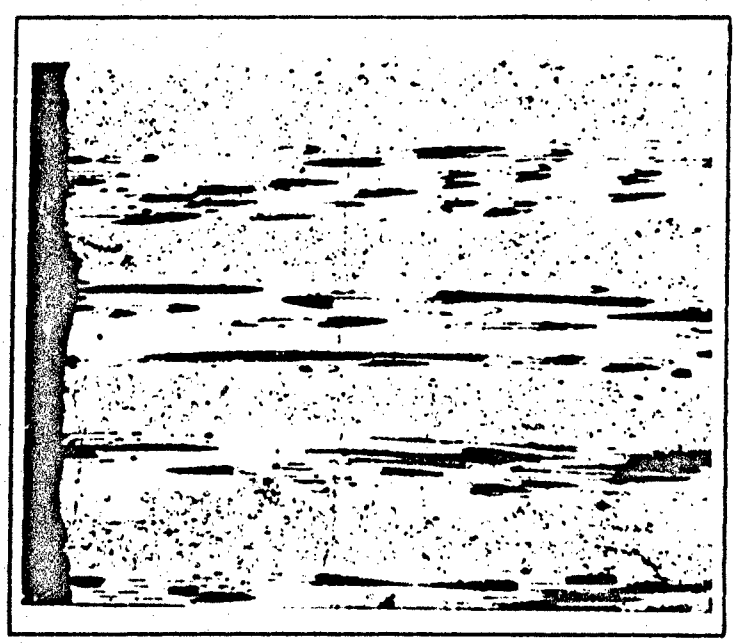

Figure 76. Preferential Crack Propagation, 10x.

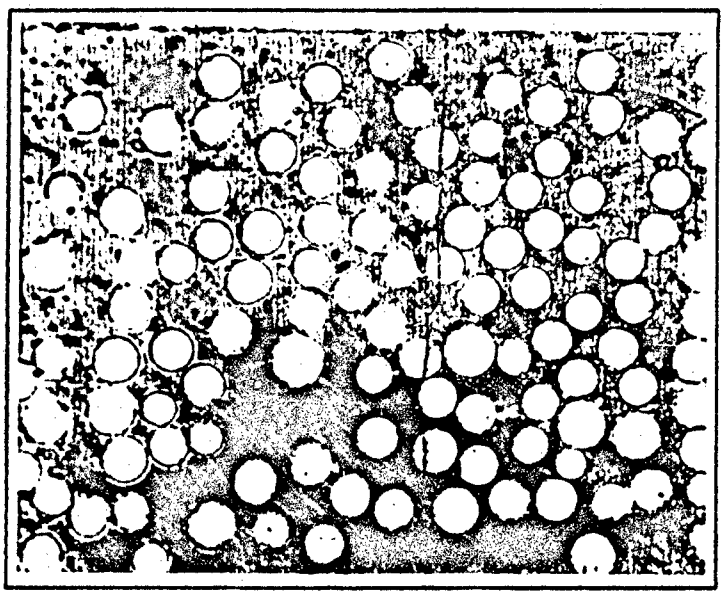

Figure 77. Brittle Fiber Cracks, 40x.

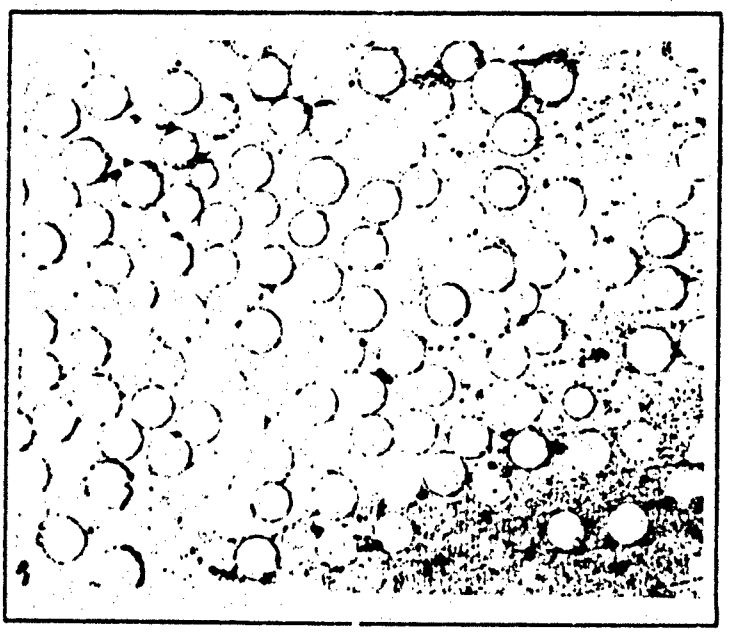

Figure 78. Combined Behavior, 40x.

behavior with a crack passing through one fiber and around the next indicating that the oxidation had not fully developed. Figures 79 and 80 are both from low temperature tests and display no tendency for crack propagation through the fibers.

In summary, the effect of the environment appears to be independent of the hold time, while the maximum stress has the effect of inducing more initial damage which may provide added paths for oxidation to occur. When arranged by exposure time at each temperature, fracture surfaces illustrate that the extent of fiber pull-out decreases with increasing time. The exposure time groupings also

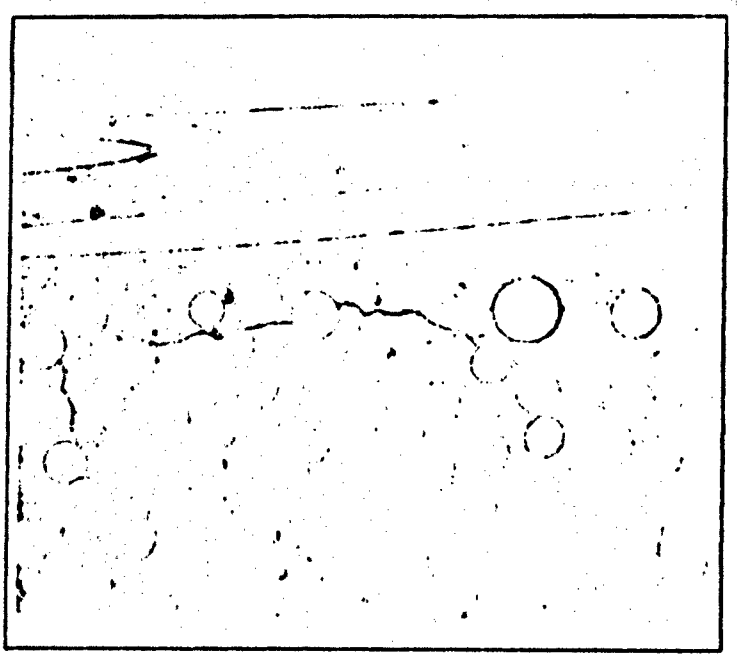

Figure 79. Low Temperature/Low Stress Non-Brittle Behavior, 40x.

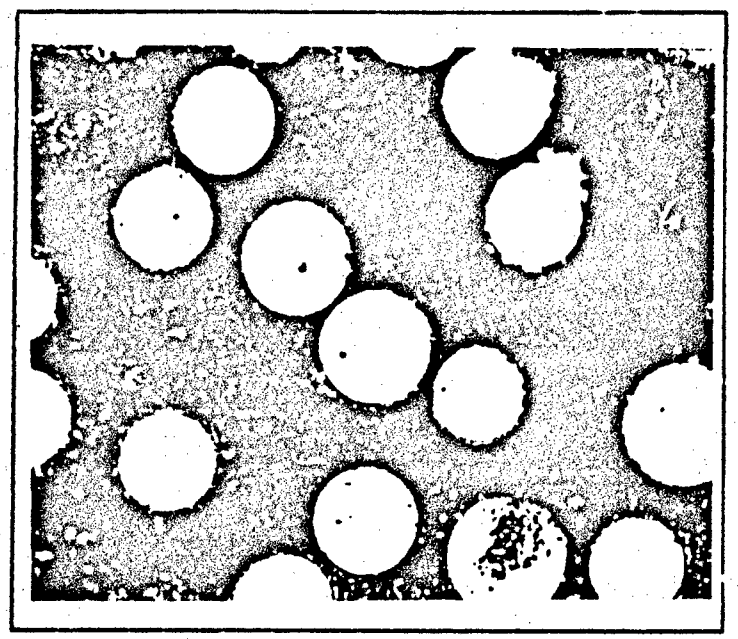

Figure 80. Low Temperature/High Stress Non-Brittle Behavior, 100x.

showed a dependence on the maximum stress in that the four high stress tests produced a lower value of exposure duration than the low stress tests. This is probably due to the initial damage caused by the stress level--the highest produces more initial damage possibly providing additional paths for environmental damage. The highest temperature produced the largest environmental effect with the added feature of increasing extent toward the center of the fracture surface with brittle behavior around the outside. Additional evidence of brittle behavior was found from examining the polished edges of representative specimens. It was found that the specimens exhibiting brittle behavior contained cracks that propagated through the matrix and the fiber via the oxygenated interface. None of

the low temperature specimens exhibited this behavior with matrix cracks propagating around the fibers indicating that the fiber/matrix interface remained un-oxidized.

V. Conclusions

In this study, the fatigue behavior of SiC-MAS5 ceramic matrix composite subjected to tension-tension cycling was studied at two elevated temperatures with hold time. The two elevated temperatures were 566°C and 1093°C and were chosen for the purpose of direct comparison to previous fatigue and stress rupture studies. Two stress levels--103 MPa and 138 MPa --for the fatigue tests were chosen, each inducing different levels of damage in the material. The hold time occurred at the maximum stress in the 1 hertz triangular wave-form and varied from 0 (a pure triangular wave) to 100 seconds (to induce a significant fraction of stress rupture behavior). The combination of all the test parameters resulted in a series of 16 tests, the results of which were compiled in the form of S-N (stress versus cycles to failure), S-T (stress versus exposure duration), and S-S*T (stress versus area under the loading wave-form) curves. In addition, normalized modulus, maximum/minimum strain, loop hysteretic energy, and loading curves were plotted as a function of normalized life. Based on these curves, a hypothesis was formed as to the damage mechanisms at work and how they varied with the loading conditions. Finally, a scanning electron microscope (SEM) was used to examine the fracture surface of each specimen, and thereby probable mechanisms contributing to the failure were deduced.

The S-N curves revealed that the fatigue life varied inversely with the amount of hold time applied at the maximum stress in the loading wave-form.

This behavior was most pronounced at the higher temperature, 1093°C. In order to isolate the environmental effect from that of fatigue, the data from the S-N curves was normalized with respect to exposure time at maximum stress (S-T curves) and a normalizing parameter involving the stress and exposure time (S-S*T curves). It was found that the data completely collapsed to a single curve at 566°C when the S-T normalization was applied implying that the fatigue life of the material at this temperature is predominantly a function of exposure time. In contrast, the 1093°C data did not uniformly collapse. Instead, the data at 138 MPa tended to collapse while the data at 103 MPa tended to remain spread. This implied a combined effect from the cycling and the environment that depended on the stress and the environment. The S-S*T normalization had a much smaller effect, and thus, the effect of temperature was pursued.

Both the rate and extent of the modulus degradation depended on the initial damage induced by the stress level, and to a lesser extent, the hold time and temperature. The damage (and hence the modulus degradation) a specimen experienced was directly related to the proportional limit or "knee" on the monotonic tensile curve (which was a function of temperature). Cycling at stresses that exceeded this critical value resulted in a rapid decrease in modulus followed by a stabilization at the decreased value to the point of failure. Damage beyond that point was predominantly due to the high temperature environment as indicated by the S-T curves. Cycling at a stress below the critical value resulted in a more gradual decrease in modulus to the point of failure. Damage at this lower

stress was due predominantly to the environment at 566°C and a synergistic combination of cycling and the environment at 1093°C. Hold time had the effect of further decreasing the modulus at the latter stages of cycling with all other parameters equal--especially at the 566°C/103 MPa loading condition. In addition the modulus of the high temperature, low stress specimens increased slightly after the initial decrease indicating an effect of crack bridging by debris [4] or possibly the effect of the stiffening of the interfacial bond [10] caused by oxidation. Again, the stress and the environment contributed to the failure of the material in differing proportions depending on the loading condition.

The loop hysteretic energy followed the modulus trend in that the greatest values corresponded to the largest increments of modulus degradation. Unlike some of the moduli, which tended to increase over time, the loop hysteretic energy decreased with increasing cycles up to the point of failure in all cases. On a percentage basis, an incremental increase in the stress from a level located below the "knee" to one beyond results in a disproportionate increase in the loop hysteretic energy. This is due to the added damage resulting from the destruction of the 90° plies. This behavior occurred at both temperatures.

The stress strain curves reflected the trends from the loop hysteretic energy data in that large amounts of cyclic damage were represented by the relatively large areas of the hysteresis loop. In the high temperature/high stress cases, the traced area of the hysteresis loops remained relatively large in the absence of a corresponding modulus decrease. This was predominantly due to creep since the

effect of the environment was to stiffen the fiber/matrix bond preventing slippage. In addition, the modulus degradations were represented by a progressive secant slope decrease in the curves.

Creep behavior in some of the specimens was indicated by the progression of ε_{min} and ε_{max}. Both increased gradually at the same rate with increasing cycles such that ε_{max}-ε_{min} was constant. This indicated that a permanent deformation was occurring within the specimen. The increasing strains were not accompanied by a modulus decrease in the high stress specimens as in the case of cyclic damage in the form of matrix cracks. In the case of cyclic damage, the value of minimum strain remains relatively constant while the maximum strain increases with cycles to the point of failure in a load controlled test. In addition, a continual modulus decrease is indicative of cyclic damage and was present only initially at the 566°C/103 MPa loading condition.

The extent of fiber pull-out on the fracture surfaces was a function of both the exposure time and the temperature. The extent of fiber pull-out varied inversely with the exposure time at a constant temperature. An increasing stress level had the effect of reducing the cycles (and the exposure time) at failure decreasing the damage due to oxidation. This was indicated by the more extensive fiber pull-out at the higher stress level. The stress level also had the effect of inducing an amount of initial damage. This is reflected in the fact that, at a constant temperature, all the higher stress specimens failed before the lower stress specimens independent of the hold time. In addition, all the high

temperature, high stress specimens exhibited a fracture surface with brittle behavior around the edges and extensive pull-out toward the center. This was a result of the environment penetrating the outer edges of the material and causing extensive oxidation. The fibers so located failed in brittle fashion at the surface effectively decreasing the cross-sectional area until catastrophic failure occurred. Finally, The high temperature tests displayed the greatest extremes of fiber pullout. This was due to the accelerated damage caused by a synergistic effect of the cycling combined with the environment. This caused the high exposure duration/low stress specimens to fail in a predominantly brittle fashion and the low exposure duration/high stress specimens to fail in a brittle fashion at the edges and in a non-brittle fashion at the center.

VI. Recommendations

Now that the behavior of SiC-MAS5 is known at elevated temperatures, it follows that a model be created to predict the behavior of this and other like CMCs at elevated temperatures in oxidizing environments. SiC-MAS5 has a fatigue life (in terms of time) that can be expressed as a function of a number of variables (in decreasing order of importance,

$$Life=f(T, \sigma, h)$$

where T is the exposure duration, σ is the maximum stress, and h is the hold time. It is possible that a non-dimensional grouping could be made, in a fashion similar to the aerodynamicist's Reynolds Number, that would predict the behavior of a number of CMCs that derive their toughness from a by-design weak fiber matrix interface.

Bibliography

1. Askeland, D.R. The Science and Engineering of Materials. Boston: PWS Publishers, 1984.

2. Worthem, D.W. Thermomechanical Fatigue Behavior of Three Ceramic Matrix Composites. Contract NAS3-25266. Brook Park, Ohio: Sverdup Technology Inc., 1993.

3. Larsen D.C, Godard H.T., Stewart R.L., Chyung K., Linsey G.D., Murphy D.S. "BSG Doped CMCs for Thermal Durability," Proceedings of the 17th Annual Conference on Composites, Materials, and Structures. New York: Corning Inc., 1993.

4. Harris B., Habib F.A., Cooke R.G. "Matrix Cracking and the Mechanical Behavior of SiC-CAS Composites," (1992).

5. Allen R.F., Beevers C.J., Bowen P. "Fracture and Fatigue of a Nicalon/CAS Continuous Fiber-Reinforced Glass-Ceramic Matrix Composite," Composites, 24: 150-156 (1993).

6. Enhanced SiC-SiC Ceramic Matrix Composites: Du Pont's New Material System For Long-Life Performance in Oxidizing Environments. Newark Delaware: Du Pont Lanxide Composites Inc. 1994.

7. Headinger M.H. Du Pont Lanxide Composites Inc., Newark Delaware. Fax of test data. May 1994.

8. Karandikar P.G., Chou T. "Damage Development and Moduli Reductions in Nicalon/CaS Composites Under Static Fatigue and Cyclic Fatigue." Center for Composite Materials and Materials Science Program, University of Delaware, Newark, Delaware, 1993.

9. Steiner, C. Fatigue Behavior of a Cross-Ply Ceramic Matrix Composite at Elevated Temperature Under Tension-Tension Loading. MS Thesis, AFIT/GAE/ENY/94D. School of Engineering, Air Force Institute of Technology (AU), Wright-Patterson Air Force Base, Ohio, December 1994.

10. Larsen, D.C. Thermally Durable Glass Ceramic Matrix Composites: Interim Report, 31 December 1992. Contract F33615-90-C-5909. Corning, New York: Corning Inc., December 1992 (P-92-222-13-TP).

Appendix A: BASIC Program

Basic Program to Correct Load Versus Displacement
to Reflect Stress Versus Strain

```
      DIM X(2000), Y(2000), XL(2000), YL(2000), XU(2000), YU(2000)

      INPUT "ENTER DATA FILE (INCLUDING PATH) TO BE MODIFIED TO
REFLECT STRESS VS STRAIN"; FS
      INPUT "ENTER NUMBER OF DATA POINTS TO BE READ"; NUM
      INPUT "ENTER AREA OF THE SPECIMEN (square inches)"; AREA
      INPUT "ENTER GAUGE LENGTH OF EXTENSOMETER"; L

      OPEN FS FOR INPUT AS #1
      FOR I = 1 TO NUM
      IF I < 3 GOTO 10
      INPUT #1, X(I), Y(I)
      X(I) = X(I) * 1 / L
      Y(I) = Y(I) * 1 / AREA
10    NEXT
      CLOSE #1

      INPUT "ENTER THE DATA FILE (INCLUDING PATH) TO SAVE LOADING
DATA UNDER"; SSL$

      OPEN SSL$ FOR OUTPUT AS #2
      FOR J = 4 TO (NUM - 500) STEP 4
      XL(J) = X(J)
      YL(J) = Y(J)
      WRITE #2, XL(J), YL(J)
      NEXT
      CLOSE #2

      INPUT "ENTER THE DATA FILE (INCLUDING PATH) TO SAVE
UNLOADING DATA UNDER"; SSU$
      OPEN SSUS FOR OUTPUT AS #3
      FOR K = (NUM - 500) TO NUM STEP 4
      XU(K) = X(K)
      YU(K) = Y(K)
      WRITE #3, XU(K), YU(K)
      NEXT
      CLOSE #3
```

Appendix B: Raw Data

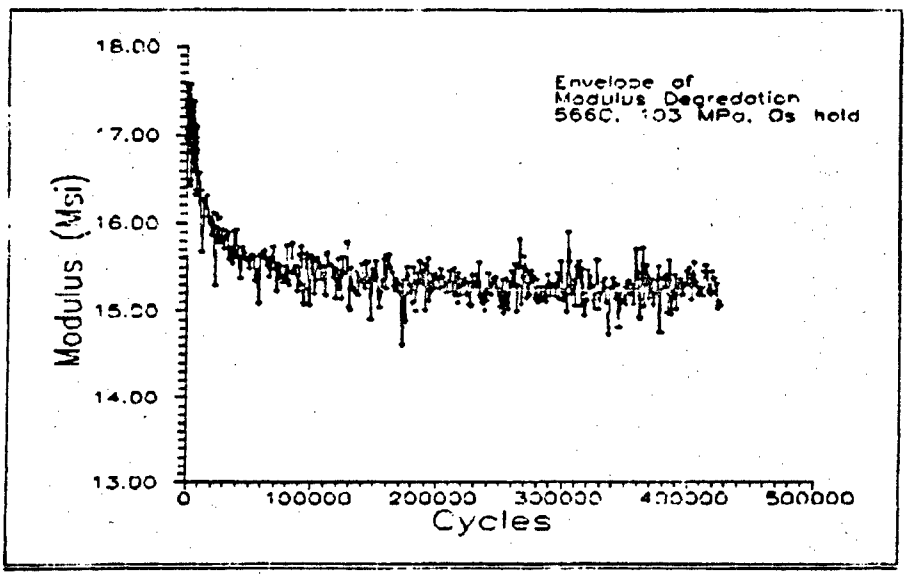

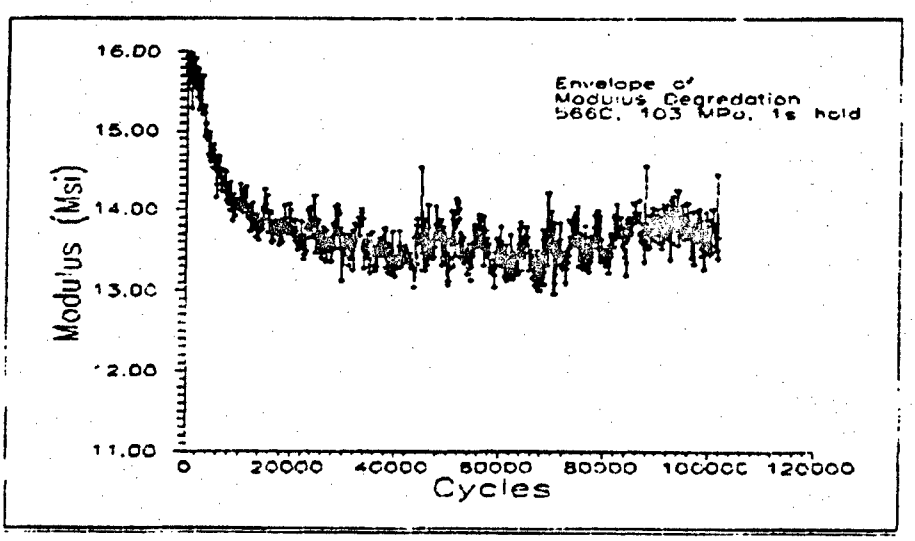

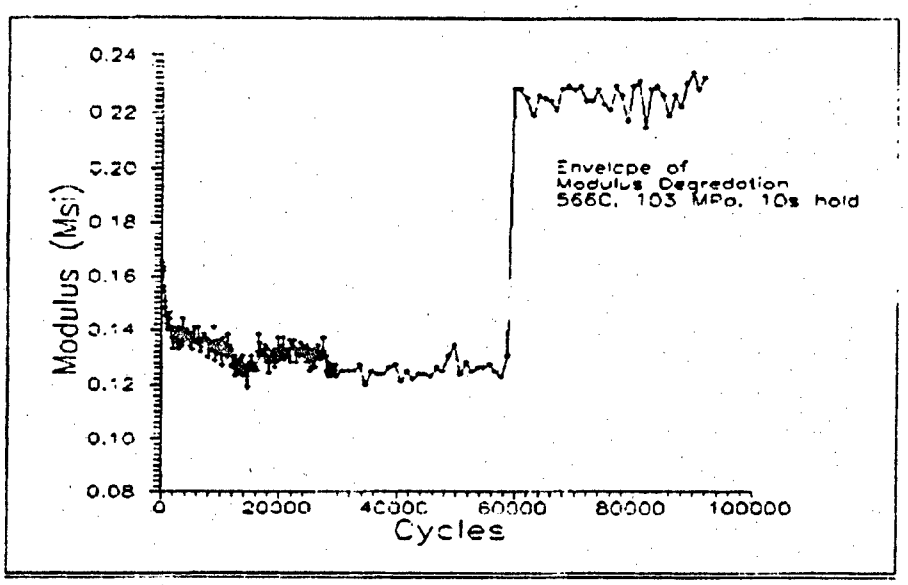
Envelope of
Modulus Degredation
566C, 103 MPa, 10s hold
Modulus (Msi)
0.24
0.22
0.20
0.18
0.16
0.14
0.12
0.10
0.08
0
20000
40000
60000
80000
100000
Cycles

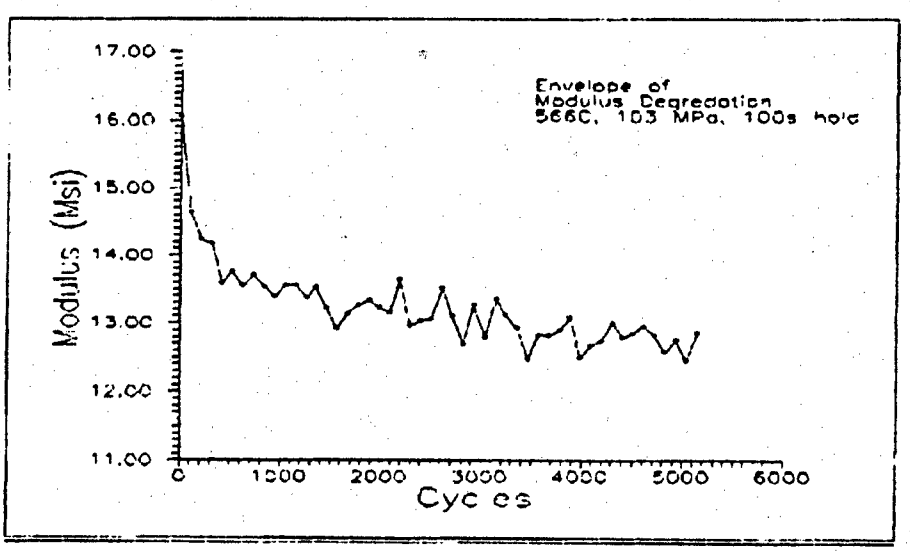
Envelope of
Modulus Degredation
566C, 103 MPa, 100s hold
Modulus (Msi)
17.00
16.00
15.00
14.00
13.00
12.00
11.00
0
1000
2000
3000
4000
5000
6000
Cycles

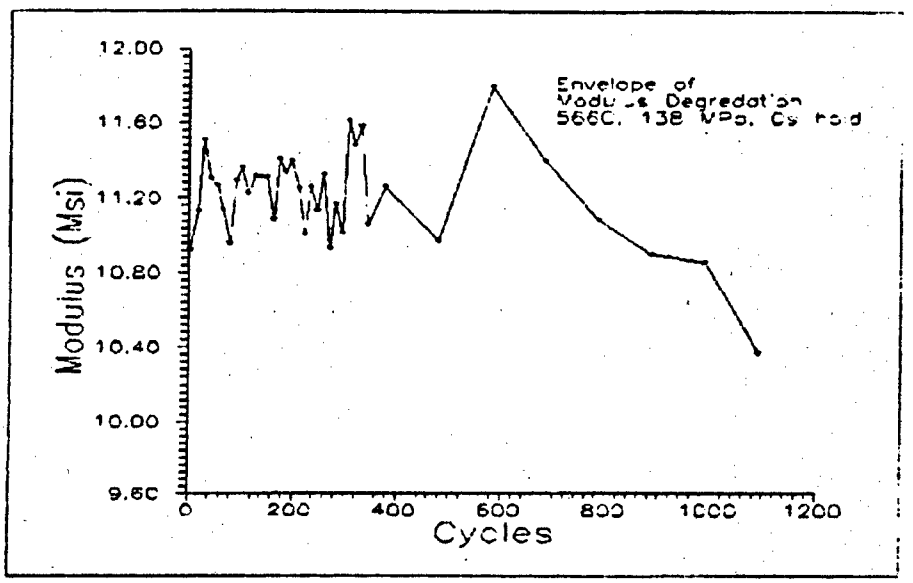
12.00
11.60
11.20
10.80
10.40
10.00
9.60
Modulus (Msi)
0
200
400
600
800
1000
1200
Cycles
Envelope of
Modulus Degredation
566C, 138 MPa, 0s hold

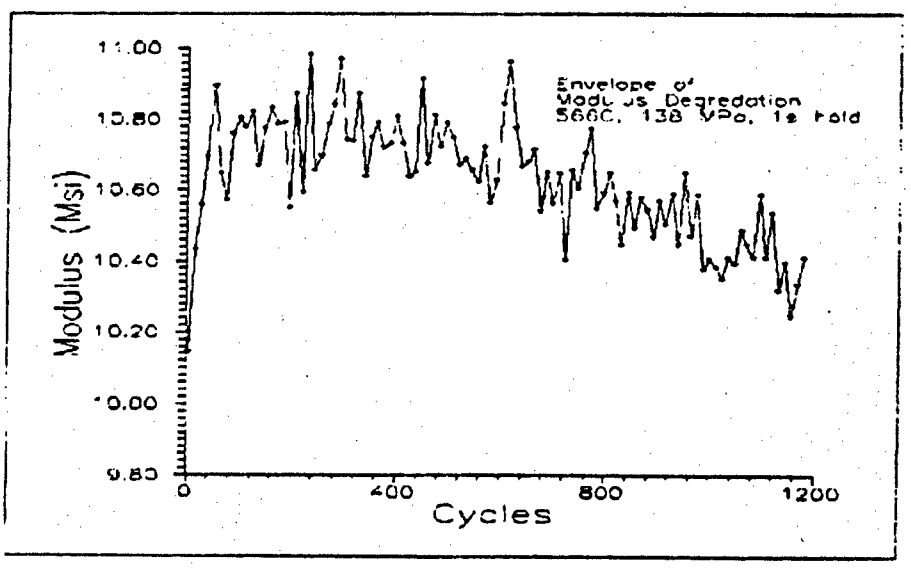
11.00
10.80
10.60
10.40
10.20
10.00
9.80
Modulus (Msi)
0
400
800
1200
Cycles
Envelope of
Modulus Degredation
566C, 138 MPa, 1s hold

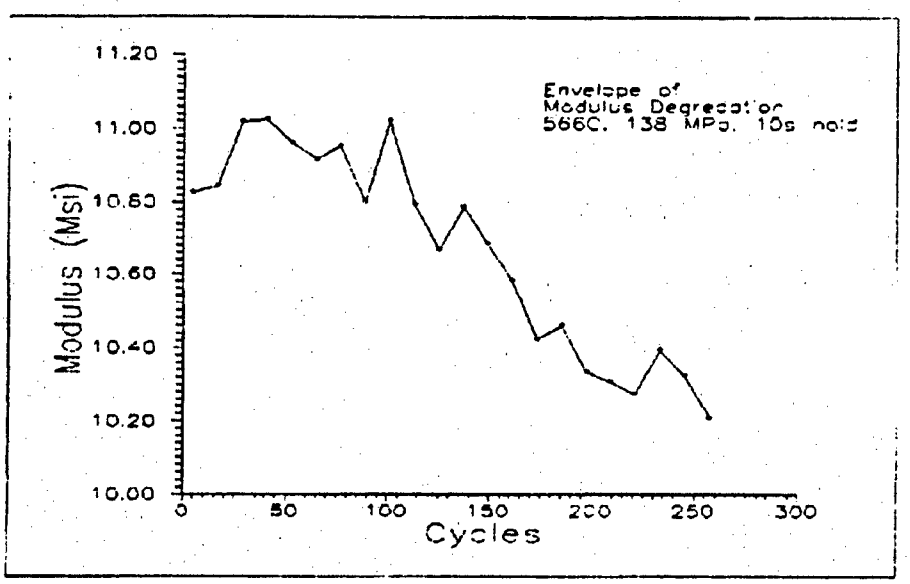
Envelope of
Modulus Degredation
566C, 138 MPa, 10s hold
Modulus (Msi)
11.20
11.00
10.80
10.60
10.40
10.20
10.00
0
50
100
150
200
250
300
Cycles

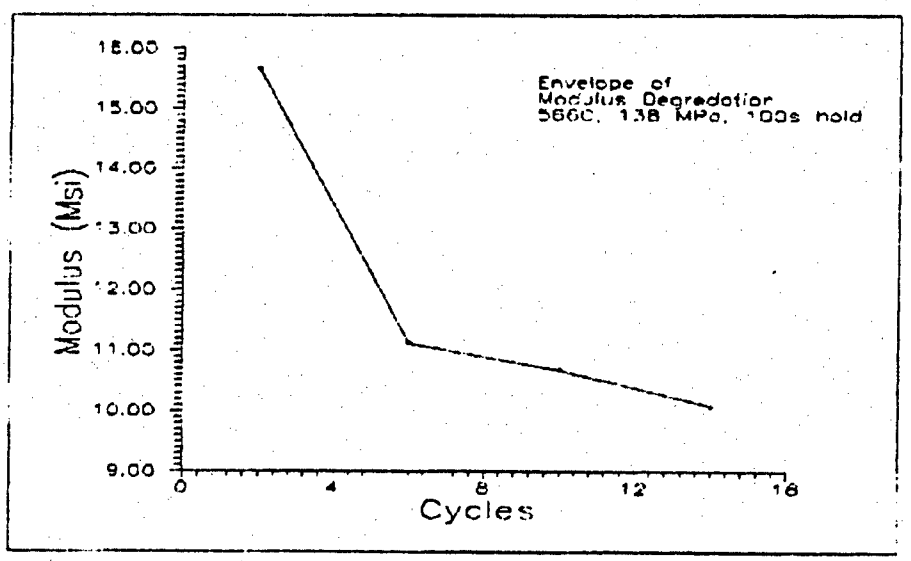
Envelope of
Modulus Degredation
566C, 138 MPa, 100s hold
Modulus (Msi)
16.00
15.00
14.00
13.00
12.00
11.00
10.00
9.00
0
4
8
12
16
Cycles

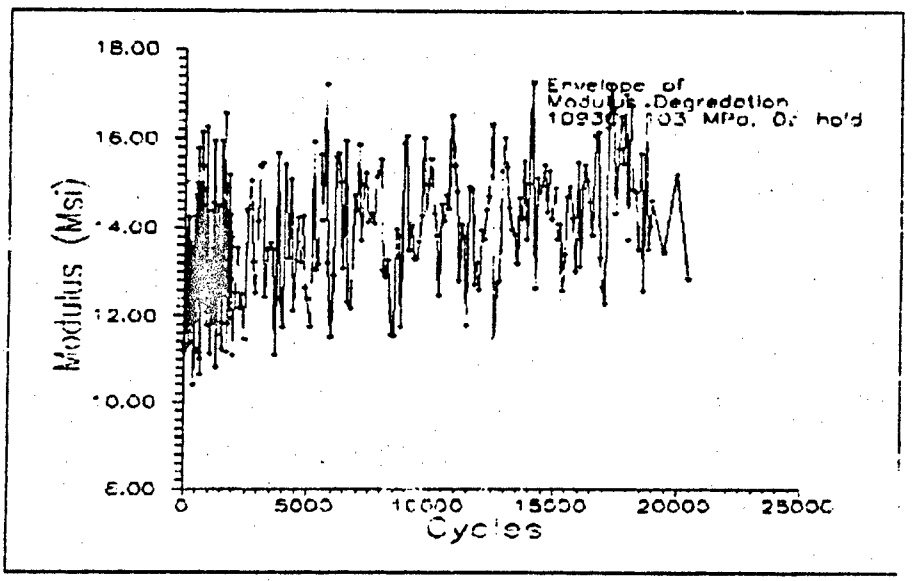
18.00
16.00
14.00
12.00
10.00
8.00
Modulus (Msi)
0
5000
10000
15000
20000
25000
Cycles
Envelope of
Modulus Degredation

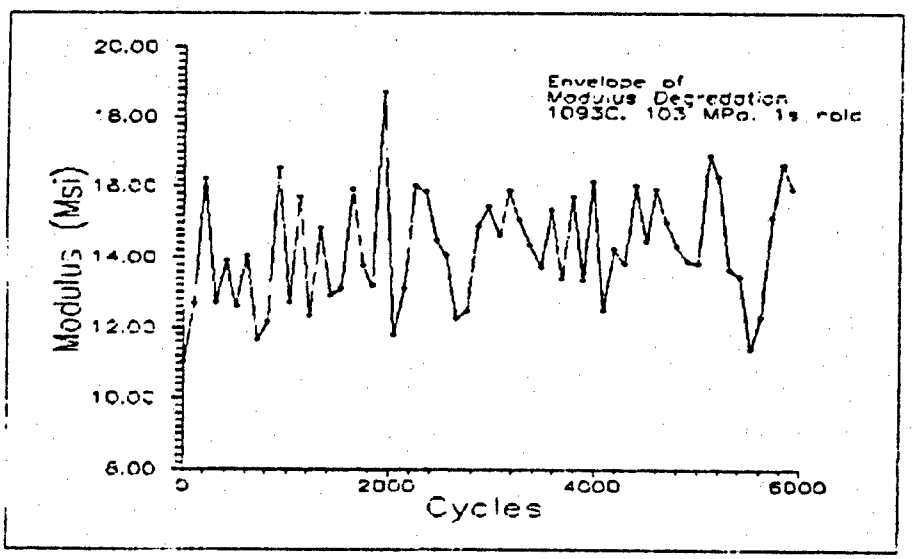
20.00
18.00
16.00
14.00
12.00
10.00
8.00
Modulus (Msi)
0
2000
4000
6000
Cycles
Envelope of
Modulus Degredation

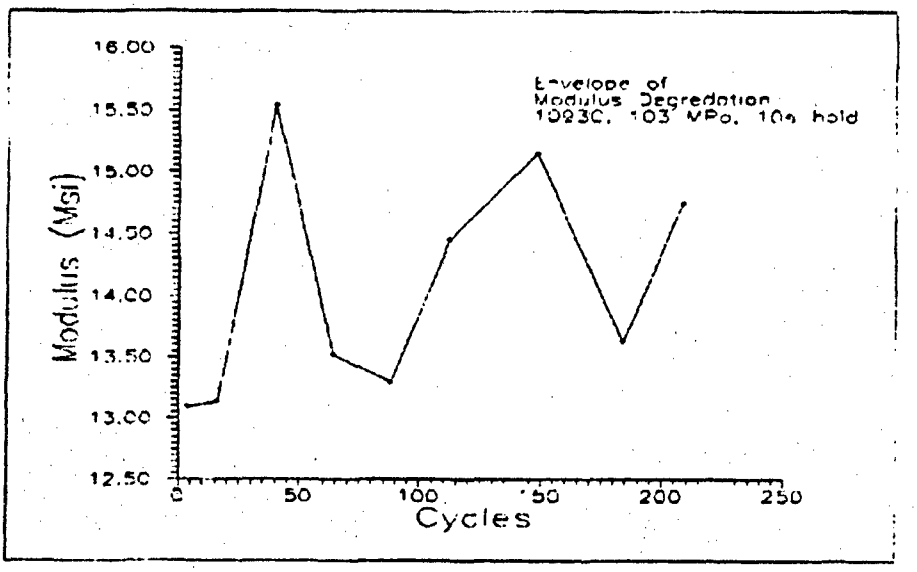
Envelope of
Modulus Degredation
1093C, 103 MPa, 10s hold
Modulus (Msi)
16.00
15.50
15.00
14.50
14.00
13.50
13.00
12.50
0
50
100
150
200
250
Cycles

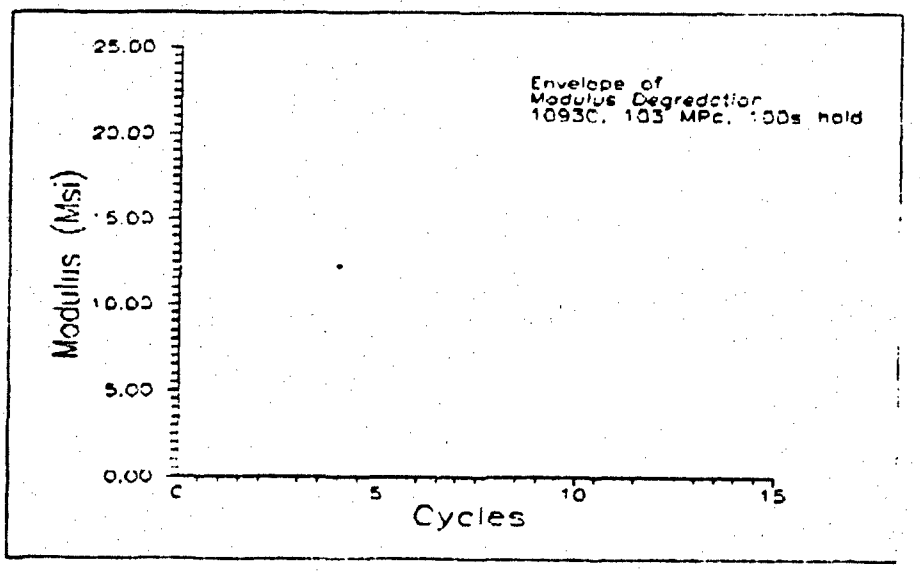
Envelope of
Modulus Degredation
1093C, 103 MPa, 100s hold
Modulus (Msi)
25.00
20.00
15.00
10.00
5.00
0.00
0
5
10
15
Cycles

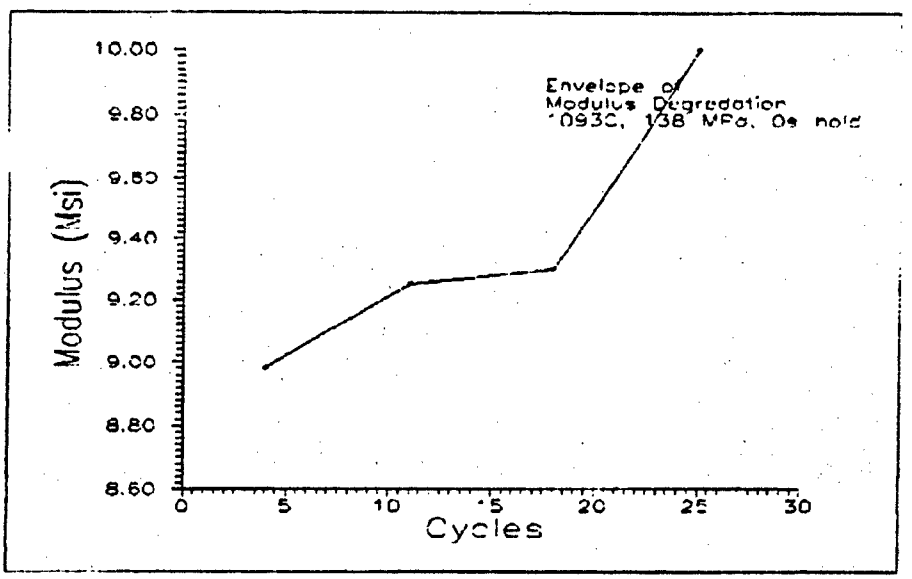
Envelope of
Modulus Degredation
1093C, 138 MPa, 0s hold
Modulus (Msi)
10.00
9.80
9.60
9.40
9.20
9.00
8.80
8.60
0
5
10
15
20
25
30
Cycles

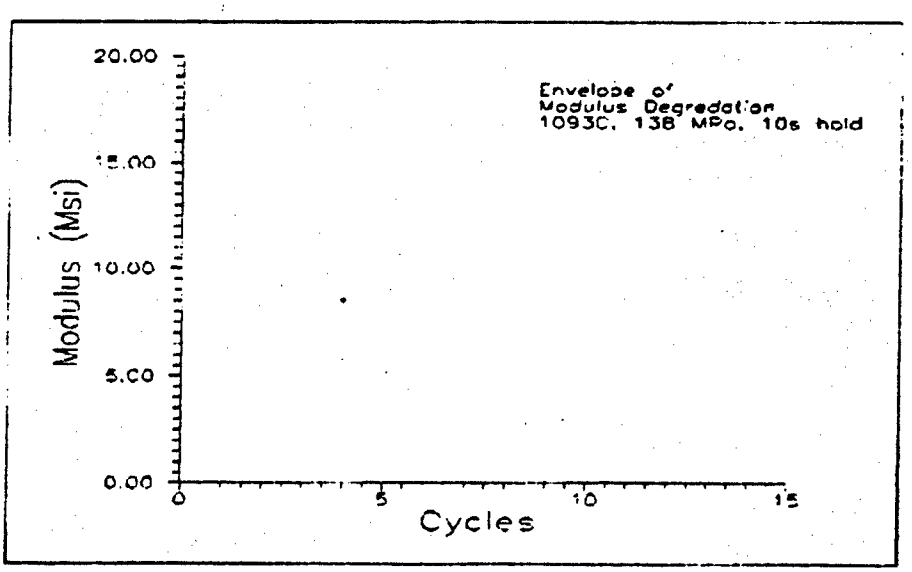
Envelope of
Modulus Degredation
1093C, 138 MPa, 10s hold
Modulus (Msi)
20.00
15.00
10.00
5.00
0.00
0
5
10
15
Cycles

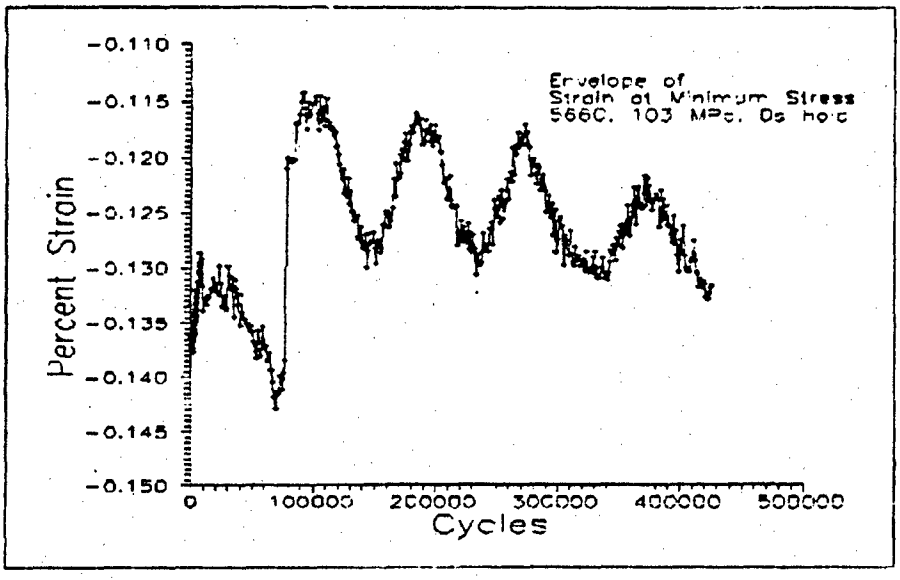
Envelope of
Strain at Minimum Stress
566C, 103 MPa, 0s hold
Percent Strain
-0.110
-0.115
-0.120
-0.125
-0.130
-0.135
-0.140
-0.145
-0.150
0
100000
200000
300000
400000
500000
Cycles

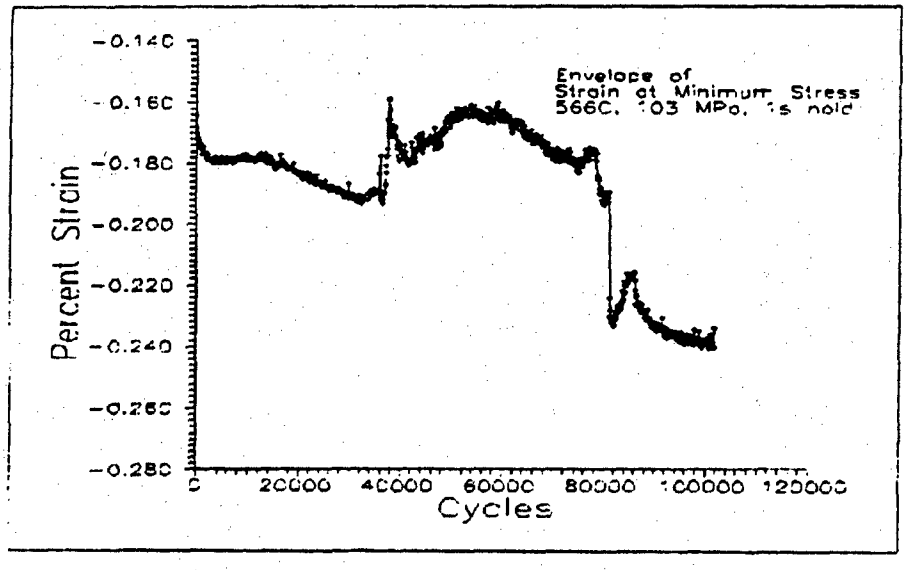
Envelope of
Strain at Minimum Stress
566C, 103 MPa, 1s hold
Percent Strain
-0.140
-0.160
-0.180
-0.200
-0.220
-0.240
-0.260
-0.280
0
20000
40000
60000
80000
100000
120000
Cycles

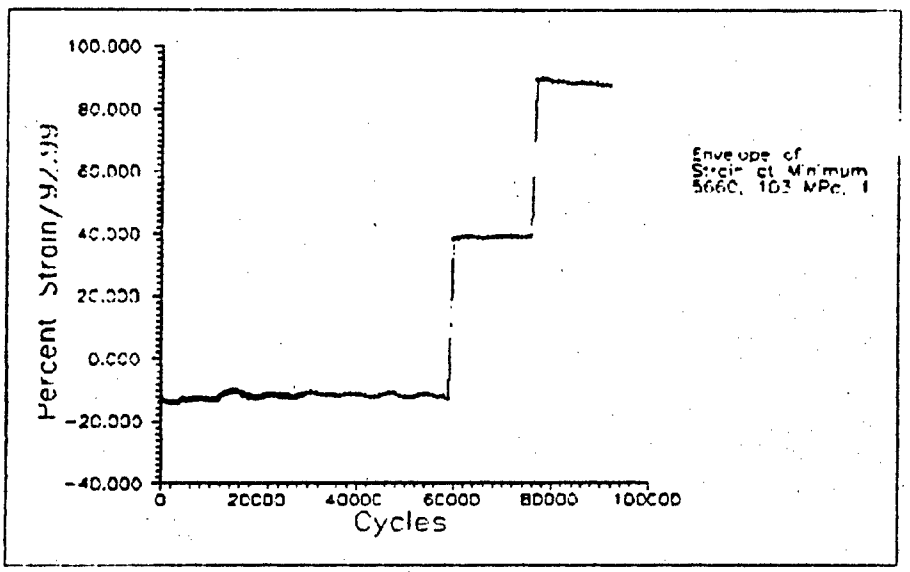
100.000
80.000
60.000
40.000
20.000
0.000
-20.000
-40.000
Percent Strain/9
0
20000
40000
60000
80000
100000
Cycles
Envelope of
Strain at Minimum
566C, 103 MPa, 1

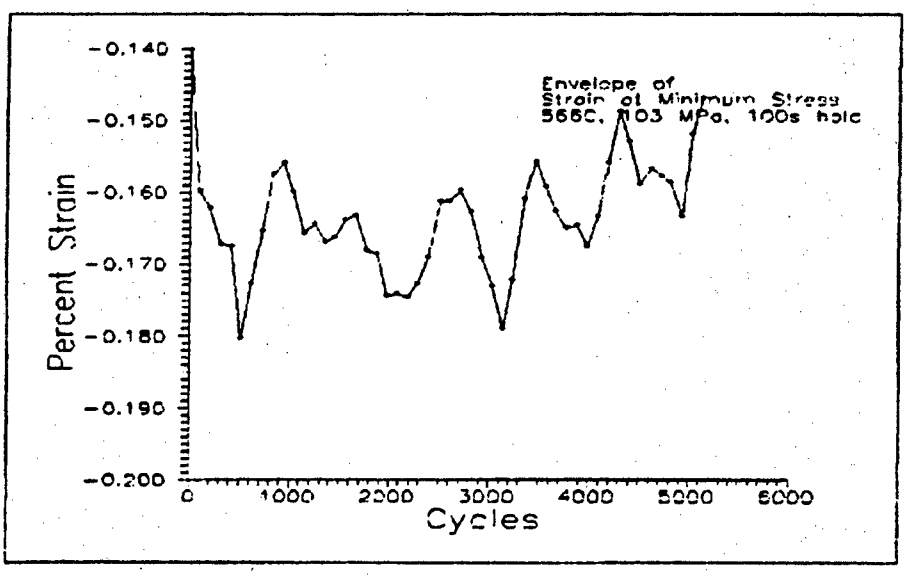
-0.140
-0.150
-0.160
-0.170
-0.180
-0.190
-0.200
Percent Strain
0
1000
2000
3000
4000
5000
6000
Cycles
Envelope of
Strain at Minimum Stress
566C, 103 MPa, 100s hold

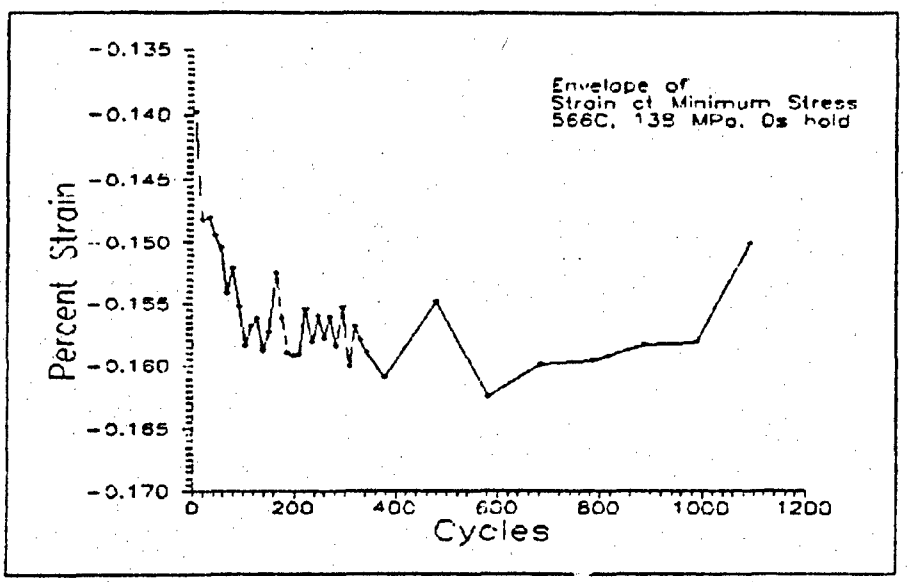
Envelope of
Strain at Minimum Stress
566C, 139 MPa, 0s hold
Percent Strain
-0.135
-0.140
-0.145
-0.150
-0.155
-0.160
-0.165
-0.170
0
200
400
600
800
1000
1200
Cycles

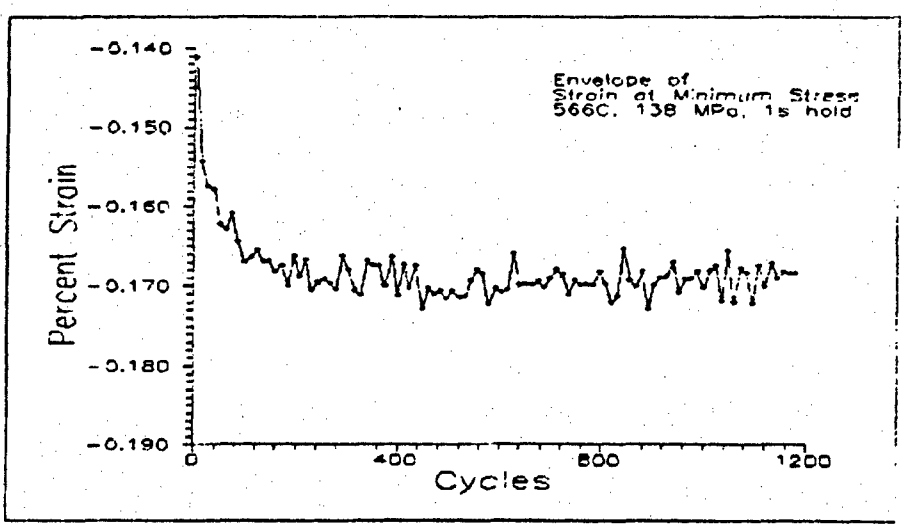
Envelope of
Strain at Minimum Stress
566C, 138 MPa, 1s hold
Percent Strain
-0.140
-0.150
-0.160
-0.170
-0.180
-0.190
0
400
800
1200
Cycles

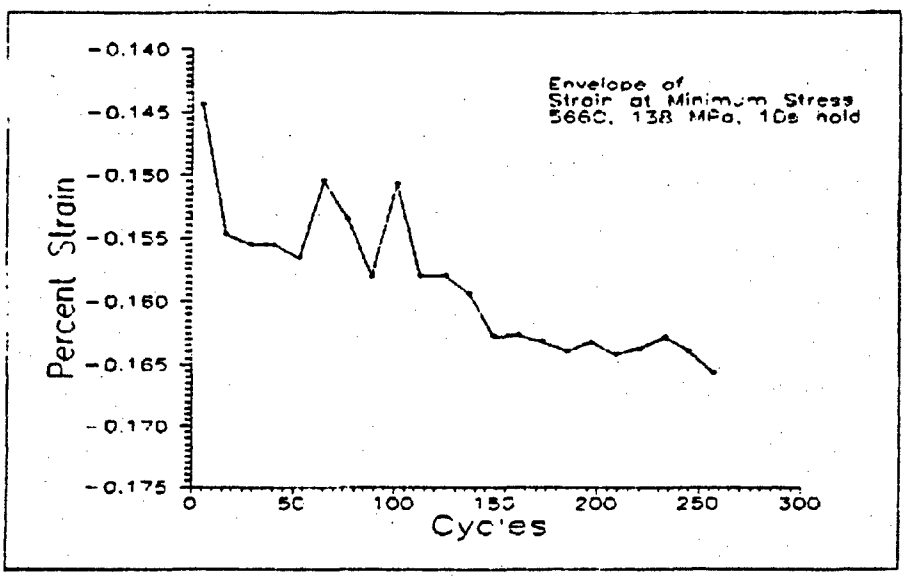
Envelope of
Strain at Minimum Stress
566C, 138 MPa, 10s hold
Percent Strain
-0.140
-0.145
-0.150
-0.155
-0.160
-0.165
-0.170
-0.175
0
50
100
150
200
250
300
Cycles

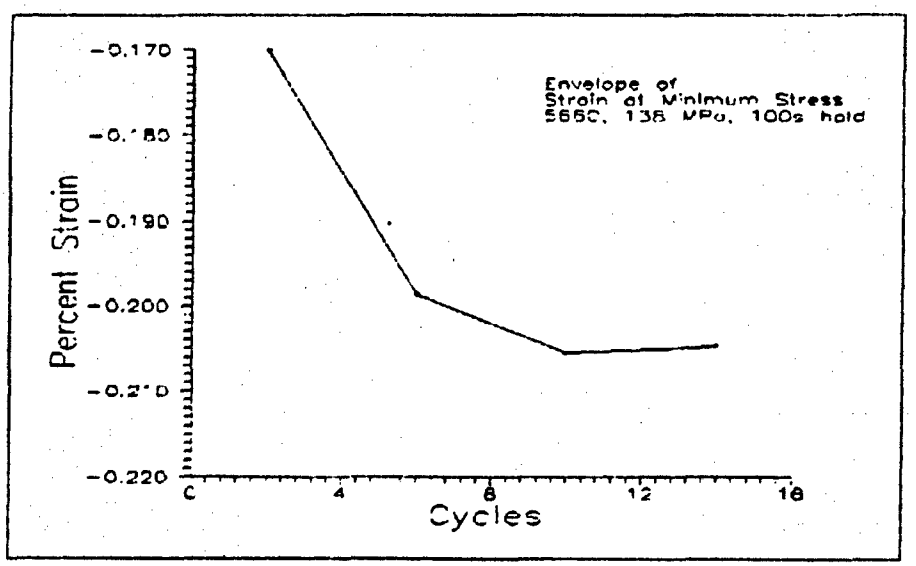
Envelope of
Strain at Minimum Stress
566C, 138 MPa, 100s hold
Percent Strain
-0.170
-0.180
-0.190
-0.200
-0.210
-0.220
0
4
8
12
16
Cycles

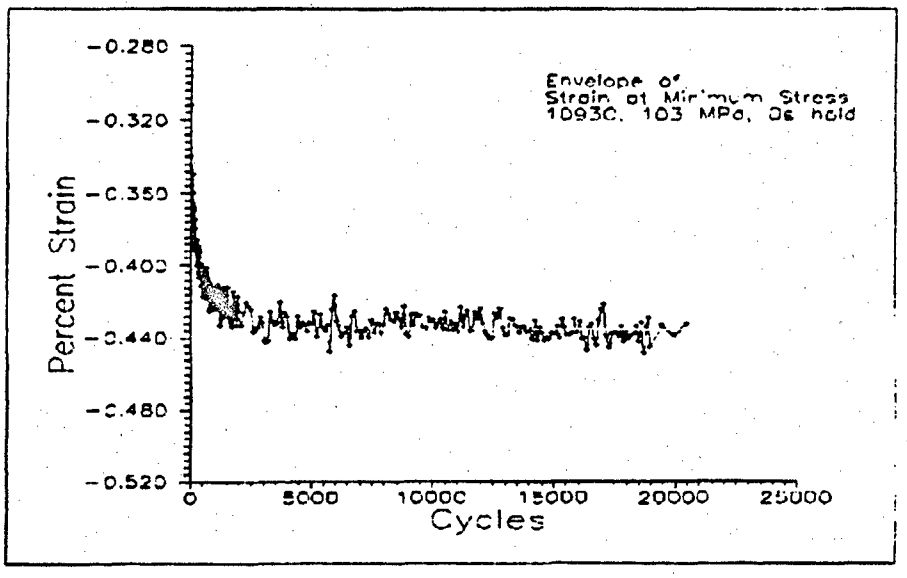
Envelope of
Strain at Minimum Stress
1093C, 103 MPa, 0s hold
Percent Strain
-0.280
-0.320
-0.360
-0.400
-0.440
-0.480
-0.520
0
5000
10000
15000
20000
25000
Cycles

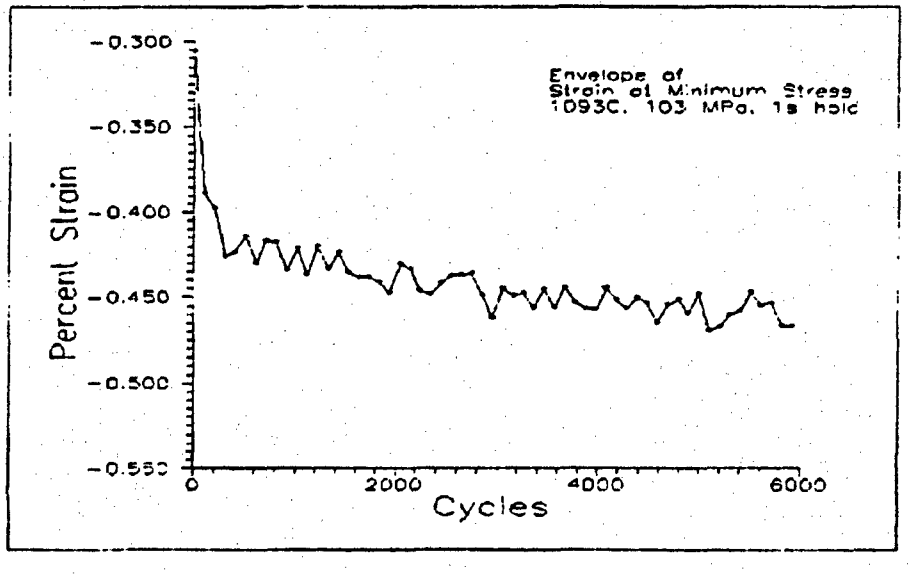
Envelope of
Strain at Minimum Stress
1093C, 103 MPa, 1s hold
Percent Strain
-0.300
-0.350
-0.400
-0.450
-0.500
-0.550
0
2000
4000
6000
Cycles

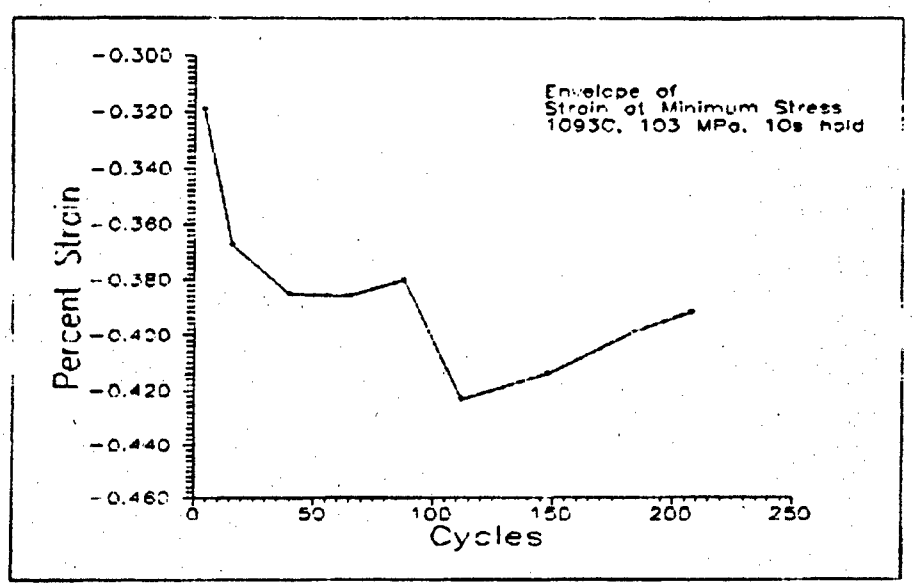
Envelope of
Strain at Minimum Stress
1093C, 103 MPa, 10s hold
Percent Strain
-0.300
-0.320
-0.340
-0.360
-0.380
-0.400
-0.420
-0.440
-0.460
0
50
100
150
200
250
Cycles

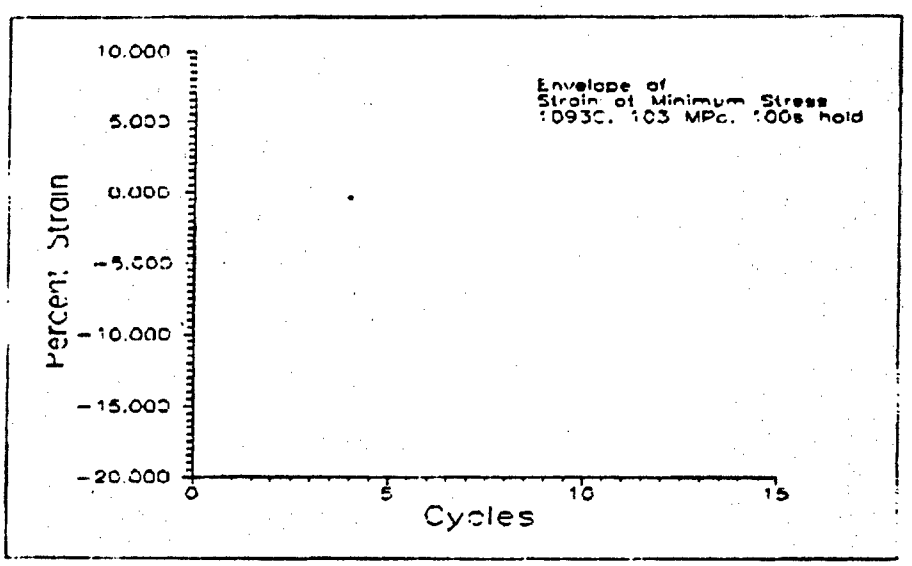
Envelope of
Strain at Minimum Stress
1093C, 103 MPa, 10s hold
Percent Strain
10.000
5.000
0.000
-5.000
-10.000
-15.000
-20.000
0
5
10
15
Cycles

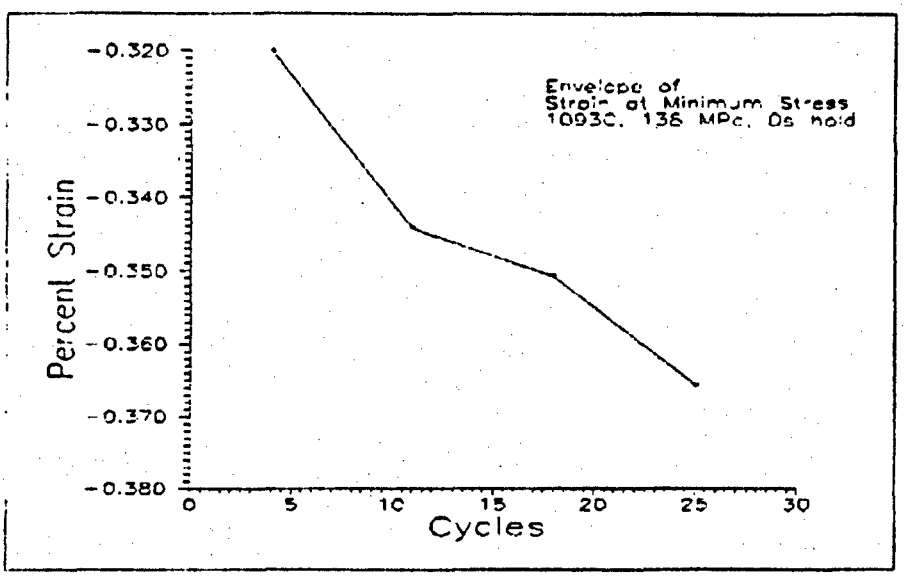
Envelope of
Strain at Minimum Stress
1093C, 138 MPa, 0s hold
Percent Strain
-0.320
-0.330
-0.340
-0.350
-0.360
-0.370
-0.380
0
5
10
15
20
25
30
Cycles

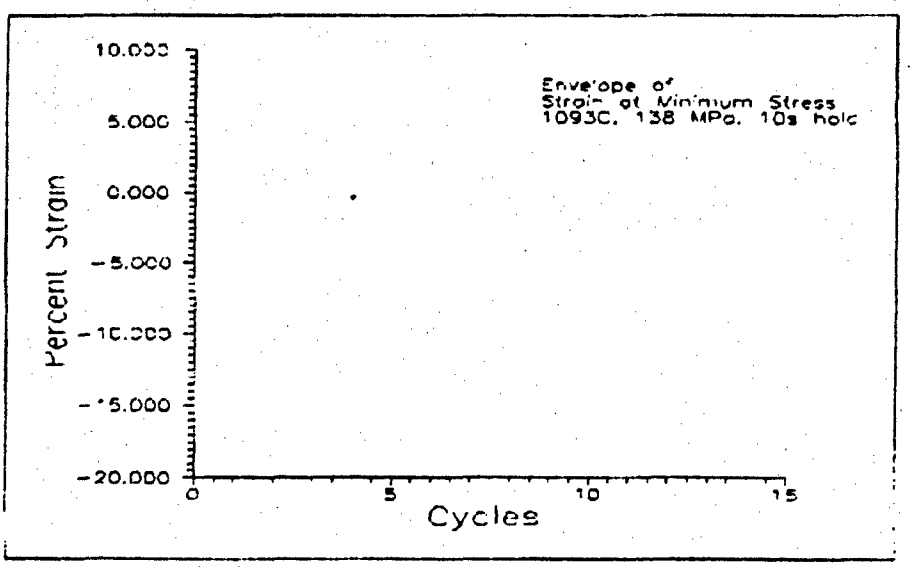
Envelope of
Strain at Minimum Stress
1093C, 138 MPa, 10s hold
Percent Strain
10.000
5.000
0.000
-5.000
-10.000
-15.000
-20.000
0
5
10
15
Cycles

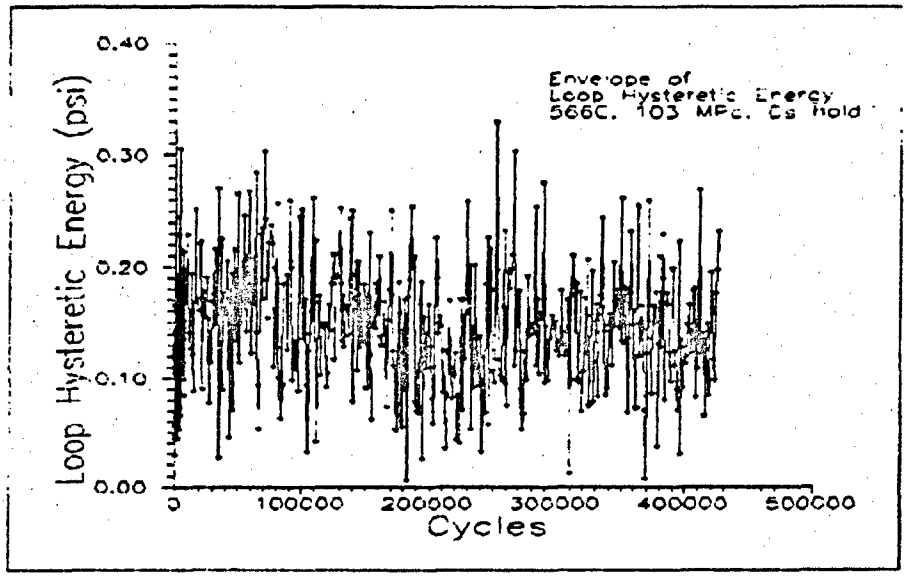
Envelope of
Loop Hysteretic Energy
566C, 103 MPa, Cs hold
Loop Hysteretic Energy (psi)
0.40
0.30
0.20
0.10
0.00
0
100000
200000
300000
400000
500000
Cycles

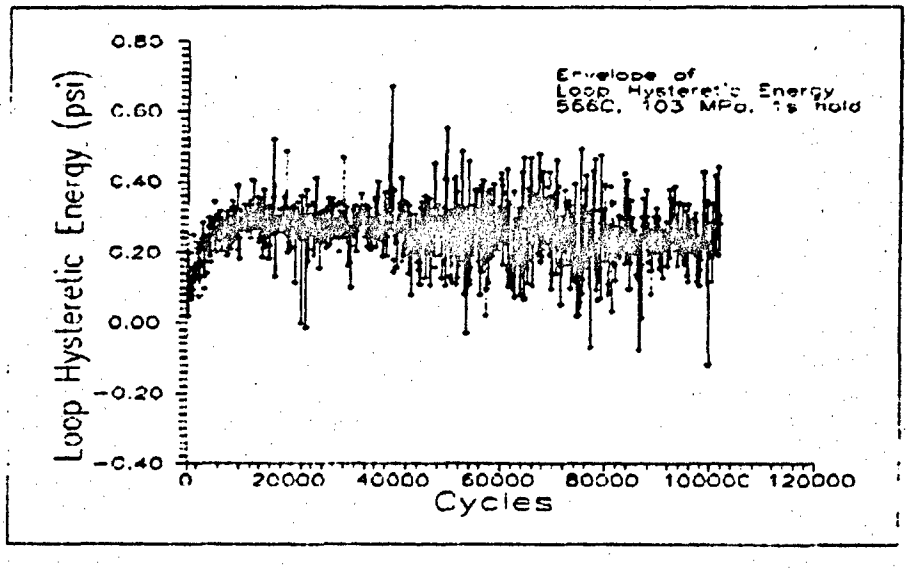
Envelope of
Loop Hysteretic Energy
566C, 103 MPa, 1s hold
Loop Hysteretic Energy (psi)
0.80
0.60
0.40
0.20
0.00
-0.20
-0.40
0
20000
40000
60000
80000
100000
120000
Cycles

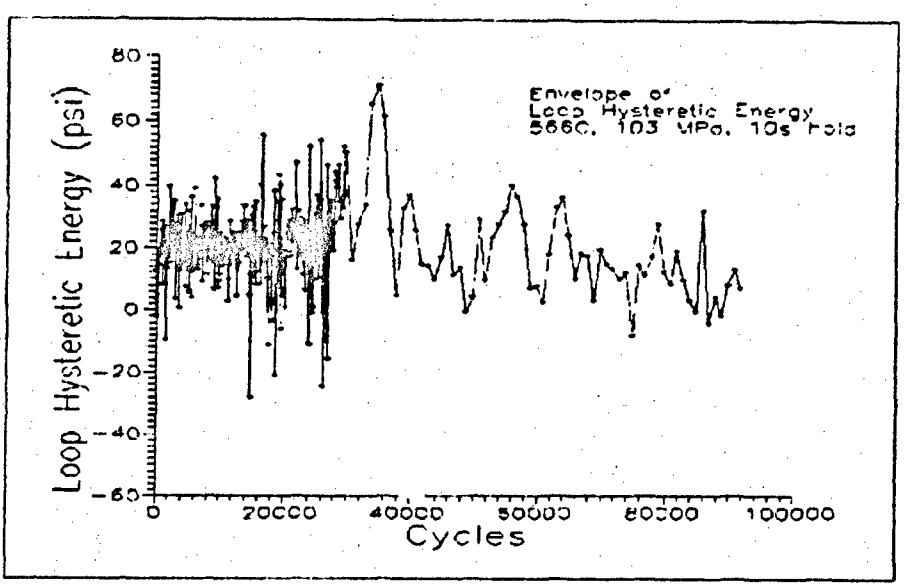
Envelope of
Loop Hysteretic Energy
566C, 103 MPa, 10s hold
Loop Hysteretic Energy (psi)
80
60
40
20
0
-20
-40
-60
0
20000
40000
50000
80000
100000
Cycles

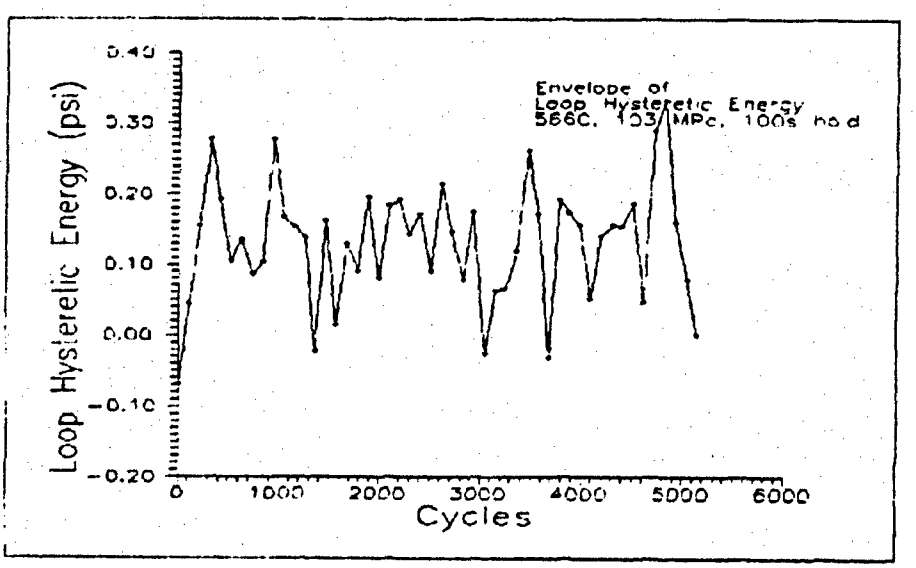
Envelope of
Loop Hysteretic Energy
566C, 103 MPa, 100s hold
Loop Hysteretic Energy (psi)
0.40
0.30
0.20
0.10
0.00
-0.10
-0.20
0
1000
2000
3000
4000
5000
6000
Cycles

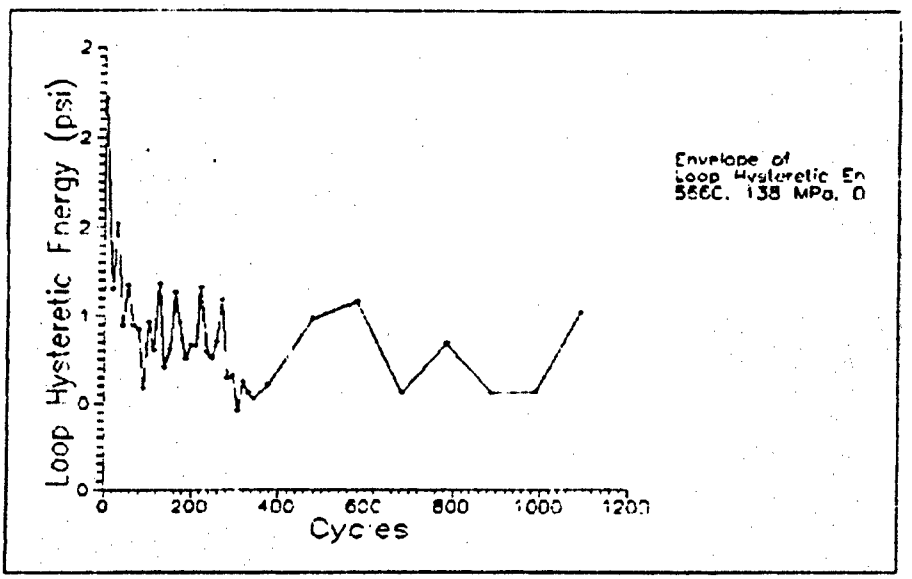
Loop Hysteretic Energy (psi)
Cycles
0
200
400
600
800
1000
1200
Envelope of
Loop Hysteretic En
566C, 138 MPa, 0

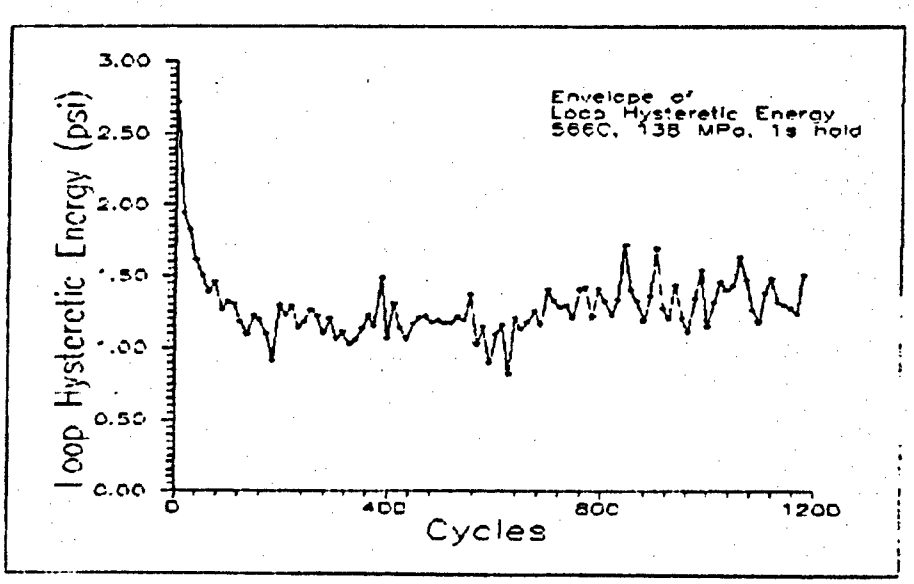
Loop Hysteretic Energy (psi)
3.00
2.50
2.00
1.50
1.00
0.50
0.00
Cycles
0
400
800
1200
Envelope of
Loop Hysteretic Energy
566C, 138 MPa, 1s hold

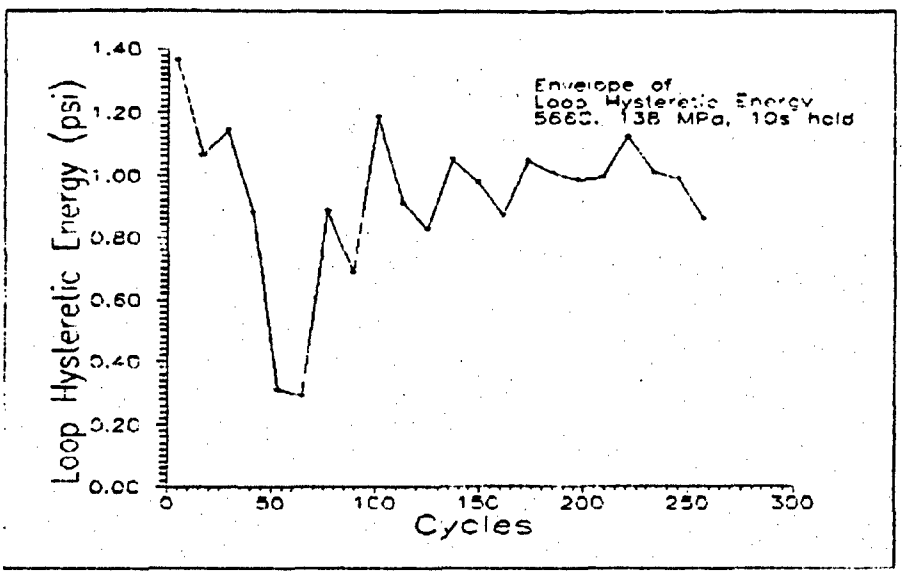
Envelope of
Loop Hysteretic Energy
566C, 138 MPa, 10s hold
Loop Hysteretic Energy (psi)
1.40
1.20
1.00
0.80
0.60
0.40
0.20
0.00
0
50
100
150
200
250
300
Cycles

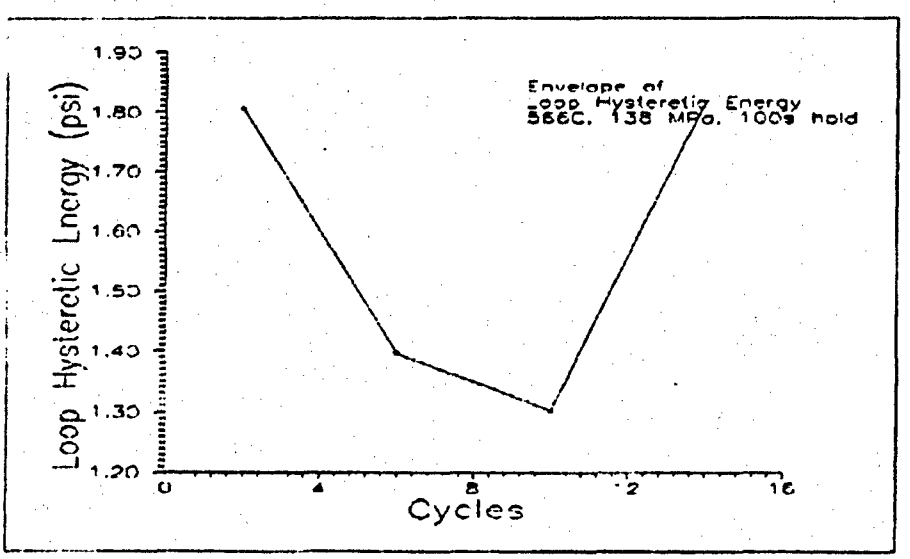
Envelope of
Loop Hysteretic Energy
566C, 138 MPa, 100s hold
Loop Hysteretic Energy (psi)
1.90
1.80
1.70
1.60
1.50
1.40
1.30
1.20
0
4
8
12
16
Cycles

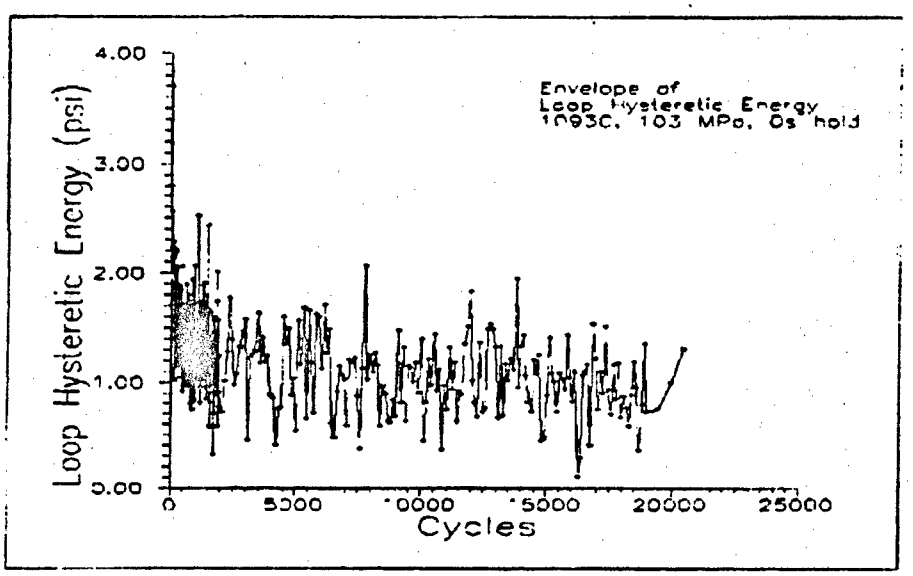
Envelope of
Loop Hysteretic Energy
1093C, 103 MPa, 0s hold
Loop Hysteretic Energy (psi)
4.00
3.00
2.00
1.00
0.00
0
5000
10000
15000
20000
25000
Cycles

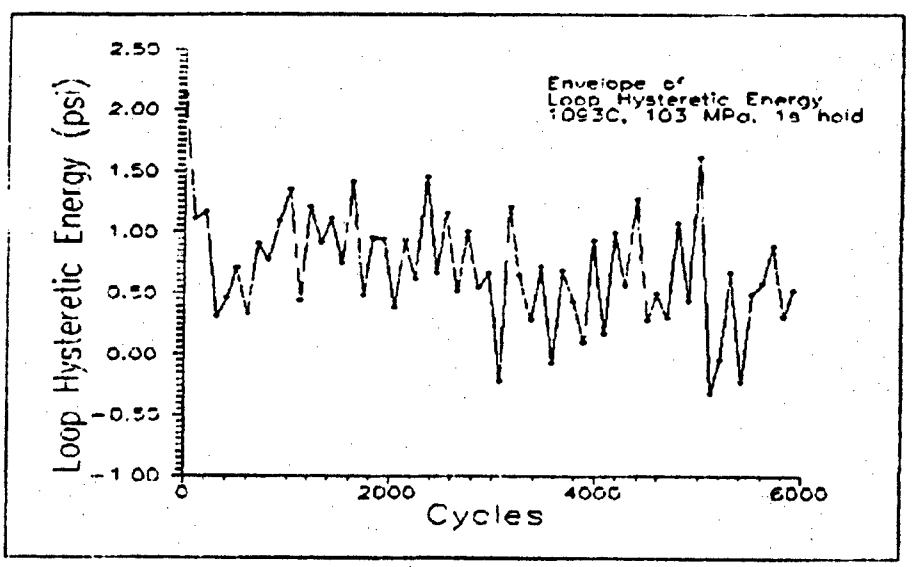
Envelope of
Loop Hysteretic Energy
1093C, 103 MPa, 1s hold
Loop Hysteretic Energy (psi)
2.50
2.00
1.50
1.00
0.50
0.00
-0.50
-1.00
0
2000
4000
6000
Cycles

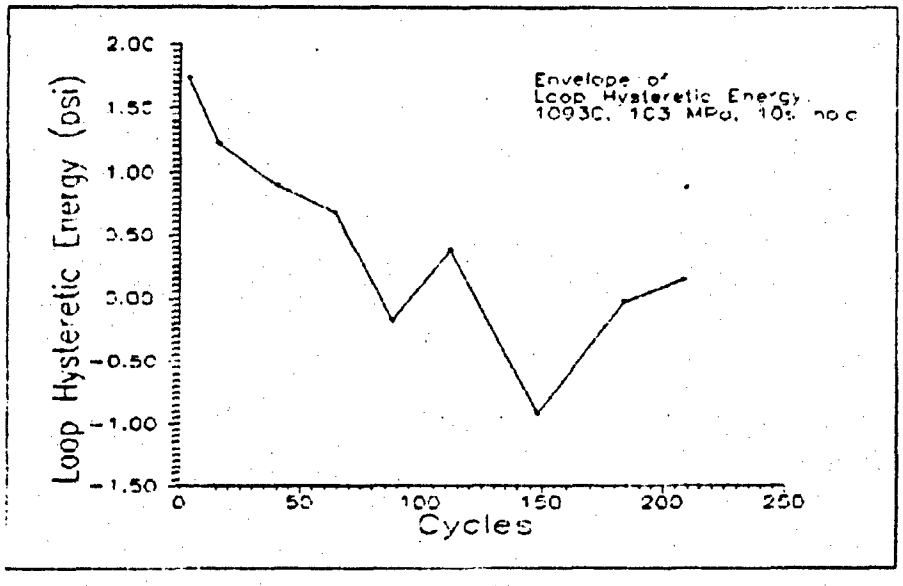
Envelope of
Loop Hysteretic Energy
1093C, 103 MPa, 10s no c
Loop Hysteretic Energy (psi)
2.00
1.50
1.00
0.50
0.00
-0.50
-1.00
-1.50
0
50
100
150
200
250
Cycles

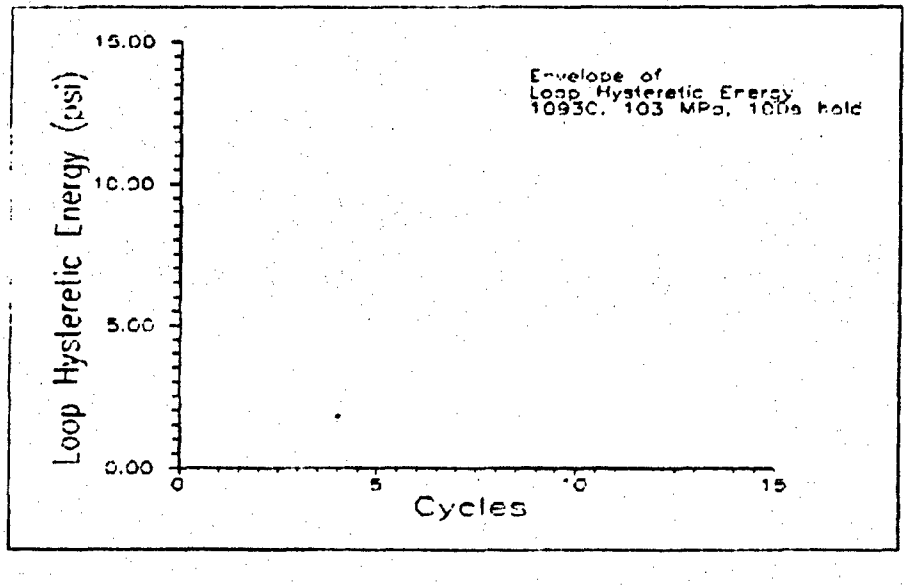
Envelope of
Loop Hysteretic Energy
1093C, 103 MPa, 100s hold
Loop Hysteretic Energy (psi)
15.00
10.00
5.00
0.00
0
5
10
15
Cycles

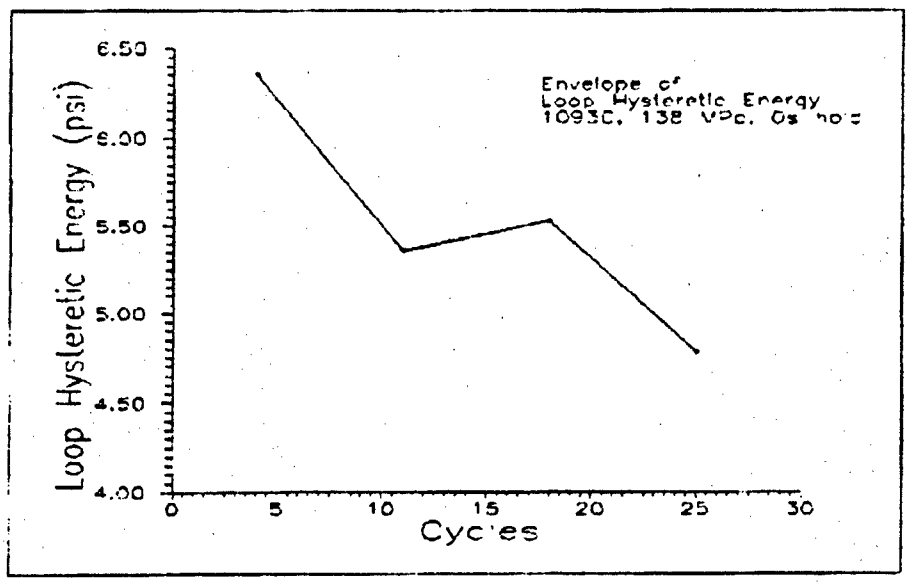
Envelope of
Loop Hysteretic Energy
1093C, 138 MPa, 0s hold
Loop Hysteretic Energy (psi)
6.50
6.00
5.50
5.00
4.50
4.00
0
5
10
15
20
25
30
Cycles

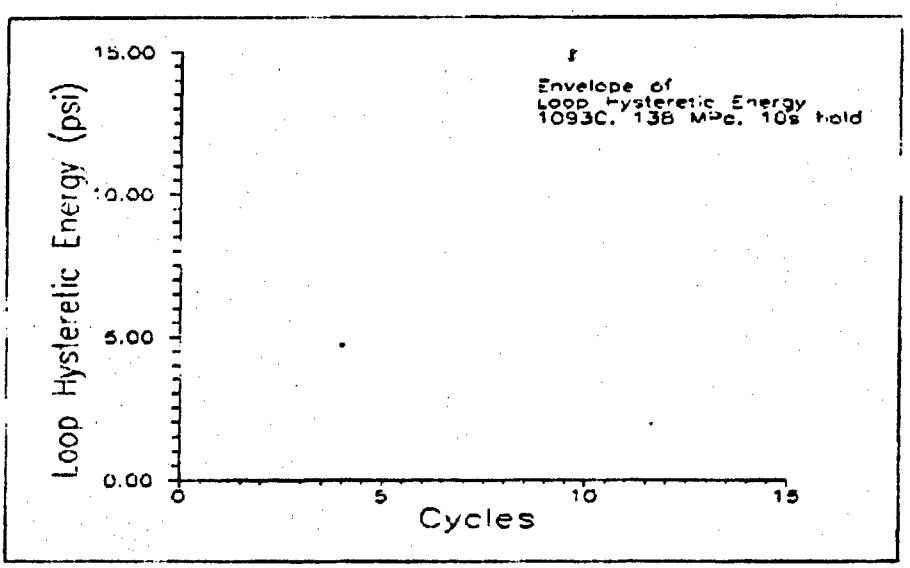
Envelope of
Loop Hysteretic Energy
1093C, 138 MPa, 10s hold
Loop Hysteretic Energy (psi)
15.00
10.00
5.00
0.00
0
5
10
15
Cycles

This Page Intentionally Left Blank

Appendix C: Fractured Surfaces

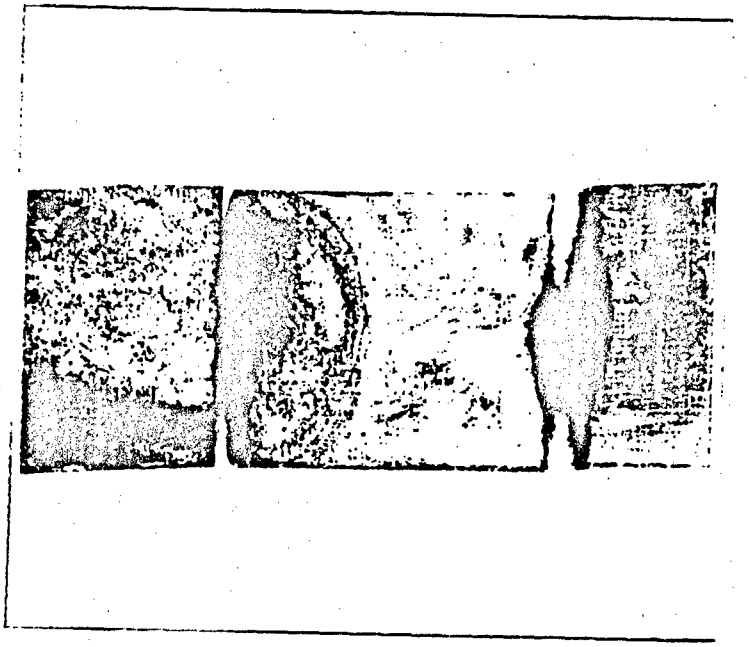

Fractured Surface at T=1156 seconds, 8x.

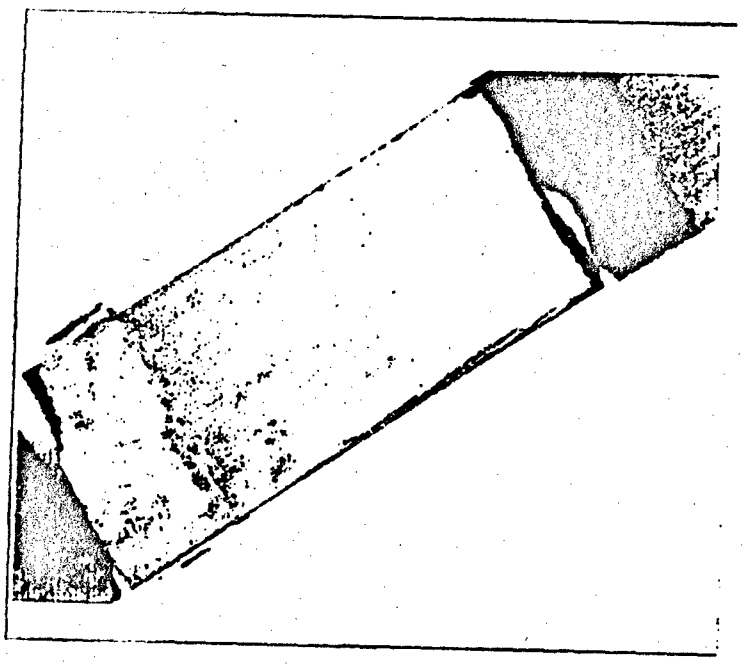

Fractured Surface T=1414 seconds, 8x.

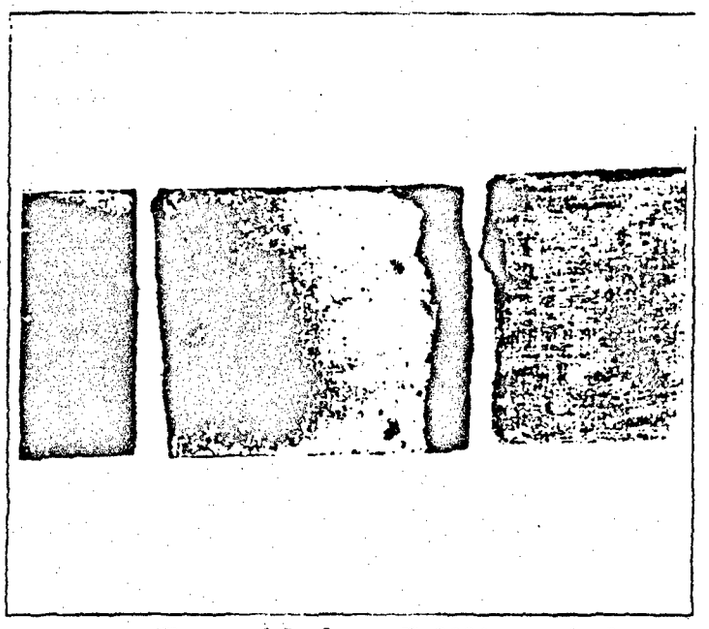

Fractured Surface at T=2390 seconds, 8x.

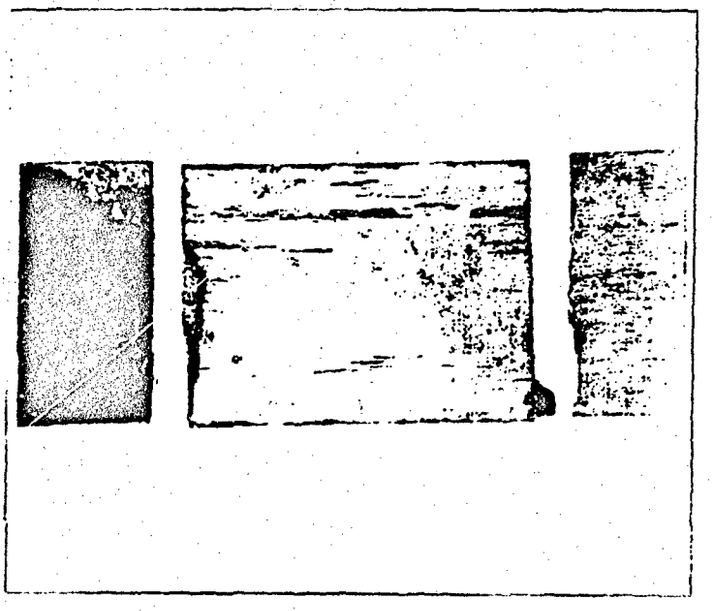

Fractured Surface at T=2915 Seconds, 8x.

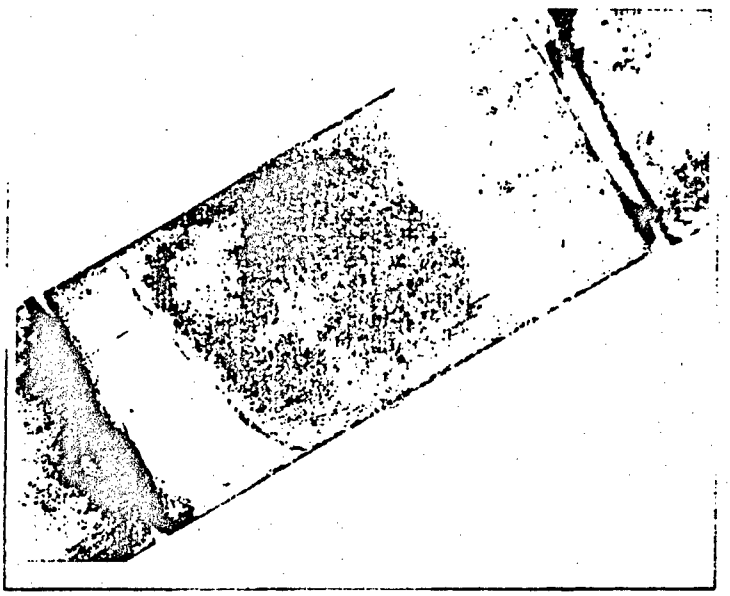

Fractured Surface at T=203700 seconds. 8x.

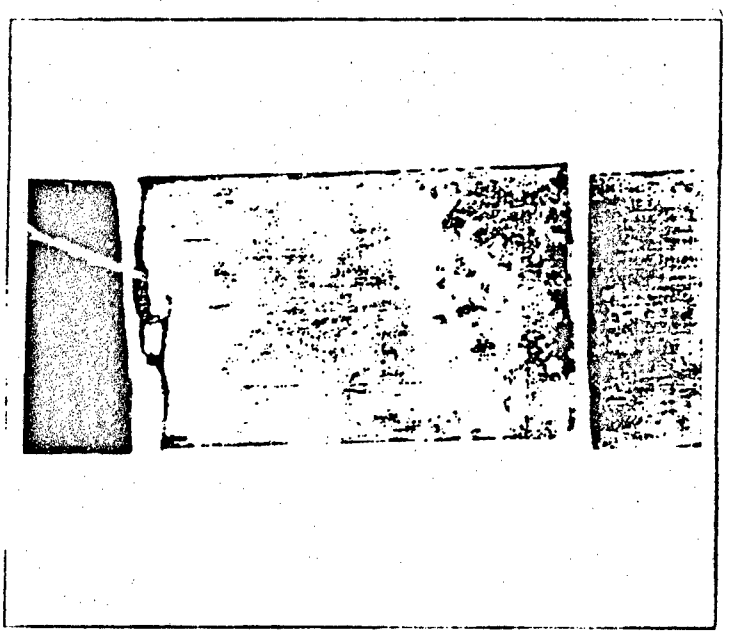

Fractured Surface at T=425299 seconds, 8x.

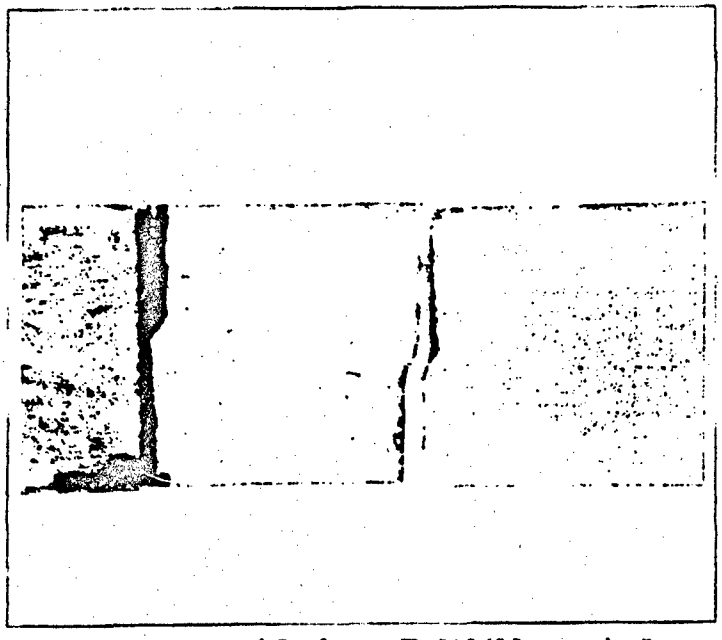

Fractured Surface at T=518635 seconds, 8x.

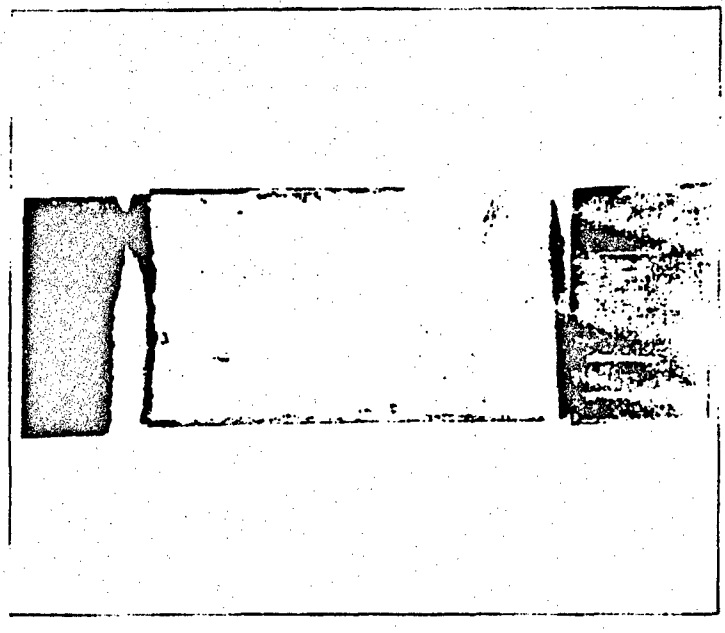

Fractured Surface at T=1009129 seconds, 8x.

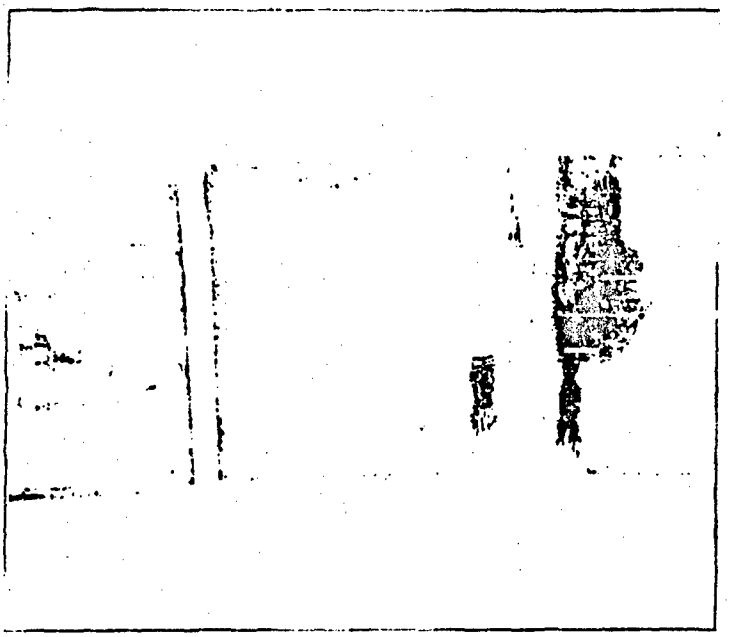

Fractured Surface at T=32 seconds, 8x.

Fractured Surface at T=36 seconds, 8x.

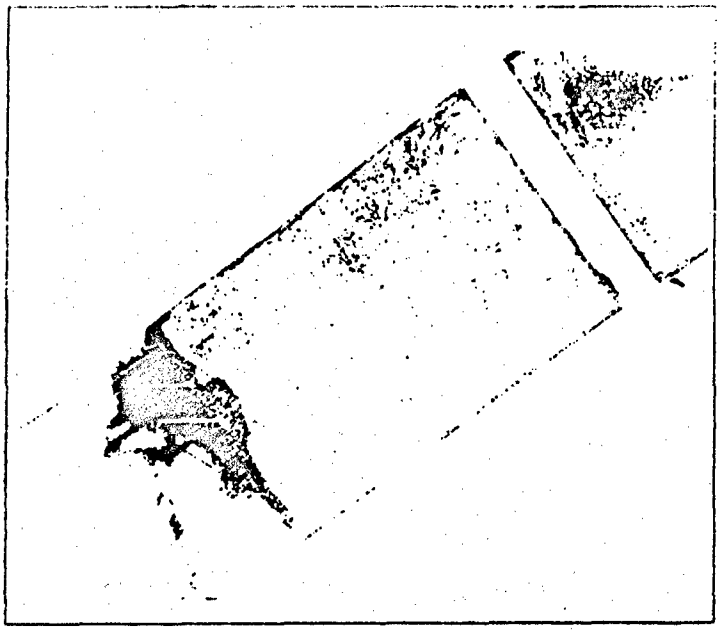

Fractured Surface at T=101 seconds. 8x.

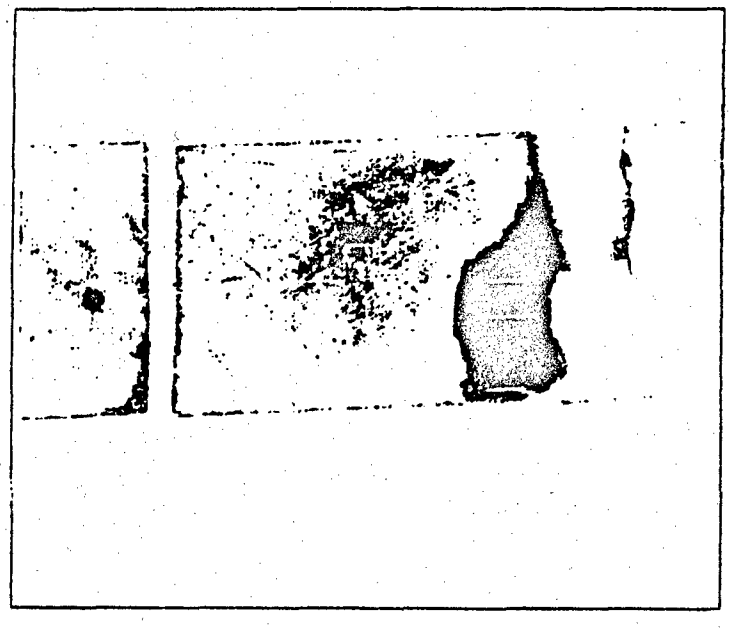

Fractured Surface at T=121 seconds. 8x.

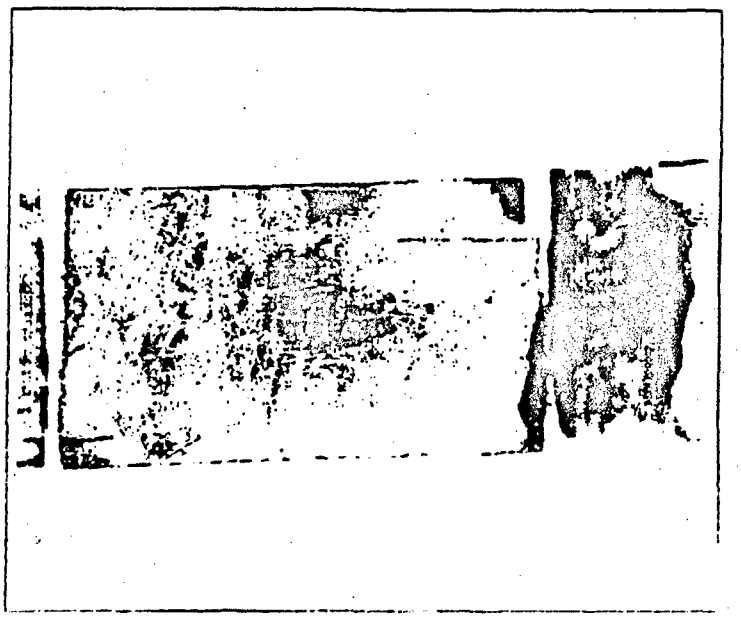

Fractured Surface at T=1010 seconds, 8x.

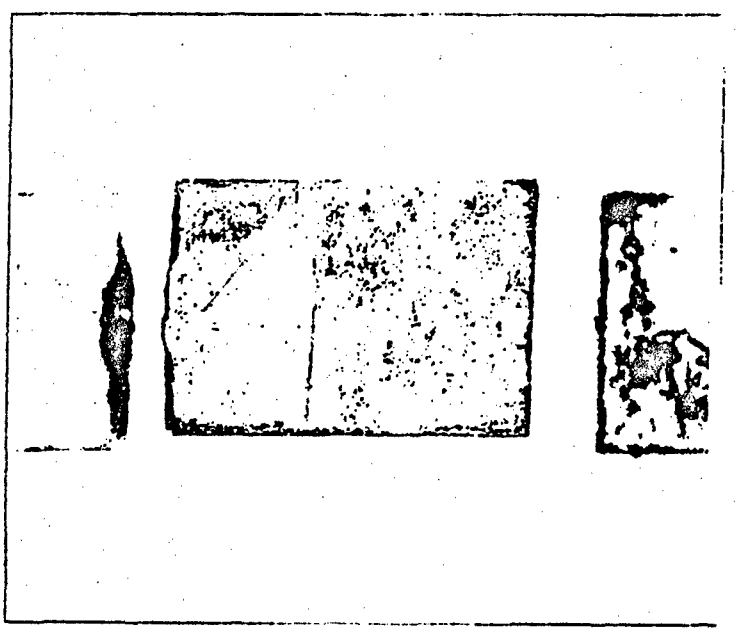

Fractured Surface at T=2376 seconds, 8x.

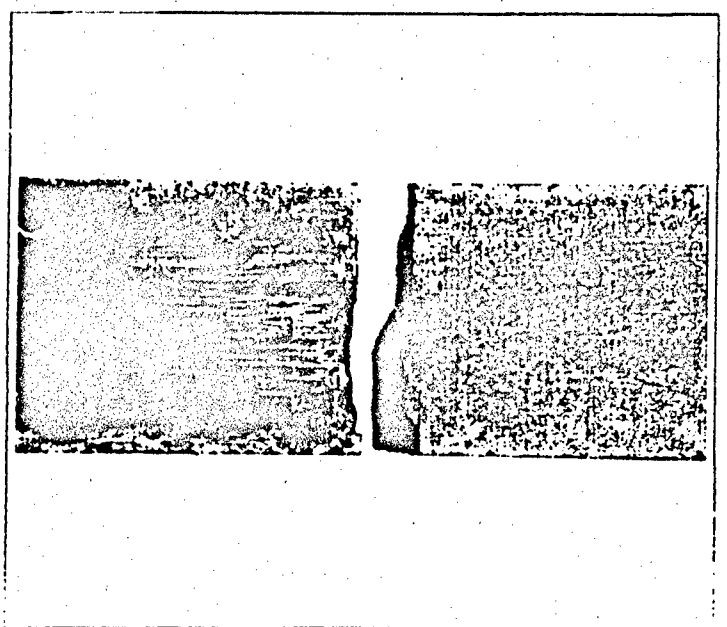

Fractured Surface at T=12030 seconds, 8x.

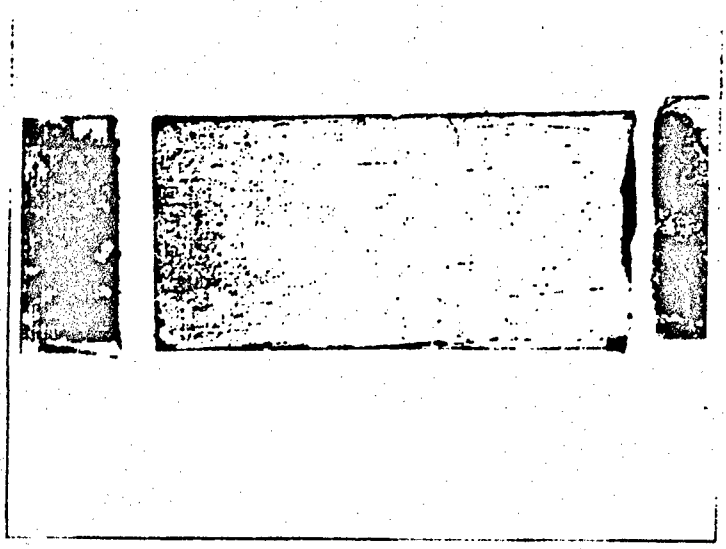

Fractured Surface at T=20237 seconds, 8x.

Vita

Captain Scott A. Grant was born on 3 March 1963 in Santa Barbara, California. He graduated from Carpenteria High School in Carpenteria, California in 1981. He enlisted in the United States Air Force in the summer of 1981, graduating from the Minuteman ICBM electrical maintenance school at Chanute Air Force Base in the Spring of 1982.

During his first tour at Malmstrom Air Force Base as a Minuteman ICBM electrical maintenance team chief and instructor, he was selected to attend Texas A&M University beginning January 1986 through the Airman's Education and Commissioning Program after completing preliminary course work at the College of Great Falls.

He graduated from Texas A&M University in December 1988 with a Bachelor of Science Degree in Aerospace Engineering, and was assigned to the (then) Air Force Weapons Laboratory, Kirtland Air Force Base, New Mexico following graduation from Officers Training School. He entered the school of engineering, Air Force Institute of Technology, in May of 1993.

REPORT DOCUMENTATION PAGE

Form Approved
OMB No 0704-0188

1. AGENCY USE ONLY (Leave blank)	2. REPORT DATE	3. REPORT TYPE AND DATES COVERED
	December 1994	Master's Thesis

4. TITLE AND SUBTITLE
FATIGUE BEHAVIOR OF A CROSS-PLY CERAMIC MATRIX COMPOSITE UNDER LOAD CONTROLLED TENSION-TENSION COMBINED LOADING AT ELEVATED TEMPERATURE

5. FUNDING NUMBERS

6. AUTHOR(S)
Scott A. Grant, Captain, USAF

7. PERFORMING ORGANIZATION NAME(S) AND ADDRESS(ES)
Air Force Institute of Technology
2750 P Street
WPAFB OH 45433-6583

8. PERFORMING ORGANIZATION REPORT NUMBER
AFIT/GAE/ENY/94D-16

9. SPONSORING / MONITORING AGENCY NAME(S) AND ADDRESS(ES)
Mr. Ted Fecke
WL/POTC
WPAFB, OH, 45433-6583

10. SPONSORING / MONITORING AGENCY REPORT NUMBER

11. SUPPLEMENTARY NOTES

12a. DISTRIBUTION / AVAILABILITY STATEMENT
Approved for public release; distribution unlimited

12b. DISTRIBUTION CODE

13. ABSTRACT (Maximum 200 words)

This study was carried out to investigate the elevated temperature behavior of the SiC-MAS5 cross-ply $[0/90]_{4s}$ ceramic matrix composite manufactured by Corning Inc. to fatigue with loading waveforms that combine the characteristics of stress rupture and high cycle fatigue. The test results were compiled in the form of S-N (cycles to failure), S-T (exposure time versus cycles to failure), S-S (energy exposure versus cycles to failure), normalized modulus degradation, strain progression, and hysteresis loop progression. From the mechanical behavior demonstrated by these curves, relationships between the effect of the environment and loading waveform were developed. In addition, a post-mortem SEM analysis of the fracture surface was conducted and the results compared to the mechanical behavior.

14. SUBJECT TERMS	15. NUMBER OF PAGES
Ceramic matrix composites, Tension-Tension Fatigue, Load control, Stress rupture	125
	16. PRICE CODE

17. SECURITY CLASSIFICATION OF REPORT	18. SECURITY CLASSIFICATION OF THIS PAGE	19. SECURITY CLASSIFICATION OF ABSTRACT	20. LIMITATION OF ABSTRACT
Unclassified	Unclassified	Unclassified	UL